HORMA domain proteins in Autophagy initiation

Dissertation

for the award of the degree

"Doctor rerum naturalium"

of the Georg-August-Universität Göttingen within the

doctoral program

"Biomolecules: Structure-Function – Dynamics" (GGNB)

Submitted by

FRANCESCA LUGARINI

From Frascati, Rome, Italy

Göttingen, February 2022

TAC

Dr. Alex Caspar Faesen

Biochemistry of Signal Dynamics, Max Planck Institute for Multidisciplinary Sciences

Prof. Dr. Michael Thumm

Department of Cellular Biochemistry, Center for cellular Biochemistry, University Medical Center Göttingen (UMG)

Dr. Alexander Stein

Research Group Membrane Protein Biochemistry, Max Planck Institute for Multidisciplinary Sciences

---

First reviewer: Dr. **Alex Caspar Faesen,** Biochemistry of Signal Dynamics, Max Planck Institute for Multidisciplinary Sciences

Second reviewer: Prof. Dr. **Michael Thumm,** Department of Cellular Biochemistry, Center for cellular Biochemistry, University Medical Center Göttingen (UMG)

Further members of the Examination Board:

- Dr. **Alexander Stein**, Research Group Membrane Protein Biochemistry, Max Planck Institute for Multidisciplinary Sciences
- Prof. Dr. **Henning Urlaub**, Research Group Bioanalytical Mass Spectrometry, Max Planck Institute for Multidisciplinary Sciences
- Dr. **Sonja Lorenz**, Research Group Ubiquitin Signaling Specificity, Max Planck Institute for Multidisciplinary Sciences
- Prof. Dr. **Prof. Dr. Rubén Fernández-Busnadiego** University Medical Center, University of Göttingen, Germany, Institute of Neuropathology

Date of oral examination: 21 March 2022

ZUSAMMENFASSUNG

Der autophagische Signalweg ist eine, unter eukaryotischen Zellen, evolutionär konservierteStrategie zur Aufrechterhaltung der Zellhomöostase auf basalem Niveau und unter Stressbedingungen. Durch ihn werden Proteinaggregate, beschädigte Organellen und Krankheitserreger entfernt. Außerdem wird er benötigt, um die Energiequellen in entscheidenden Stadien der normalen Entwicklung und der Tumorbildung auszugleichen. Er wird als Reaktion auf Hunger, DNA-Schäden, Hypoxie und Amino- oder ATP-Mangel aktiviert (Levine und Klionsky, 2004; Levine und Kroemer, 2008; Glick, Barth und Macleod, 2010; Feng *et al.*, 2014; Hurley and Young, 2017; Mizush, 2018). Da die Autophagie eine Qualitätserhaltung- und Abwehrsystem und ein Abwehrsystem ist, kann eine unausgewogene Modulation des Signalwegs schädlich sein und erfordert daher eine strenge Regulierung.

An der ER-Kontaktstelle kolokalisieren der ULK1-Komplex sowie andere Proteine wie ATG9, das Lipidtransfermodul ATG2-WIPI und das PI3KC, um eine Autophagie auszulösen (Mari *et al.*, 2010; Obara and Ohsumi, 2011; S. W. Suzuki *et al.* , 2015a; Yamamoto *et al.* , 2016; Chowdhury *et al.* , 2018; Noda, 2021a). Es ist jedoch unklar, wie die einzelne Bestandteile zusammenfinden, um die Expansion des Autophagosoms zu starten und voranzutreiben Innerhalb des ULK1-Komplexes ATG13 und ATG101 dimerisieren die beiden HORMA-Proteine (Qi *et al.*, 2015; Suzuki *et al.*, 2015), ähnlich wie MAD2, das am besten untersuchte HORMA-Domain-Protein (Luo *et al.*, 2002; Sironi *et al.*, 2002). Diese Proteine sind in ihrer HORMA-bezogenen Funktion bei der Einleitung der Autophagie weitgehend uncharakterisiert.

In dieser Arbeit haben wir den Einfluss der HORMA-Domänenstruktur von ATG13 und ATG101 auf die Rekrutierung einiger Subkomplexe der Autophagie-Initiation untersucht (Jao *et al.*, 2013; S. W. Suzuki *et al.* , 2015; Kim *et al.* , 2018; Park *et al.* , 2019; Kannangara *et al.* , 2021). Dies geschah mittels eines *in vitro* biochemischen Rekonstitutionsansatzes unter Verwendung von aufgereinigten Proteinen. Wir konnten nachweisen, dass ATG13-ATG101 direkt mit der Lipid-Scramblase ATG9 interagiert und die Komplexbildung durch eine kinetisch kontrolliert Dimerisierung von ATG101-ATG13 eng reguliert wird. Wir haben auch festgestellt, dass dieser Drei-Protein-Komplex mit anderen Komponenten der Autophagie-Initiierung einen einzigen Komplex bildet und vermuten deshalb, dass diese Wechselwirkung Teil eines größeren Apparats sein könnte, welcher an der ER-Kontaktstelle angefügt wird. In diesem Zusammenhang stellen ATG13 und ATG101 den Master-Regulator der Autophagie dar, indem sie ihre Rolle als zeitlimitierender Faktor ausüben und gleichzeitig einen Interaktionspunkt für Proteine schaffen, die an der autophagosomalen Biogenese beteiligt sind.

ABSTRACT

The autophagic pathway is an evolutionarily conserved strategy among eukaryotic cells for maintaining cell homeostasis at the basal level and during stressful conditions. It removes protein aggregates, damaged organelles, and pathogens. In particular, it is necessary for balancing energy sources at crucial stages of normal development and tumor progression, and it is upregulated in reaction to starvation, DNA damage, hypoxia, amino acid, and ATP deficiency (Levine and Klionsky, 2004; Levine and Kroemer, 2008; Glick, Barth and Macleod, 2010; Feng *et al.*, 2014; Hurley and Young, 2017; Mizushima, 2018). Since autophagy is quality maintenance and a defensive mechanism, an unbalanced modulation of the pathway can be harmful and, therefore, requires stringent regulation.

At the ER contacts site, the ULK1 complex, as well as other proteins like ATG9, the lipid transfer complex ATG2-WIPI and the PI3KC colocalize to initiate autophagy (Mari *et al.*, 2010; Obara and Ohsumi, 2011; S. W. Suzuki *et al.*, 2015a; Yamamoto *et al.*, 2016; Chowdhury *et al.*, 2018; Noda, 2021a). However, it is not clear how all these components coalesce to form and progress the expansion of the autophagosome. Inside the ULK1 complex, ATG13 and ATG101, dimerize through their HORMA structure (Qi *et al.*, 2015; Suzuki *et al.*, 2015), similarly to MAD2, the most described HORMA (Luo *et al.*, 2002; Sironi *et al.*, 2002). These proteins are largely uncharacterized in their HORMA-related function in autophagy initiation.

In this work, we investigated the impact of the HORMA domain structure of ATG13 and ATG101 in the recruitment of some of the autophagy initiation subcomplexes (Jao *et al.*, 2013; S. W. Suzuki *et al.*, 2015; Kim *et al.*, 2018; Park *et al.*, 2019; Kannangara *et al.*, 2021) by an *in vitro* biochemical reconstitution approach using purified proteins.

We show that ATG13 and ATG101 directly interact with the lipid scramblase ATG9 in an incredibly slow fashion and that the complex formation is accelerated by a conformationally-sensitive dimerization of ATG101-ATG13. We also assessed that ATG13-ATG9-ATG101 form a super-complex with other components of autophagy initiation and propose that ATG13-ATG101 interaction to ATG9 is the rate-limiting factor that regulates assembly at the ER contact sites of this super-complex involved in autophagosome biogenesis and elongation.

Table of Contents

Table of Figures

Abbreviations

AcMNPV	Autographa Californica Multicapsid Nucleopolyhedrovirus
APC	Anaphase Promoting Complex
BAR	Bin-Amphiphysin-Rvs
BATS	Barkor/ATG14 Autophagosome Targeting Sequence
BM	Binding Motif
BP	Binding Partner
BS3	Bissulfosuccinimidyl Suberate
C	Closed
CBASS	Cyclic Oligonucleotide-Based Antiphage Signaling System
CCD	Coiled-Coil Domain
CMA	Chaperone-Mediated Autophagy
CMC	Critical Micelles Concentration
CVT	Cytoplasm to Vacuole Targeting
DDM	N-Dodecyl-B-D-Maltoside
DFCP1	FYVE Domain–Containing Protein 1
DSB	Double-Strand Breaks
ERES	ER Exit Site
ERGIC	ER-Golgi Intermediate Compartment
FIP200	FAK Family-Interacting Protein of 200 kDa
FL	Full Length
GABARAP	Gamma-Aminobutyric Acid Receptor-Associated Protein
GEC	Gene Expression Constructs
GOI	Gene Of Interest
GSH	Glutathione-S-Transferase
GST	Glutathione S-Transferase
HORMA	Hop1, Rev7 and Mad2
HORMAD	HORMA Domain–containing Proteins
HR	Homologous Recombination
HyPAS	Hybrid PAS
IDPR	Intrinsically Disordered Protein Regions
IPTG	Isopropyl B-D-1-Thiogalactopyranoside

LAMP-2A	Lysosomal-Associated Membrane Protein 2A
LC3	Microtubule-Associated Protein Light Chain 3
LIR	LC3-Interacting Region
MBP	Maltose Binding Protein
MBP1	MAD2-Binding Peptide 1
MCC	Mitotic Checkpoint Complex
MIM	MAD2 Interacting Motif
mTORC1	Mammalian TORC1
NHEJ	No Homologous End Joining
O	Open
ON	Overnight
PBS	Phosphate Buffered Saline
PCR	Polymearse Chain Reaction
PD	Pull Dwn
PE	Phosphatidylethanolamine
PI	Phosphatidylinositol
PI3KC1	Phosphatidylinositol (3-Kinase) Complex I
PI3P	Phosphatidylinositol 3-Phosphate
RT	Room Temperature
SAC	Spindle Assembly Checkpoint
SEC	Size Exclusion Chromatography
TGN	Trans-Golgi Network
TORC1	Target Of Rapamycin Complex 1
ULK	Uncoordinated-51-Like Kinase
ULK	Unc-51-Like Kinase
UVRAG	Uv Radiation Resistance-Associated Gene
VPS34	Vacuolar Protein-Sorting 34
WIPI	WD-40 Repeat-Containing Protein That Interacts With PI
XLMS	Mass-Spectrometry
YFP	Yellow Flourescent Protein

1 Introduction

1.1 Prelude

At the beginning of autophagy research, Christian De Duve drifted his attention from the mechanism of insulin metabolism to the 'dense bodies' with an high acid phosphatase activity: the lysosome. He won the Nobel Prize for Physiology or Medicine (shared with George Palade Albert Claude) in 1974 for his discovery. During his pivotal work on lysosomes, Christian de Duve (re)-invented the term 'autophagy' that is derived from the Greek word 'αὐτόφαγος' or 'autóphagos', and can be translated as 'self-devouring' or 'self-eating'. The word was already used since the second half of the 19th century to identify the effects of nutrient deprivation (Mizushima, 2018). De Duve decided to use the name 'Autophagy' to distinguish the intracellular degradation system from the 'heterophagy', mechanism of absorption and destruction of external molecules (Mizushima, 2018).

Most of the studies on autophagy were mostly based on microscopy approaches until the beginning of the 90s when different groups identified autophagy defective mutants (Tsukada and Ohsumi, 1993; Thumm *et al.*, 1994; Harding *et al.*, 1995). The genes identified were termed ATG from 'AuTophaGy' (Harnett *et al.*, 2017). The spark that the Autophagy genes discovery represented for the biology field led, in 2016, Yoshinori Oshumi to get the Nobel Prize in Physiology or Medicine (Takeshige *et al.*, 1992; Tsukada and Ohsumi, 1993; Baba *et al.*, 1994; Ohsumi, 1999; Harnett *et al.*, 2017). At the time of his discovery, Oshumi's research was devoted to the protein degradation system of yeast, the vacuole, a lysosome-like organelle. His approach was based on cultivating yeast mutants lacking vacuolar enzymes while also starving the cells to trigger autophagy. He screened specifically for the accumulation of tiny vesicles inside vacuoles and classified his mutants in 15 groups, suggesting at least 15 genes involved in the control of autophagy in yeast. Up to now, 41 ATG genes have been identified in yeast and most have human orthologs.

To this day, we may include up to 604 genes as regulators and 'core' components of autophagy in humans, and they are classified into six groups: 135 genes belong to mTOR and downstream pathways, 197 genes are involved in the autophagy core, 68 genes are autophagy regulators, 80 genes are involved in mitophagy, 22 genes regulate docking and fusion, 162 genes compose the lysosome, and 34 are lysosome-related genes (Bordi *et al.*, 2021).

1.2 Autophagy pathway and diseases

The autophagic pathway is an evolutionarily conserved mechanism to maintain cell homeostasis during stressful conditions. In particular, its role is to eliminate protein aggregates, damaged organelles, or pathogens, but more, in general, is extremely crucial for balancing energy sources at critical developmental stages and in response to nutritional stress (Glick, Barth and Macleod, 2010; Feng *et al.*, 2014). Autophagy pathway defects are linked to various diseases because of their essentiality in cell quality maintenance and their role in recycling macromolecules. In particular, its disbalance is involved in non-alcoholic fatty liver disease (NAFLD), cancer, neurogenerative diseases, diabetes, kidney diseases, heart diseases, infectious diseases, and Inflammatory Bowel Disease (Wong, Cheung, and Ip, 2011; Ichimiya *et al.*, 2020).

Overnutrition causes NAFLD, which is typically linked to diabetes and dyslipidemia. Hepatotoxicity and lipid droplet buildup lead to hepatocyte mortality, and both caused by reduced autophagy in NAFLD hepatocytes. Autophagy disruption in pancreatic cells produces anomalies in cellular organelle turnover and function, leading to insulin insufficiency and hyperglycemia, which is the base for diabetes mellitus where there is marked impaired insulin production, secretion, and activity (Ichimiya *et al.*, 2020). Out of all the diseases in which autophagy is involved, probably cancer and neurodegeneration are the most striking.

Autophagy deficit in neurons is linked to mutations or deletions of ATG genes, causes a variety of neurodegenerative disorders. Among the most prominent gene mutation, we can underline Parkin, PINK1 (Parkinson's disease), OPT1(Amyotrophic Lateral Sclerosis), RAB7A (Charcot–Marie–Tooth disease), APP (Alzheimer's disease) (Levine and Kroemer, 2008; Wong, Cheung, and Ip, 2011; Ichimiya *et al.*, 2020; Li, He and Ma, 2020; Watanabe, Taguchi and Tanaka, 2020).

In cancer, autophagy represents a "double-edged sword". The reason is that autophagic cell quality control can be disrupted and lead to tumor formation. But at the same time, tumor development is also linked to cell nutrition supply via autophagy activation. As a result, both autophagy suppression and activation contribute to tumor genesis and proliferation through distinct routes. Advanced lung cancer, pancreatic ductal adenocarcinoma, melanoma, breast cancer, and colorectal cancer all benefit from autophagy. This double-faced role of autophagy in cancer is influenced by food availability, microenvironment stress, pathogenic circumstances, and the existence of a functional immune system in the organism. Indeed, at the early stages of tumorigenesis, autophagy can preserve genome stability, prevent severe cell damage and inflammation responses, and also block the accumulation of oncogenic protein aggregates, acting in tumor suppressive manner. However, at later stages, autophagy works as a shield for the

cancerous cells by assisting the cell energetically by maintaining the quality of mitochondria, preventing DNA damage, and enhancing survival and resistance in a stressful environment. Therefore, promoting tumor development. Autophagy has also been linked to cancer aggressiveness through aiding metastasis (Wong, Cheung, and Ip, 2011; Ichimiya *et al.*, 2020; Li, He, and Ma, 2020).

Since it is certain that autophagy can help tumor cells survive, the normal cancer treatment combined with autophagy activity regulators can be regarded as a viable anticancer therapy in the near future. The core approach would be increasing or blocking autophagy activity by autophagy inducers or inhibitors dependent on tumorigenesis and cancer stages. However, we have to keep in mind that further research is needed to better understand and define how autophagy relates to cancer evolution and how autophagy is regulated at the early stages of development as preventing approach (Li, He, and Ma, 2020).

Needless to say, the scientific community is in desperate need of new potential targets and regulators to screen, and what the autophagy field lack, at the moment, is a deep structural and functional understanding of the biochemistry of the pathway.

1.3 Different types of Autophagic pathway

The proteasome and the vacuole-lysosome are two key pathways for protein and organelle degradation in eukaryotic cells. The proteasome is a compartmentalized protease machine and its degradative capability is limited to partially denatured protein substrates (Voges, Zwickl and Baumeister, 1999). Proteins in the cytoplasm and nucleus, as well as misfolded proteins destined for destruction in this context, are tagged with ubiquitin signals. While proteasomes provide optimal processing for soluble proteins, their capacity to operate on membrane proteins and protein complexes is limited. To this purpose, yeast vacuoles and mammalian lysosomes are capable of digesting bigger and more complex substrates such as protein complexes and organelles (Teter and Klionsky, 2000). The vacuole and lysosome organelles represent a way to compartmentalize enzymes within a membrane to protect the cytoplasm from the unregulated enzymatic activity. This eliminates the necessity to use the substrate-limited proteasome system but introduces substrate delivery problems (Huang and Klionsky, 2002).

Autophagy is that elegant and sophisticated solution to delivery cytoplasmic cargos that eukaryotic cells evolved to upgrade their recycle capability. There are three types of autophagy: micro-autophagy, macro-autophagy, and chaperone-mediated autophagy (CMA) (Figure 1.0a). Macro-autophagy transports cytoplasmic cargo to the lysosome through a double membrane vesicle termed 'autophagosome' that engulfs the substrate, merges with the lysosome to generate an 'autolysosome'. By contrast, in micro-autophagy, cytosolic components are directly taken up by

the lysosome by invagination of the lysosomal membrane. These two autophagy mechanisms may swallow huge structures via both selective and non-selective manner (Huang and Klionsky, 2002).

Micro-autophagy is generally considered a non-selective process (with very few exceptions like micro-pexophagy, micro-mitophagy, etc.), while macro-autophagy can be either.

Figure 1.0

a

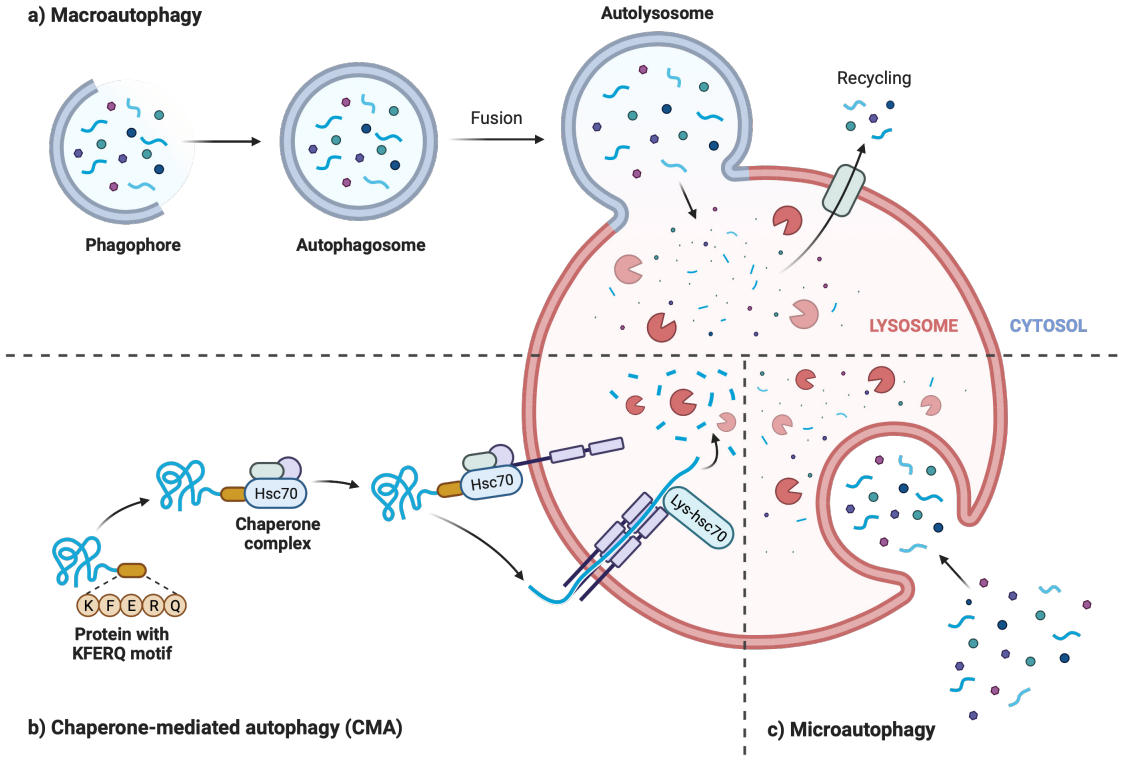

b

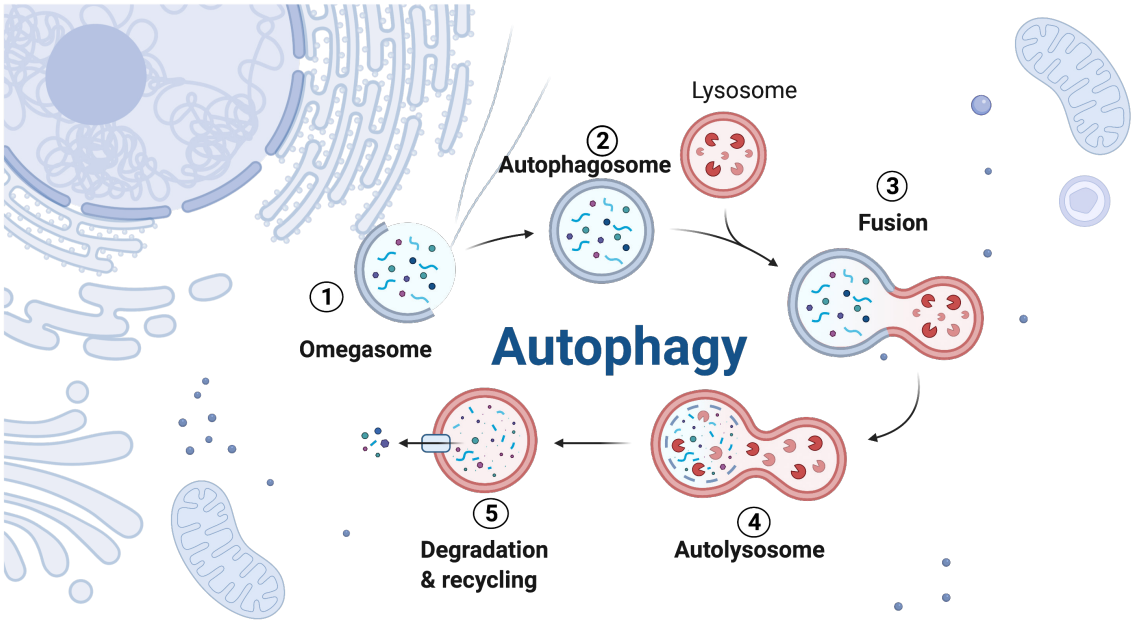

Figure 1.0 Types of Autophagy and Macroautophagy in detail

(a) Schematic depiction of autophagy processes: Macroautophagy -a-, CMA -b- and -c- (macro)autophagy; **(b)** Schematic representation of autophagy in mammals. The images were modified from BioRender templates.

Non-selective macro-autophagy is used for the cytoplasm turnover under starvation, whereas selective macro-autophagy specifically targets damaged or superfluous organelles, such as mitochondria or peroxisomes, as well as bacteria or viruses. Each selective process involves a core set of machinery as well as specific components, and thus is labeled accordingly: We have mitophagy for selective mitochondria degradation, xenophagy for viruses and bacteria, pexophagy for peroxisomes degradation, etc. (Feng *et al.*, 2014). One form of selective macro-autophagic-specific pathway in yeast is the CVT pathway. The cytoplasm to vacuole targeting (CTV). At least two hydrolases are transported to the vacuole via the Cvt pathway: α-mannosidase (Ams1) and aminopeptidase I. (Ape1). Ape1 is synthesized as an inactive proto-enzyme in the cytoplasm. The Cvt pathway sequesters the precursor Ape1 into a Cvt vesicle that delivers it into the vacuole, where it is converted into its active form (Lynch-Day and Klionsky, 2010).

CMA, which only occurs in mammals, differs from micro-autophagy since it does not employ membranous structures to trap cargos. Targeted proteins are translocated through the membrane of the lysosome by forming a complex with chaperone proteins (like Hsc-70) (Glick, Barth and Macleod, 2010). These proteins are then recognized by the lysosomal membrane receptor lysosomal-associated membrane protein 2A (LAMP-2A), resulting in their unfolding and degradation in chaperone-mediated autophagy (CMA) (Glick, Barth and Macleod, 2010). Therefore, CMA differs from micro-autophagy since does not employ membranous structures to trap cargo and the chaperones detect cargo proteins via a specific pentapeptide motif (Huang and Klionsky, 2002).

From this moment on, we will discuss macro-autophagy and therefore, for simplicity, it will be termed 'Autophagy' (Figure 1.0b).

1.3.1 Autophagy process in yeast

Most of the studies of autophagy have bourgeoned from the ATG genes discovery at the beginning of 90s. Therefore, both micro- and macro-autophagy mechanisms have been more deeply characterized in yeast rather than more complex systems like mammals. Even though the mechanism is strongly evolutionarily conserved, there are a few differences that pushed most of the autophagy field to shift attention towards mammals.

It can be stated that autophagy is the formation of a *de novo* vesicle in the cytoplasm (Noda, Suzuki, and Ohsumi, 2002). In *Saccharomyces cerevisiae*, in particular, autophagy originates at the PAS ('pre-autophagosomal structure' or 'phagophore assembly site') a separate cellular component that acts in autophagosome formation but does not turn into an autophagosome. Indeed, the ATG proteins colocalize to the PAS, interact with the expanding phagophore to support autophagosome formation, but detach when the autophagosome is completed (Hollenstein and Kraft, 2020).

The PAS act as a membrane seeder, recruiting membrane from various sources, e.g. existing organelles. Also, fusion with other vesicles may promote phagophore enlargement, however, more studies are necessary to clarify this aspect (for more information see ATG9 section) (Noda, Suzuki and Ohsumi, 2002; Suzuki and Ohsumi, 2010; Hollenstein and Kraft, 2020). Autophagosomes compartmentalize their cargo from the surrounding cytoplasm, which may contain cytosol, organelles, or microbes, and transport it to the vacuole. The outer autophagosome membrane merges with the vacuole and, consequently, the inner membrane vesicle, and its content is discharged into the vacuolar lumen. The last stage involves vacuolar hydrolases breaking down cargo and converting it back to building blocks for reuse. From the molecular point of view, the PAS formation and the development of the autophagosome, until fusion to the vacuole, is an incredibly complex cascade of proteins that interact with each other. Autophagosomes in yeast form within 10 minutes and can be between 0.3 and 0.9 μm in size (Takeshige *et al.*, 1992; Baba *et al.*, 1994; Geng *et al.*, 2008). We may easily understand that indiscriminate autophagy would be disastrous; hence, autophagosome formation must be strictly and spatiotemporally controlled (Suzuki and Ohsumi, 2010). Indeed, although adequate levels of autophagy are essential to maintain homeostasis under stress conditions, excessive or uncontrolled autophagy can result in cell death (Liu and Levine, 2015; Denton and Kumar, 2019).

In yeast, the ATG proteins are classified into various groups: the Atg1–Atg13 subcomplex and the Atg17–Atg29–Atg31 subcomplex (the Atg1 kinase complex), Atg9, the PI3 kinase complex I (the phosphatidylinositol (3-kinase) complex I, PI3KC1), the Atg2–Atg18 complex, the Atg12 conjugation system, and the Atg8 system.

The most frequent approaches used to induce autophagy are to use drugs targeting autophagy regulators or by inducing starvation (Figure 1.1a). One of the most used drugs is rapamycin, a TORC1('target of rapamycin complex 1') inhibitor. The cascade that regulates TORC1 inhibition is incredibly complicated, however, it can be summarized as follows.

PI3KCIα p85 and p110 subunits couple to an active receptor tyrosine kinase (like epidermal growth factor or the insulin receptor). They catalyze the phosphorylation of PIP3 at the membrane. With the binding of PIP3 by the Akt-kinase PDK1 and Akt, this PIP3 acts as a ligand for Akt kinase PDK1 and Akt. At the membrane, PDK1 phosphorylates and activates Akt. Akt modulates the TORC1 functional state, one of which includes suppression of TSC. The release of an inhibitory switch by AKT phosphorylation of the TSC allows the Ras-related GTPase-Rheb to load GTP and activate TORC1. Negative regulators like PTEN have a strong influence on the PI3K signal to maintain the equilibrium by a negative feedback loop (Papa and Pandolfi, 2019) (Figure 1.1a).

In both fed and starving conditions, Atg13 is necessary for Atg1 kinase activity and autophagy progression. Atg13 is phosphorylated in nutrient-rich conditions but rapidly dephosphorylates under nutrient depletion or rapamycin treatment. Rapamycin suppression of TORC1 triggers an enhanced Atg1 kinase activity and the activation of bulk autophagy. The dephosphorylation of Atg13 was proposed to be essential for its interaction with Atg1, leading to a scenario in which Atg13 interacts with Atg1 only during starvation. However, this concept has recently been amended, as Atg13 binding is required for Atg1 function in fed cells as well (Noda and Ohsumi, 1998; Kamada *et al.*, 2000; Kraft *et al.*, 2012).

Furthermore, starvation and TORC1 suppression allow Atg13 to bind to Atg17, another component of the 'core' autophagy. Atg17 is required for PAS assembly and Atg1 kinase activity in starvation-induced autophagy. Atg29 and Atg31 form a stable subcomplex with Atg17, and both are required for proper Atg17 localization and function. Atg17 is proposed to engage curved membranes directly given that the S-shaped homo-dimers that form when homo-dimerizing are similar to two BAR ('Bin-Amphiphysin-Rvs') domain dimers binding to each other. This supports the hypothesis that Atg17, like Atg1complex, is involved in binding Atg9-positive vesicles at the PAS (Kawamata *et al.*, 2008; Ragusa, Stanley, and Hurley, 2012; Simunovic *et al.*, 2019). *In vitro*, Atg17 has been proposed to directly bind to Atg9 (Rao *et al.*, 2016a). Additionally, also the N-terminus domain of Atg13 (HORMA) is supposed to bind Atg9 *in vivo* (S. W. Suzuki *et al.*, 2015a). Atg9 is the only transmembrane protein of the 'core' autophagy machinery and is a lipid scramblase involved in membrane expansion at the PAS (Matoba *et al.*, 2020).

The phosphatidylinositol (3-kinase) complex I (PI3KC1) is recruited and accumulates at the omegasome and catalyzes phospho-inositol (PI) phosphorylation, resulting in PI3-phosphate

(PI3P). The recruitment of the PI3KC1, in particular of Atg14 is directly or indirectly mediated by Atg13 (Jao *et al.*, 2013). In a PI3P-dependent way, the Atg2-Atg18 complex interacts with the omegasome Atg18 is a PI3P sensor (Busse *et al.*, 2015), while Atg2 is a phospholipid transport protein (Suzuki *et al.*, 2017; Gómez-Sánchez *et al.*, 2018; Osawa and Noda, 2019; Osawa *et al.*, 2019).

Autophagy requires two ubiquitin-like conjugation processes (Mizushima *et al.*, 1998; Ichimura *et al.*, 2000; Suzuki *et al.*, 2001): the Atg8 and the Atg12. Atg12 was identified to be the first ubiquitin-like Atg protein (Mizushima *et al.*, 1998). Ubiquitin is produced as a precursor and subsequently processed to expose the carboxy-terminal glycine. After activation by an E1 enzyme, ubiquitin is transferred to an E2 enzyme (formation of a thioester bond). An E3 ubiquitin ligase recognizes the target protein and then transfers the ubiquitin from the E2 to a lysine residue on the target protein (Cappadocia and Lima, 2018).

Atg12 has a glycine residue already at the end of its amino-acid sequence and it can be directly activated by establishing a thioester bond with Atg7 (E1) (Tanida *et al.*, 1999). After activation, Atg12 is transported to Atg10 (E2) enzyme (Shintani *et al.*, 1999), and then conjugated to the target protein Atg5. The conjugate of Atg12–Atg5 then forms a non-covalent bond with Atg16. Atg16-Atg5-Atg12 can be therefore localized to the PAS (Mizushima *et al.*, 1998; Mizushima, Noda and Ohsumi, 1999; Kuma *et al.*, 2002).

In the second system, the ubiquitin-like protein Atg8 is conjugated to the head group of the membrane lipid PE (phosphatidylethanolamine). First, Atg8 is cleaved by Atg4 to expose the glycine residue (Kirisako *et al.*, 2000). The conjugating enzymes Atg7 (E1) and Atg3 (E2) have a major role in this reaction. Differently from Atg12-Atg5, Atg8-PE conjugation is reversible and the reaction is mediated again by Atg4 (Kirisako *et al.*, 2000). The Atg8 and Atg12 conjugation systems are strongly connected because the Atg12–Atg5–Atg16 complex is required for Atg8–PE synthesis *in vivo* (Hanada *et al.*, 2007). Atg8–PE has been shown to recruit cytoplasmic cargos to the isolation membrane, enabling their absorption into autophagosomes. Furthermore, Atg8–PE is thought to aid membrane tethering and fusion, hence facilitating autophagosomes expansion (Nakatogawa, Ichimura, and Ohsumi, 2007).

1.3.2 Autophagy initiation in mammals and the ULK1 complex

Figure 1.1

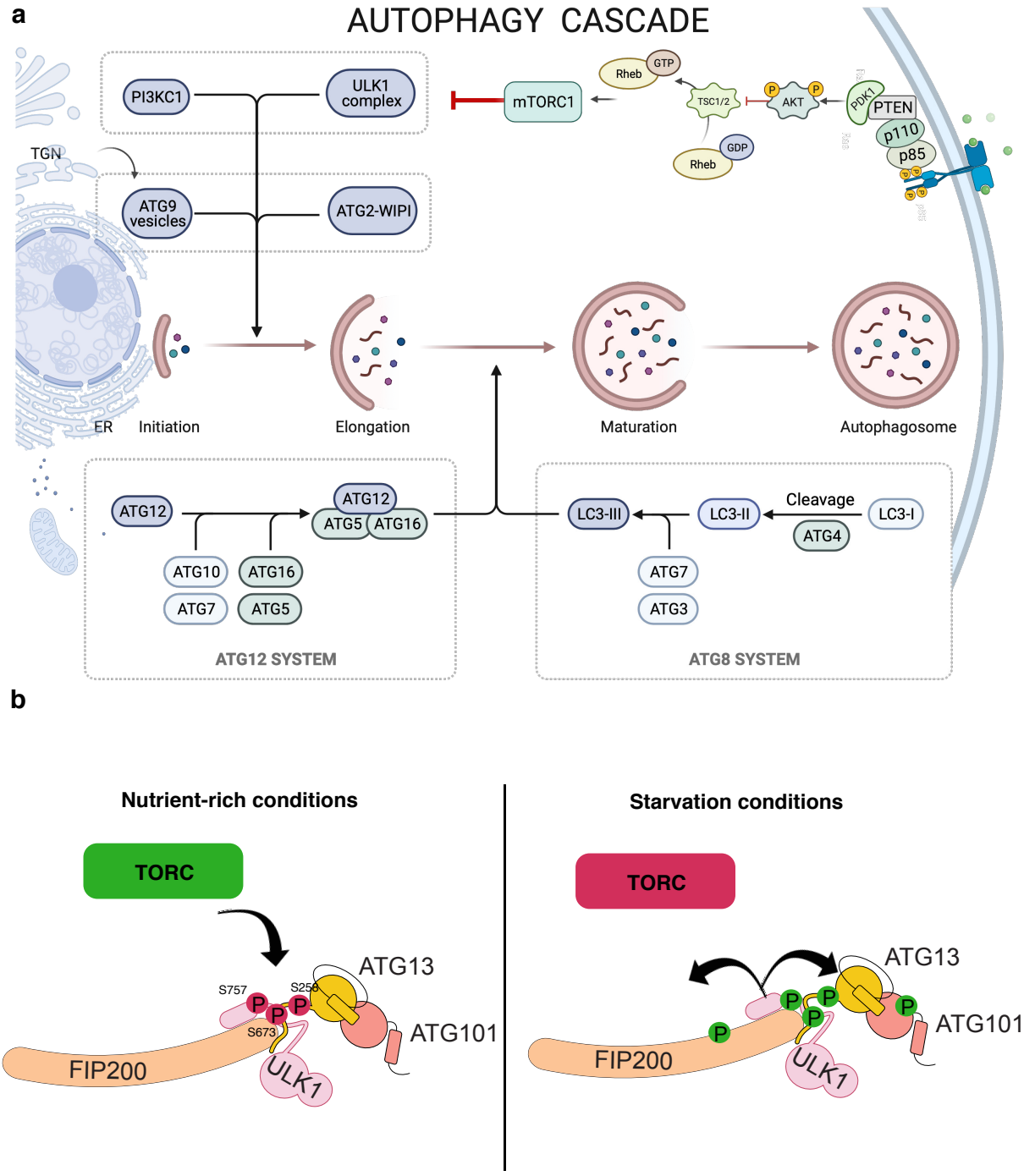

Figure 1.1 Mammalian autophagy cascade regulation and complexes involved

(a) Schematic depiction of autophagy processes from the molecular point of view. Image modified from BioRender; **(b)** Schematic representation of TORC regulation on ULK1 complex

In general, the mammalian autophagy system is far more complicated than the yeast one. A structure analogous to the yeast PAS has not yet been reported in mammalian cells, therefore it is plausible that phagophores might have different origins in this case (Kabeya *et al.*, 2000). The ER, the ER-Golgi compartment (ERGIC), mitochondria, the plasma membrane (PM), recycling endosomes, the nuclear membrane, and other intracellular organelles with membrane structures may contribute materially to the formation of the autophagosomal membrane (Tooze and Yoshimori, 2010; Mari, Tooze, and Reggiori, 2011; Yamamoto *et al.*, 2012; Shima, Kirisako, and Nakatogawa, 2019; Ktistakis, 2020; Yang *et al.*, 2021). Recently, a study has shown also the involvement of a hybrid PAS (HyPAS) for the formation of mammalian autophagosomes via fusion of *cis*-Golgi and endosomal membranes (Kumar *et al.*, 2021). It is known however that autophagosomes include around 70% of ER-derived material (Hayashi-Nishino *et al.*, 2009). At electron tomography, the omegasome seems to rise from early autophagic structure (IM) that form from a cradle originating from an ER (Hayashi-Nishino *et al.*, 2009). DFCP1 ('FYVE domain-containing protein 1') -positive ring-like structures are a marker for the omegasome (Axe *et al.*, 2008). Mammalian cells have minimal basal autophagic activity under nutrient-rich conditions, and LC3 is distributed throughout the cytoplasm. When autophagy is initiated, LC3 puncta start to appear. Some of the positive DFCP1ring-like structures are also LC3-positive. LC3 ('Microtubule-associated protein light chain 3'), a homolog of the yeast Atg8, is a notorious phagophore marker (Tanida *et al.*, 2005).

One of the main differences between the yeast and the mammalian system resides in the composition of the ATG complexes (Grasso, Renna, and Vaccaro, 2018; Lin, Shi, and Liu, 2021). ULK1 and ULK2 ('uncoordinated-51-like kinases 1 and 2') are the mammalian homologs of Atg1 (serine/threonine kinase). ULK1 and ULK2 may work, at least partially, redundantly since ULK1 loss induces only a modest phenotype in mice (Kundu *et al.*, 2008; Demeter *et al.*, 2020). One noteworthy feature of yeast Atg1 is that its enzymatic activity appears to be strongly increased during autophagy induction, while ULK1 catalytic activity after autophagy induction is milder. In addition, unlike yeast, the binding affinities between ATG13 and ULK1 do not appear to be controlled by nutritional signaling (Hara *et al.*, 2008; Chan and Tooze, 2009; Ganley *et al.*, 2009; Jung *et al.*, 2009; Nao Hosokawa *et al.*, 2009; Papinski and Kraft, 2016).

The complexity of protein interactions involving ULK proteins was shown by gel filtration studies and revealed that the majority of ULK1 was found in a super-molecular complex of ~3MDa (Nao Hosokawa *et al.*, 2009; Hieke *et al.*, 2015). The human ULK1 ~3MDa complex comprises also ATG13 (homolog of Atg13) and RB1CC1/FIP200 ('RB1-inducible coiled-coil protein 1'), as well as ATG101, which is not found in budding yeast (Hosokawa *et al.*, 2009; Mercer, Kaliappan and Dennis, 2009). Atg29 and Atg31 do not have mammalian homologs. Due to a number of

structural and functional similarities, it has been suggested that FIP200 is a yeast Atg17 homolog, despite a very low identity in sequence (Hara *et al.*, 2008; Hara and Mizushima 2009).

Embryonic early mortality occurs when either ATG101 or ATG13 are knocked-out (Lee *et al.*, 2014; Kaizuka and Mizushima, 2016; Morishita *et al.*, 2020), while FIP200 knock out embryonic mortality is observed in mid/late gestation (Gan *et al.*, 2006). ULK1/2 knock-out mice are viable and fertile and their cells can still undergo autophagy (Lee and Tournier, 2011). Indeed, the mammalian ATG13-ATG101 subcomplex appears to have autophagic capabilities irrespective of the ULK1 complex (H. Suzuki *et al.*, 2015c; Kannangara *et al.*, 2021), despite it being commonly claimed that ULK1 is assembled constitutively in mammalian cells (Alers *et al.*, 2011; Hieke *et al.*, 2015; Wallot-Hieke *et al.*, 2018).

FIP200 binds to both ULK1 and 2. ULK1 also needs FIP200 to keep its catalytic activity. ULK1 and FIP200 interact directly, according to *in vitro* protein reconstitution assays (Hara *et al.*, 2008; Ganley *et al.*, 2009; Nao Hosokawa *et al.*, 2009). In contrast to yeast, where the Atg1-Atg17 association was nutrition-sensitive, food restriction had no influence on ULK1-FIP200 interaction (Kabeya *et al.*, 2005). The molecular weight of the complex comprising ULK and FIP200 did not change during autophagy induction, indicating that their molecular composition may remain constant under a range of physiological circumstances (Hosokawa *et al.*, 2009). However, when autophagy was induced, FIP200 and ULK1 were shown translocating towards autophagosomal structures, suggesting that subcellular redistribution of ULK complexes might be a way of controlling this complex. FIP200 is a ULK substrate and its phosphorylation is elevated under autophagy-stimulated circumstances, albeit the functional importance of this mechanism is unknown (Hara *et al.*, 2008; Ganley *et al.*, 2009; Jung *et al.*, 2009; Nao Hosokawa *et al.*, 2009). Furthermore, the ULK1-ATG13-FIP200-ATG101 complex comprises also of mTORC1 ('mammalian TORC1'), but this is quickly removed from the ULK1 complex upon nutritional deprivation. Reduced mTORC1 activity causes dephosphorylation of ULK1 and ATG13, activation of ULK1, and phosphorylation of ATG13 and FIP200 under starvation (Jung *et al.*, 2009; Nao Hosokawa *et al.*, 2009) (Figure 1.1b). The phosphorylation motif of ULK1 is unique, with aromatic or aliphatic residues at positions 3, +1, and +2 relative to the phosphorylation acceptor (Papinski and Kraft, 2016).

The modulation of ULK1 kinase activity is one of the most significant tasks of ATG13 and FIP200; they can independently stimulate ULK1 kinase activity but both are required for ULK1 to be appropriately localized to the isolation membrane, as described above (Ganley *et al.*, 2009). Some examples of phosphorylation events within this complex are the phosphorylation of ULK1 are ATG13 S318 (S355 isoform 1) and FIP200 S943, S986, S1323. Most of the functions of these phosphorylation are unknown. The only known function of phosphorylation within the ULK1

complex is the auto-phosphorylation of ULK1 itself T180, S1042, T1046, involved in its kinase activity and its degradation (Bach *et al.*, 2011; Egan *et al.*, 2015; Liu *et al.*, 2016) (Figure 1.1b). ATG101 is also a target of ULK1 phosphorylation however is not clear what effect its phosphorylation might have on autophagy initiation (Egan *et al.*, 2015).

The binding sites between ATG13 and ULK1 were first identified in human than in yeast (Jung *et al.*, 2009; Kamada *et al.*, 2010; Kraft *et al.*, 2012) and all localize at the ATG13 long unstructured C-terminal region. Aside from the catalytic domain, ULK1 presents also a non-catalytic EAT domain, which is responsible for ATG13 binding. This binding is required for ULK1 recruitment to phagophore sites in human cells, a mechanism very similar to what has been observed in yeast (Chan *et al.*, 2009). The auto-phosphorylation of ULK1 might be mediated probably by a not completely clarified oligomerization of FIP200 and this EAT domain might be involved as well (Hurley and Young, 2007). Indeed, Ragusa *et al.* have determined the crystal structure of the Atg17-Atg31-Atg29 complex. They noticed that Atg17 is a dimer unable to bind liposomes but, surprisingly, they show that Atg1 EAT exhibits lipid tethering and curvature sensing characteristics (Ragusa, Stanley and Hurley, 2012). Shi *et al.* show that the N-terminus of FIP200 is able to dimerize *in vitro* and that the EAT domain has weak interaction for the FIP200 N-terminal dimer (Shi *et al.*, 2020). The EAT domain is flexible, but it folds into a folded domain when in interaction with Atg13, as revealed by hydrogen-deuterium exchange coupled to mass spectrometry (Stjepanovic *et al.*, 2014). The same is also true for the N-terminal dimer of FIP200: the FIP200 N-terminal domain is flexible, but when ATG13 is present, FIP200 assumes a C-shaped structure. In yeast, it resembles more an S-shaped structure (Ragusa, Stanley, and Hurley, 2012; Shi *et al.*, 2020). Chen *et al.* narrowed the binding site between ATG13 and FIP200 to 4 residues (LQFL) (Cheong *et al.*, 2005; Jung *et al.*, 2009; Alers *et al.*, 2011; Chen *et al.*, 2016).

ATG101 interacts with ATG13 but not ULK1 and FIP200 (Hosokawa *et al.*, 2009). It is proposed to have other potential interactors more downstream the autophagy pathway (like DFCP1, LC3 - Qi *et al.*, 2015-; or ATG14 -Kim *et al.*, 2018). ATG101 has no similarity to other ATG proteins and is not found in *S. cerevisiae*, *L. thermotolerans,* and *E. gossypii* (Hosokawa *et al.*, 2009; Qi *et al.*, 2015). One of the hypotheses is that ATG101 has been lost during evolution (Qi *et al.*, 2015; Almutairi, 2018; Yajie Gu *et al.*, 2022). The role of ATG101 has yet not been clarified. Might exert the role of stabilizing the expression of ATG13, while protecting it from proteasomal degradation (Qi *et al.*, 2015; Mercer, Kaliappan and Dennis, 2009).

1.4 Potential interactors of ATG13 and ATG101

1.4.1 ATG9

Figure 1.2

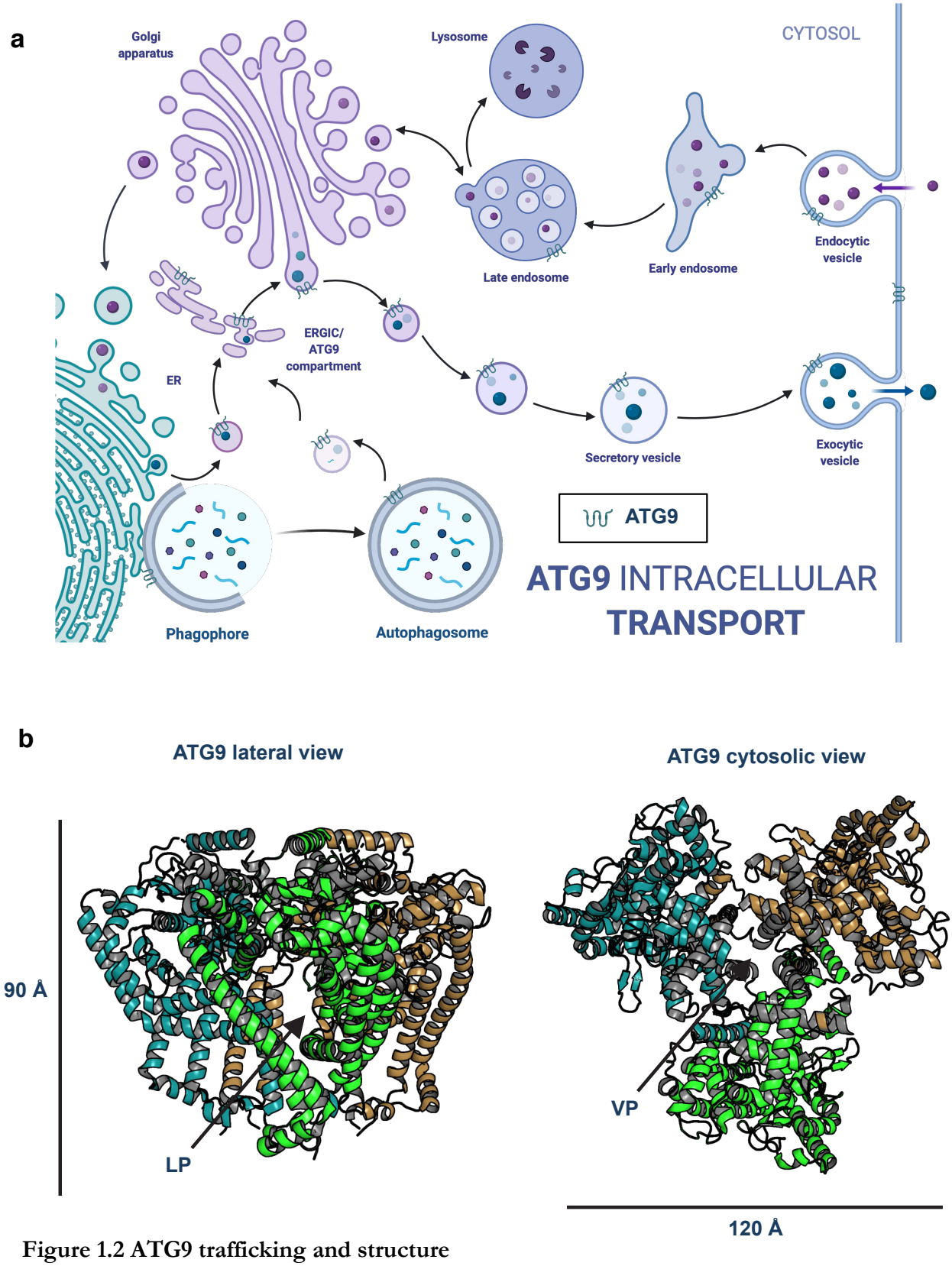

Figure 1.2 ATG9 trafficking and structure

(a) schematic representation of ATG9 trafficking within all the cell compartments. This image was created with BioRender; **(b)** structure of ATG9 (43-587) with the lateral view (first panel) and cytosolic view (second panel) and (PDB: 7JLQ).

ATG9 has been proposed as one of the direct potential interactors of ATG13 (S. W. Suzuki *et al.*, 2015b; Kannangara *et al.*, 2021) both in yeast and mammals. However, no direct interaction has been proved so far. ATG9 was identified in yeast by Ohsumi's labs (Noda *et al.*, 2000) and Thumm's lab (Lang *et al.*, 2000). ATG9 is a highly dynamic integral membrane protein (Yamamoto *et al.*, 2012). In yeast is localized to the PAS and can travel to the mitochondria (Reggiori *et al.*, 2004) through vesicles of 30-60 nm radius (Yamamoto *et al.*, 2012). ATG9 vesicles shuttle between the trans-Golgi network (TGN) and the 'ATG9 compartment' (tubular vesicular compartment in the neighborhood of the Golgi also known as ERGIC) (Orsi *et al.*, 2012). ATG9 vesicles also shuttle back and forth from the plasma membrane (Moreau and Rubinsztein, 2012; Zhou *et al.*, 2017) and endosomes (Young *et al.*, 2006) (Figure 1.2a). SRC kinase (fed conditions) and ULK1 (starving conditions) (Papinski *et al.*, 2014) phosphorylate $ATG9^{N}$ to control its trafficking (Zhou *et al.*, 2017). The fact that ULK1 phosphorylates ATG9 and is in complex with ATG13-ATG101 during starvation-induced autophagy correlates with ATG9 and ATG13-ATG101 being part of a stable complex, at least temporarily, during autophagy induction. In support of this, it is known that ATG9 trafficking is inhibited when ULK1 and ATG13 are knocked out (Young *et al.*, 2006; Chen *et al.*, 2016; Zhou *et al.*, 2017). Karanasios *et al.* observed that during autophagy induction ~85% of the ATG13 positive autophagy puncta were colocalizing together with the ATG9 positive structures (Karanasios *et al.*, 2013, 2016). It also seems that, at least in yeast, Atg13 interaction (direct or indirect) is enhanced by starvation-induced autophagy (S. W. Suzuki *et al.*, 2015b) and Atg9 recruitment to the PAS is dependent on Atg13 (Reggiori *et al.*, 2004).

The autophagic membrane is created *de novo* upon autophagy induction (Noda, Suzuki, and Ohsumi, 2002). ATG9 vesicles can fuse with the outer membrane of the phagophore, providing, at least partially, lipids for the autophagic membrane to grow (Yamamoto *et al.*, 2012; S. W. Suzuki *et al.*, 2015b; Rao *et al.*, 2016b; Noda, 2017; Sawa-Makarska *et al.*, 2020). Indeed, Trs85 and other components essential for fusing to the nascent autophagosome are found in these vesicles(Kakuta *et al.*, 2012). Autophagosomes have an average diameter of 500 nm (Baba *et al.*, 1994) and because the quantity of phospholipids imported by ATG9 trafficking vesicles is expected to be inadequate to manufacture autophagosomes, it is thought that a major part of the phospholipids that make up autophagosomes come from membrane sources other than Atg9 vesicles. Indeed, Hayashi-Nishino and colleagues show that ER composes roughly 70% of the omegasome in mammals (Hayashi-

Nishino *et al.*, 2009). Upon its arrival to the nascent omegasome, ATG9 exerts the important role of maintaining the equilibrium between the two leaflets of the growing phagophore. ATG9 is a scramblase and its active unite is a trimer. Its transmembrane helices and its lipid transfer activity have been recently characterized in both yeast and human (Guardia, Tan, *et al.*,2020; Maeda *et al.*, 2020; Matoba *et al.*, 2020). All the structures published until now show only the core of the trimer. The N-terminus (1-43) and C-terminus (587-839) of ATG9 are predicted to be almost completely unstructured (Figure 1.2b). ATG9 structure shows two distinctive pores that the authors termed 'LP' (lateral, that lies laterally to the cytoplasmic leaflet nearby the adjacent protomer) and 'VP' (at the trimer center and therefore traverses the membrane vertically) that make up for the unicity of this scramblase compared to translocase/scramblases proteins (Brunner, Schenck and Dutzler, 2016; Nagata, Sakuragi, and Segawa, 2020 (Figure 1.2b). The mechanism of lipid transportation between the two leaflets is still unknown, although these holes are critical for lipid translocation.

Under autophagy-inducing starvation, knocking down ATG9 reduced ATG13 and WIPI2 puncta concurrently by ~50% (Karanasios *et al.*, 2016) and ATG9 colocalizes with both early and late autophagy components (Orsi *et al.*, 2012; Karanasios *et al.*, 2016). ATG9 probably directly interacts with ATG2 (Gómez-Sánchez *et al.*, 2018b), also co-localizes with it in the area between the ER and the IM (Valverde *et al.*, 2019). ATG2 has a ~20 nm long rod-shaped structure and it is long enough to bridge the two compartments (Hayashi-Nishino *et al.*, 2009). It is not surprising that ATG2 theaters liposomes without inducing their fusion (Chowdhury *et al.*, 2017; Maeda, Otomo, and Otomo, 2019) and it also has a lipid transferase activity (Obara *et al.*, 2008; Chowdhury *et al.*, 2018; Gómez-Sánchez *et al.*, 2018b; Osawa and Noda, 2019; Otomo and Maeda, 2019; Osawa, Ishii and Noda, 2020; Noda, 2021) that is enhanced by WIPIs (Osawa, Ishii, and Noda, 2020). Since all these components seem to colocalize at the ER contact site at the same time, is possible that they combine their effort in promoting the autophagosome formation. ATG9-ATG2-WIPI4 might form a single complex where ATG2 transfer lipids from ER to omegasome, while ATG9 maintains the equilibrium between the outer and the inner leaflet by flipping lipids within the omegasome membrane (Guardia, Christenson, *et al.*, 2020; Guardia, Tan, *et al.*, 2020; Maeda *et al.*, 2020; Matoba *et al.*, 2020). If the ATG13 role is only to bind and recruit ATG9 to the omegasome, it is not clear why it would reside there longer than the necessary time to deliver ATG9.

1.4.2 ATG14

WIPIs are PI3P and PI3,5P2 sensors and fold into a seven-bladed β-propeller. WIPIs (WD-40 repeat-containing PI-interacting protein) are mammals PROPPINs (Proikas-Cezanne *et al.*, 2004; Thumm M & Kühnel K, 2012). WIPI1 and WIPI2 are orthologs of Atg18, WIPI3 and WIPI4 are relatives of Hsv2b (Krick *et al.*, 2012; Bueno-Arribas *et al.*, 2021). WIPI3 and WIPI4 are redundant for elongation (Bakula *et al.*, 2017) while WIPI1 is the least characterized, but it might be involved in the recruitment of the lipidation machinery together with WIPI2 (Proikas-Cezanne *et al.*, 2004; Polson *et al.*, 2010; Liang *et al.*, 2019). ATG2-WIPI4 complex tether PI3P-positive vesicles *in vitro* (Chowdhury *et al.*, 2018; Otomo, Chowdhury and Lander, 2018; Osawa, Ishii and Noda, 2020) and interact with PI3P also at the nascent autophagosome (Bakula *et al.*, 2017).

PI phosphorylation into PI3P is deposited by the ATG14-containing PI3KC1(Obara and Ohsumi, 2011). Therefore, it is not surprising that ATG14 has also been proposed as a direct interactor of ATG13 (Jao *et al.*, 2013b; Park *et al.*, 2016) and of ATG101 (Kim *et al.*, 2018). Jao et al., propose that the Atg13 HORMA domain is essential for autophagy and the recruitment of the Atg14 to the autophagosomal structure, but it is not necessary Atg13 recruitment (Jao *et al.*, 2013b. Park et al., identified the potential interactor region within ATG14 (the coiled-coil region) (Park *et al.*, 2016). Another Korean group proposes that also the C-terminus of ATG101 is an interactor of ATG14 (Kim *et al.*, 2018).

1.5 HORMA domains proteins

ATG13 and ATG101 are the only HORMA domain proteins in the autophagy pathway (Hosokawa *et al.*, 2009; Mercer, Kaliappan and Dennis, 2009; Jao *et al.*, 2013; H. Suzuki *et al.*, 2015; Qi *et al.*, 2015; Noda and Mizushima, 2016). They could not be identified by the sequence alignment that Aravind and Koonin carried out at the end of the 90s (Aravind and Koonin, 1998). HORMA domain proteins (from Hop1, Rev7, and Mad2) are present in both eukaryotes and bacteria (Almutairi, 2018) and share the same fold. It took almost 15 years after Aravind and Koonin discovery to classify as HORMA domain proteins also p31^{comet}, ATG13, and ATG101 as well (Yang *et al.*, 2007; Hosokawa, Sasaki, *et al.*, 2009; Mercer, Kaliappan and Dennis, 2009; Jao *et al.*, 2013a; Hegedus *et al.*, 2014).

HORMA domain structure determinates certain specific features (Ye Gu *et al.,* 2021*,* Rosemberg and Corbett., 2015):

1) They are all regulatory proteins of survival and quality control mechanisms. In eukaryotes, HORMA is involved in autophagy, DNA damage response, mitosis, meiotic control. Whereas in prokaryotes, it's involved in antiviral immunity.
2) The globular core of the protein (length ~200 residues) is composed of three main α-helices (αA, αB, and αC) and a three-stranded β-sheets (β4, β5, and β6). The N-terminus and the C-terminus are usually regulatory regions. Inside the C-terminus, we can identify a flexible region, known as the 'seatbelt' or 'safety belt' involved in interacting with secondary binding partners (BP) with an internal motif. The C-terminal tail can pack against the HORMA domain core in two distinct ways, resulting in open (O) or closed (C) conformation. The seatbelt folds into two strands (β7 and β8) that stretch over one side of the core in the O condition. The safety belt wraps completely around the domain in the C state, forming two additional strands (β8' and β8") against the opposing side of the HORMA domain core.
3) Each HORMA recognizes its own preferred motif inside a BP. The BP internal motif is usually localized inside a flexible unstructured region of the BP itself. The binding motif, other than the safety belt, also interacts with part of the core of the HORMA (usually one of the β-sheet). The overall unicity aspect of this interaction is that the whole C-terminus of the HORMA wraps around the BP like a seatbelt and associates with the other side of the HORMA core. To make this happen, however, the N-terminus need to be displaced from the location prior to the arrival of the C-terminus docking. All this mechanism requires a partial unfolding and refolding of both N-terminus and C-terminus. This also indicates a huge energy expenditure which creates a kinetics bottleneck inside the pathway where the HORMA proteins are involved. Usually, the O-HORMA is the 'inactive' HORMA (meaning no BP and N-terminus still docked at the β5), while the (C) is usually the 'active' (meaning BP wrapped, N-terminus disembarked, and C-terminus docked on the β5 side).
4) The interaction that is created after this is usually so strong that requires an AAA+ ATPase to be remodeled.
5) The dimerization between two HORMAs is also an essential feature. They can form both homo- and heterodimers. Usually, homo-dimerization is involved in assembly mechanisms, while hetero-dimers are part of the disassembly. Dimerization is localized in the so-called 'dimerization interface' composed by two HORMA facing each other (and inverted) through their α-helix αC and the β2-β3 hairpin (a pair of β strands at the back of the protein). The dimerization is an essential part of the acceleration for the O

to C conversion (see the following section for more details) and it is usually limited to opposite conformers, at least for assembly mechanisms (DeAntoni *et al.*, 2005).

It's important to notice that HORMAs are not the only protein able to switch folds. A polypeptide chain with a given amino acid sequence can have only a single native form that is most thermodynamically stable (monomorphic), however, to be more precise, the native form of a protein is the one in which the "Gibbs free energy of the whole system is the lowest"(Anfinsen, 1973). Therefore, if a protein has two or more states (metamorphic) where the Gibbs free energy is at its lowest, the protein can undergo topological changes to convert from one to another.

Similar to HORMAs, some proteins can undergo significant changes in their secondary structure that involve unfolding and refolding on the core of the protein itself. These major changes can reveal new interacting surfaces while determining two or multiple states of the same protein. Lymphotactin, Chloride intracellular channel 1 (CLIC1) protein, PimA (a bacterial glycosyltransferase), the β-pore-forming lysenin, TRAP1N, human calcineurin, amilyn are all different examples of this protein with a propensity for switching their topology (Bryan and Orban, 2010; Kim and Porter, 2021).

The conformational change of the transition-prone proteins has distinctive requirements:

1) The protein has to undergo states of decreased stability so that alternate folds may become more accessible;
2) There have to be flexible regions that undergo secondary structural change between one conformer and the other;
3) The alternate fold has to have a functional value. Usually, the new conformation reveals a new binding surface for protein interactions that favours stabilization of the new state as well.

Figure 1.3

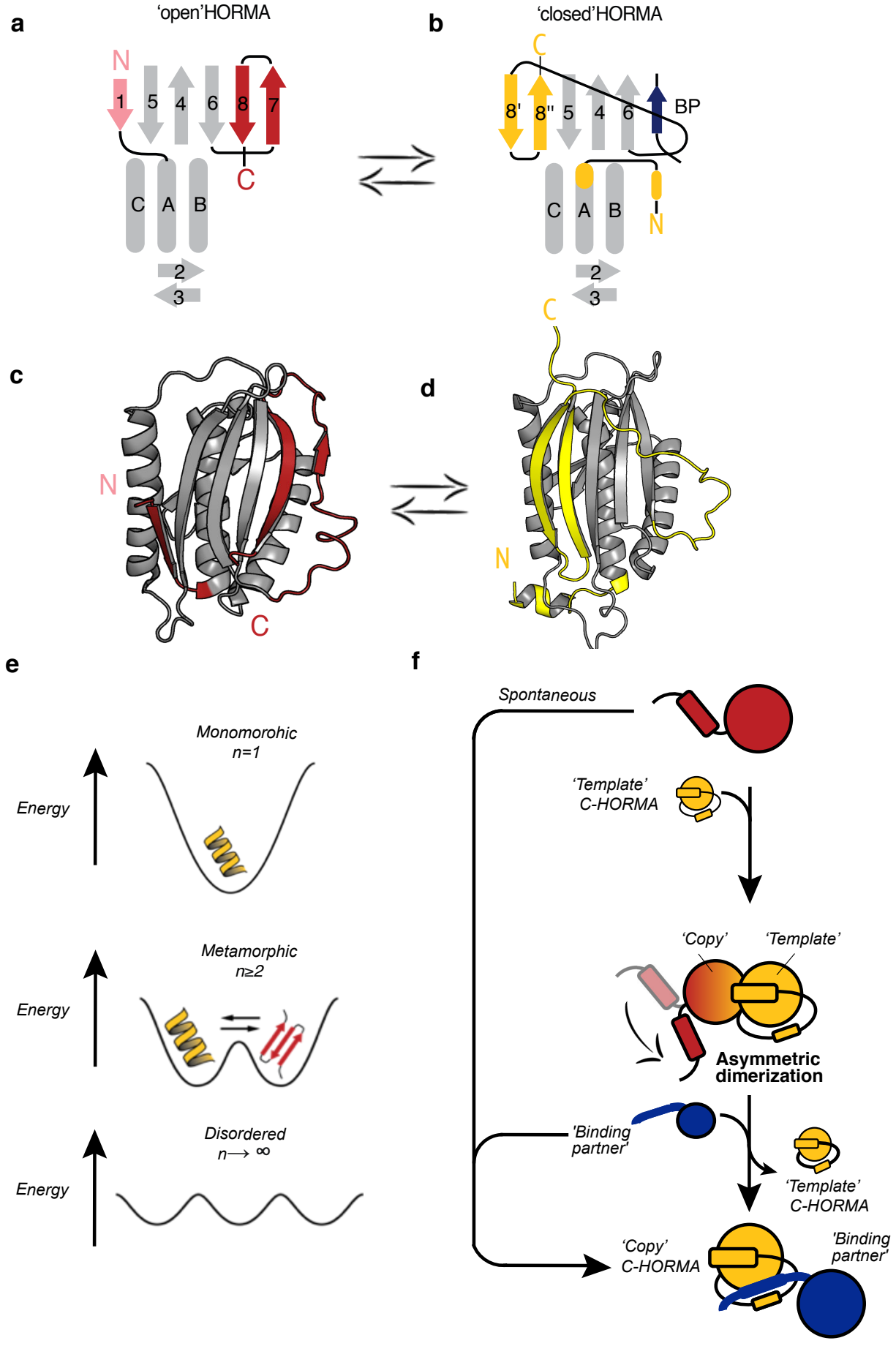
a
'open'HORMA
N
1
5
4
6
8
7
C
C
A
B
2
3
b
'closed'HORMA
C
8'
8''
5
4
6
BP
C
A
B
N
2
3
c
N
C
d
C
N
e
Monomorohic
n=1
Energy
Metamorphic
n≥2
Energy
Disordered
n⟶ ∞
Energy
f
Spontaneous
'Template'
C-HORMA
'Copy'
'Template'
Asymmetric
dimerization
'Binding
partner'
'Template'
C-HORMA
'Copy'
C-HORMA
'Binding
partner'

Figure 1.3 HORMA domain proteins are metamorphic proteins

(a) schematic representation of the open (O) conformation of a HORMA (MAD2); **(b)** schematic representation of the closed (C) conformation of a HORMA (MAD2); **(c)** published structure of O-MAD2 and **(d)** C-MAD2 from Mapelli *et al.* 2007 PDB:2V64; **(e)** schematic representation of different energy-dependent secondary folding states of proteins; **(f)** schematic representation of the 'template model' described in section 1.5.1.

1.5.1 MAD2

MAD2 is the most studied HORMA. Therefore, most of the generic features of HORMAs have been extrapolated from studies on this SAC (Spindle assembly checkpoint) protein.

MAD2 and many other SAC proteins co-localize to kinetochores, the scaffold dedicated to the capture of spindle microtubules during mitosis (DeAntoni *et al.*, 2005; Mapelli *et al.*, 2007; Musacchio and Salmon, 2007).The SAC proteins monitor the establishment of proper kinetochore-microtubule attachments at kinetochores and are essential for chromosomal alignment at the metaphase plate, as well as for sister chromatid separation at anaphase(Maiato *et al.*, 2004; Garcia *et al.*, 2021). SAC proteins prevent chromosomal segregation problems induced by premature mitotic exit by forming the MCC (mitotic checkpoint complex) that inhibits APC (anaphase-promoting complex).

The MCC comprises MAD2, CDC20, BUBR1, and BUB3. MAD2 interaction with the CDC20 binding motif (MIM) is the rate-limiting step in MCC assembly, and unattached kinetochores dramatically speed up MAD2–CDC20 binding (Faesen *et al.*, 2017). When CDC20 is sequestered by a C-MAD2, it cannot activate the APC for the mitosis exit (Musacchio and Salmon, 2007).

To understand the mechanism through which MAD2 forms a complex with CDC20, we need to consider 'the template model' (DeAntoni *et al.*, 2005): two O-MAD2s are recruited by a homo-dimer of MAD1 protein and form a tetramer through the MAD1-binding motif that is very similar to a MIM (to an extent that, few studies used a hybrid of the two sequences and termed it 'MBP1', from MAD2-binding peptide) (Sironi *et al.*, 2002b). On one side of the tetramer, the MAD1–C-MAD2 complex (MAD1-C-MAD2, the 'template') binds to soluble O-MAD2, forming an 'asymmetric' dimer through the interaction interface shared by the two HORMA domain proteins. This MAD1–C-MAD2 primes the O-MAD2 protomer for an intermediate state known as 'unbuckled' for the BP (CDC20) closure motif binding by accelerating the conversion of the O-MAD2 to a C-MAD2 (Sironi *et al.*, 2002; de Antoni *et al.*, 2005; DeAntoni *et al.*, 2005; Yang *et al.*,

2008; Hara *et al.*, 2015; Lara-Gonzalez *et al.*, 2021; Piano *et al.*, 2021) (Figure 1.3f).The C-MAD2–CDC20 complex then separates from the MAD1–C-MAD2 core complex (Luo and Yu, 2008). MAD2 can dimerize as O-C or C-C/I, however this second is less stable than the O-C (Yang *et al.*, 2008; Hara *et al.*, 2015).

MAD2 asymmetric dimerization regulates the speed of the O-MAD2 to C-MAD2 conversion. O-MAD2 can spontaneously convert to C-MAD2 with slow kinetics because of the huge energy barrier separating the two conformational states(Luo *et al.*, 2004; Mapelli *et al.*, 2007; Simonetta *et al.*, 2009). O-MAD2, the β1 disembarks from β5, treads through the β5-αC loop, and also forms a new turn nearby αA. If this doesn't happen, the C-terminal region of β7, β8, and the rest of the flexible C-terminal that disengage from β6, rearrange into a hairpin, but can't dock at the β5(Lou *et al.*, 2000; Sironi *et al.*, 2002b; Mapelli *et al.*, 2007; Luo and Yu, 2008). Therefore, the dissociation of the N-terminus from the core and its passage through the loop is the rate-limiting factor in the conversion of O-MAD2 to C-MAD2 (Yang *et al.*, 2007b). In support of this hypothesis, the 'loopless' MAD2 ($MAD2^{LL}$) mutant, designed by Mapelli *et al.*, has a shorter the β5-αC loop and tends to adopt the O conformation (Mapelli *et al.*, 2007). For the folding and structure of MAD2 see Figure 1.5a and b.

It has been predicted by the 'template model' that O-MAD2 converts first into an unbound-C/I-MAD2, which then quickly binds the $CDC20^{MIM}$ (Luo and Yu, 2008; Yang *et al.*, 2008). However, recently, Valentina Piano and colleagues discovered that unbound C-MAD2 did not interact at an appreciable rate to $CDC20^{FL}$. Only with $CDC20^{MIM}$ an unbound-C-MAD2 could interact. $CDC20^{FL}$ does not tread into I/C-MAD2, therefore, CDC20 has to be there before the closure (Piano *et al.*, 2021). She also proved that CDC20 favors its own inclusion in the MCC complex by having additional interactions with MAD1 and BUB1 and accelerates of ~35-fold the MCC assembly (Piano *et al.*, 2021).

1.5.2 $p31^{comet}$ and PCH2/TRIP13

The interaction between CDC20 and MAD2 is strong: MAD2 has a 10-fold greater affinity for the CDC20 motif (K_D =~10^{-7} M) than Mad1 (K_D = ~10^{-6} M) (Luo *et al.*, 2002; Sironi *et al.*, 2002b; Faesen *et al.*, 2017). Even in absence of MAD1, MAD2 can interact with CDC20 and convert spontaneously from O to C. The disassembly of the complex is also spontaneous but it is catalysed by AAA+ PACH2/TRIP13 and an adaptor protein $p31^{comet}$ to disassemble(Yang *et al.*, 2007b; Westhorpe *et al.*, 2011; Ye *et al.*, 2015).

ATP hydrolysis causes synchronized conformational changes inside the homo-hexameric ring-shaped TRIP13, which then pulls substrate proteins through its central pore, causing partial

unfolding of the substrate (Sauer and Baker, 2011). The N-terminus of CDC20-bound C-MAD2 is TRIP13's substrate (Miniowitz-Shemtov *et al.*, 2015; Ye *et al.*, 2015; Brulotte *et al.*, 2017; Alfieri, Chang and Barford, 2018). p31^{comet} takes part in MAD2-CDC20 disassembly by dimerizing with a CDC20-C-MAD2 using the same interaction interface of the MAD2-MAD2 dimer (Mapelli *et al.*, 2006; Yang *et al.*, 2007; Westhorpe *et al.*, 2011). p31^{comet} is a peculiar HORMA that appears to be closed on itself. p31^{comet} N-terminus, however, docks on the side of protein and it doesn't tread through the loop, like in MAD2. Therefore, it appears both open and closed at the same time (no conformational change has been seen so far) (Yang *et al.*, 2007b). p31^{comet}, other than binding to a CDC20-C-MAD2 and bridging it to TRIP13.

In the last 10 years, the discovery of bacterial HORMAs inside operons that also contain a TRIP13 ortholog and are associated with bacteriophage immunity, lead to the hypothesis that the HORMA-TRIP13 module has its origin from a prokaryotic survival mechanism (Burroughs *et al.*, 2015; Tromer *et al.*, 2019; Ye *et al.*, 2020). Therefore, the fact that MAD2 is not the only HORMA that p31^{comet}-TRIP13 might disassemble from their BP is not that far-fetched (Sarangi *et al.*, no date; Clairmont *et al.*, 2020; Sarangi, Clairmont and D'Andrea, 2020; de Krijger, Boersma and Jacobs, 2021; de Krijger *et al.*, 2021).

Figure 1.4

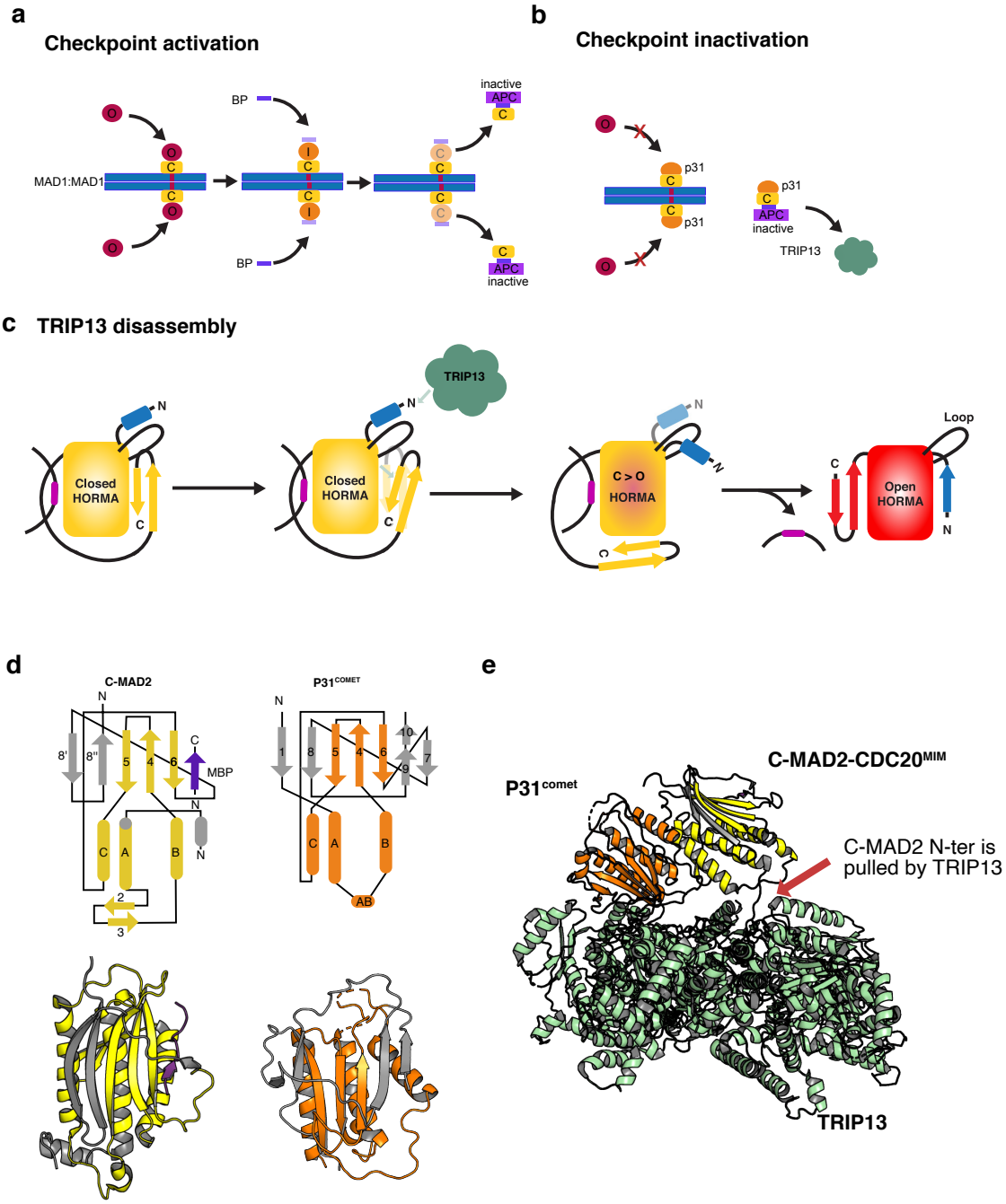

Figure 1.4 TRIP13-p31comet mediated disassembly of C-MAD2

(a) schematic representation of the checkpoint activation; **(b)** schematic representation of the checkpoint inactivation; **(c)** schematic representation of the TRIP13-mediated disassembly; **(d)** schematic representation of p31^{comet} and C-MAD2 folding and comparison of structures of p31^{comet} (PDB: 2QYF, Tomchick *et al.,* 2007) and C-MAD2 (PDB: 2V64); **(e)** Structure of TRIP13-C-MAD2- p31^{comet} (PDB: 6F0X, Alfieri *et al.,* 2018). Panels (a) (b) and (c) were adapted from Yang *et al.*, 2007 and Yajie Gu *et al.,* 2022.

1.5.3 REV 7

Figure 1.5

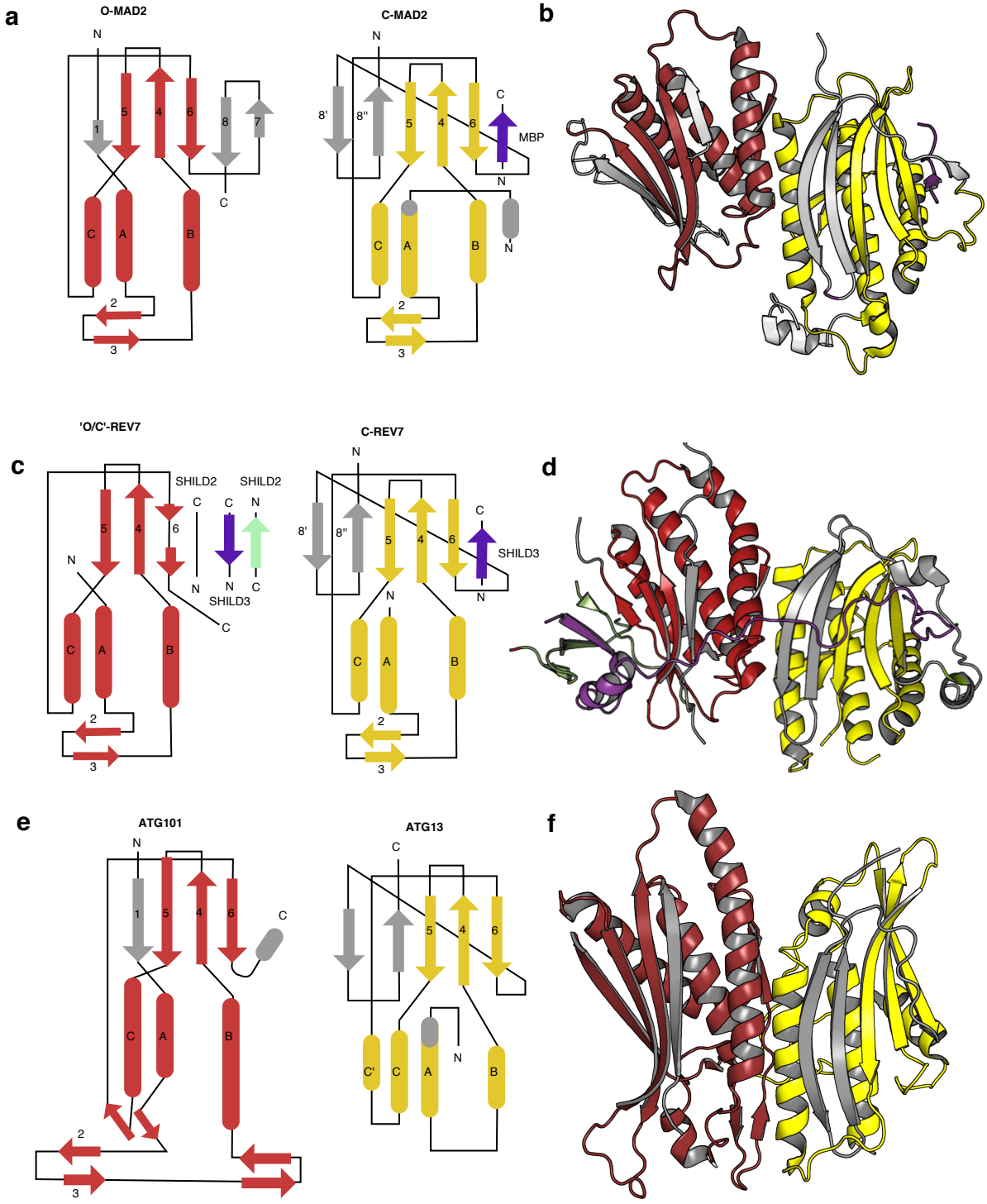

Figure 1.5 HORMAs comparison

(a) schematic representation of the folding of C-MAD2 and O-MAD2; **(b)** dimer structure of C-MAD2 and O-MAD2 (PDB: 2V64); **(a)** schematic representation of the folding of C-REV7 and O-REV7; **(b)** dimer structure of C-REV7 and O-REV7 (PDB: 6KTO); **(a)** schematic representation of the folding of ATG101 and ATG13; **(b)** dimer structure of ATG101 and ATG13 (PDB: 5C50)

REV7 is the most similar to MAD2 within the overall HORMA panorama(Hanafusa *et al.*, 2010; de Krijger, Boersma and Jacobs, 2021). It was identified in yeast by three different groups (Lemontt, 1971; Lawrence, Das, and Christensen, 1985; Torpey *et al.*, 1994), but only during the last 20 years has been possible to determine how REV7 is involved in numerous pathways: mitotic progression (Chen and Fang, 2001; Pfleger *et al.*, 2001)and translesion synthesis(Lawrence, 2002), and is also a key component of the recently discovered Shieldin complex(Boersma *et al.*, 2015; Xu *et al.*, 2015; Gubta *et al.*, 2018; Noordermeer *et al.*, 2018; Setiaputra and Durocher, 2019), which is involved in DNA double-strand break (DSB) repair.

REV7, like MAD2, homo-dimerizes, and also hetero-dimerizes with both p31comet and MAD2 (Murakumo *et al.*, 2000; Rosemberg and Corbett., 2015; Rizzo *et al.*, 2018). It contains a classical 'seatbelt' that can directly recognize the REV7 binding motif (φφxPxxxpP, φ is an aliphatic residue) on BPs(Hanafusa *et al.*, 2010; Tomida *et al.*, 2015). The RMB mostly differs from the MIM but has a very well conserved proline on the last residue (Sironi *et al.*, 2002b; Luo *et al.*, 2002).

REV7 binding partners family include REV3 and SHLD3, the chromosome alignment-maintaining phosphoprotein (CAMP), the small GTPase RAN, ELK1, ADAM9, and IpaB (Hara *et al.*, 2009; Hanafusa *et al.*, 2010; Ghezraoui *et al.*, 2018; Gupta *et al.*, 2018; Noordermeer *et al.*, 2018; Wang *et al.*, 2019). MAD2, interestingly, doesn't have this wide range of interactors from so many different pathways (CDC20, MAD1, Cdh1, SGO2) (Sironi *et al.*, 2002b; Orth *et al.*, 2011).

In higher eukaryotes, REV7 is part of the Shieldin complex, which is recruited to DSB to inhibit resection of damaged DNA, reducing homologous recombination (HR) repair and boosting no homologous end joining (NHEJ). In this context, REV7 forms an unusual asymmetric homo-dimer bridging SHLD3 (a recruitment subunit) and SHLD2 (the DNA-binding subunit). The 'O'-REV7 in this context assumes a non-canonical conformation stabilized by SHLD2 and SHLD3 (Ghezraoui *et al.*, 2018; Liang *et al.*, 2020). In particular, in Liang's structure, one of the two REV7 uses the canonical seatbelt closure with the RBM2 within SHLD3, while the other 'O'-REV7, interact with SHLD2 using its β5, which is rather unusual. In MAD2 and in the other REV7, β5 is used for docking the C-terminus in the C conformation while, in this case, is forming a 'sandwich' with RBM1 of SHLD2 and with SHLD3 (Liang *et al.*, 2020). This second REV7 is classified as 'open' even though its C-terminus is still docked in β6, like in C-REV7 and C-MAD2. This

divergent REV creates a precedent where a HORMA is interacting with a BP without any seatbelt direct involvement. For the folding and structure of REV7 see Figure 1.5c and d.

Important new steps in the field are being made to try to understand the kinetics of REV7-SHLD3-SHLD2 complex formation and disassembly mediated by TRIP13-p31^{comet} (Sarangi *et al.*, 2020; Clairmont *et al.*, 2020; Dai *et al.*, 2020; Sarangi, Clairmont, and D'Andrea, 2020; de Krijger *et al.*, 2021; Vivek Susvirkar and Bastian Föhr, unpublished data). MAD2 represents the main model of study, however, it is clear that HORMA domain proteins diverged under different evolutionary pressures to exert different roles in different pathways. Therefore, even if some features might be conserved, each HORMA has to be studied in the context of its own pathway.

1.5.4 HORMAD 1 and HORMAD2

HORMA domain-containing proteins (HORMADs) are essential for meiotic interhomolog recombination. Crossover events are governed by the 'chromosomal axis', which includes also the meiotic HORMADs. They are found throughout the whole length of chromosomes and stimulate Spo11- mediated DSB in DNA (Rosemberg and Corbett., 2015).

HORMAD1 and HORMAD2 are recruited by different methods in mammals and do appear to have different roles, with HORMAD1 binding directly to meiotic cohesin complexes and HORMAD2 attaching to the axis core protein SYCP2 (Wojtasz *et al.*, 2009; Fujiwara *et al.*, 2020). Hop1 (*S. pombe* and *cerevisiae*) is the most studied member of the meiotic HORMAD protein family, which also includes ASY1/2 from *A. thaliana*, and *C. elegans* HIM-3/HTP-1/-2/-3 (Hollingsworth, Goetsch and Byers, 1990; Caryl *et al.*, 2000; Lorenz *et al.*, 2004; Martinez-Perez and Villeneuve, 2005; Wojtasz *et al.*, 2009). Differently from other HORMAs, HORMADs and their other family components seem not to be able to dimerize. However, they encode of a 'self-closure' motif within the C-terminus (Kim *et al.*, 2014). It seems that this 'inactive' form of HORMAD is likely converted to an 'active' HORMAD by the TRIP13, allowing for the HORMAD recruitment at the chromosome axis. This is typical of HORMADs from plants (Herruzo *et al.*, 2021). In higher organisms, TRIP13 seems to be involved in later stages of miosis to remove HORMADs from the chromosomal axis (Li and Schimenti, 2007; Wojtasz *et al.*, 2009). *C. elegans* has the best-characterized closure motifs among the HORMADs. This comprises of conserved residues like a tyrosine and a glycine that mainly hidden by the safety belt wrapping over the closure motif, similarly to REV7 and MAD2 BM (Kim *et al.*, 2014).

The p31^{comet} remains one of the more unclear aspects of HORMADs, since its involvement has always been observed in plants ASY1 PCH2-dependent remodeling (Balboni *et al.*, 2020) and

there are evidences of examples like Hop1 who can bind TRIP13 (Pch2) directly (West, Komives and Corbett, 2018; Raina *et al.*, 2020).

1.5.5 Bacterial HORMAs

A family of enzymes related to cyclic GMP–AMP synthase (cGAS), a mammalian innate-immune sensor, was discovered in a 2015 study by Arvind (Burroughs *et al.*, 2015). HORMA-like proteins were discovered within the same operon. Bacteria like *E.coli* or *P.aeruginosa* employ HORMA-like proteins (HORMA 1/2/3) to detect particular peptides part of the array of proteins from bacteriophages employing the classical C-HORMA-BP system. This complex then binds and activates a cGAS/DncV-like nucleotidyltransferase (CD-NTase) to form cyclic di- or triadenylate (cAA or cAAA) second messenger.This creates a cascade of events were an endonuclease effector is activated and leads to cells death to stop viral replication. A homolog of the Pch2/TRIP13, which binds and disassembles the active HORMA-CD-NTase complex, reduces this signaling. Along with the cGAS-related enzyme and effector protein, around 10% of CBASS (cyclic oligonucleotide-based anti-phage signaling system) operons encode one or two HORMA proteins and a TRIP13-like ATPase, as discussed above. These operons are classified by the numbers of HORMA-like protein they encode within themselves. HORMAs in eukaryotes likely derive from the class that contains two (like in *P. aeruginosa*) (Ye *et al,* 2020).

Figure 1.6

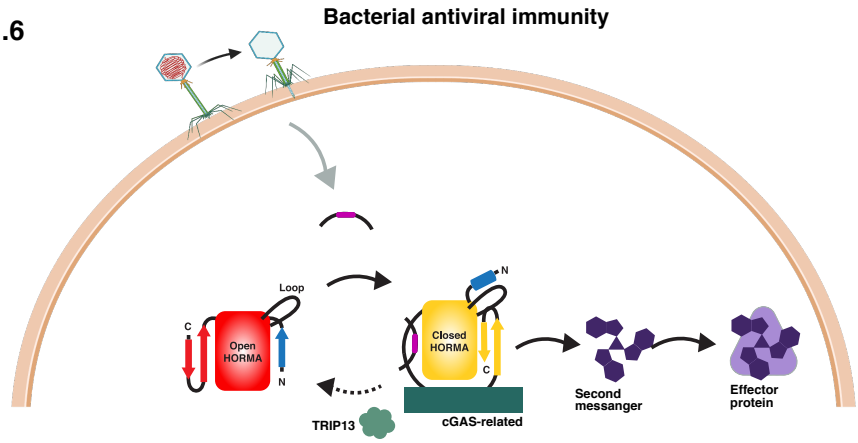

Figure 1.6 Bacterial antiviral immunity

Schematic representation of the bacterial HORMA-like dependent response. Adapted from Ye et al, 2020. Adapted with BioRender.

1.5.6 ATG101 and ATG13

In ATG101 structure, the N-terminal segment localizes between β5 and αC, while the C-terminal residues dock at the opposite side of the β-sheet β6, indicating that, conformationally, ATG101 corresponds to the O-MAD2. Regardless, there are a few notable variances: ATG101 N-terminus is substantially longer than O-MAD2 N-terminus. As a result, mobilizing this section of the molecular would need substantially more energy than MAD2 (Mercer, Kaliappan and Dennis, 2009; Qi *et al.*, 2015). ATG101 C-terminus, instead, shows a different folding in different structures: it can be found docked at the β6 or floating creating an unusual small αhelix (H. Suzuki *et al.*, 2015b; Michel *et al.*, 2015; Kim *et al.*, 2018). The other unique feature of ATG101 is that it presents three additional regions (called 'ext1', 'ext2', and 'ext3') compared to the canonical HORMAs (Michel *et al.*, 2015). 'ext1' is a WF finger motif (H. Suzuki *et al.*, 2015b; Qi *et al.*, 2015; Kim *et al.*, 2018). The WF was presented as an important interactor element by both Hurley group (in human) and the Japanese groups Noda and Mizushima (in *S. pombe*). Mutating these residues affected downstream elements like WIPI1, DFPC1, and LC3 localization in *S. pombe*, and LC3 flux in humans without affecting the recruitment of ATG14. The only interaction known for ATG101 is the one formed with ATG13 (Hosokawa, Sasaki, *et al.*, 2009; Mercer, Kaliappan and Dennis, 2009; H. Suzuki *et al.*, 2015b; Qi *et al.*, 2015). Homo-dimerization of ATG101 seems also a possibility (Hegedus *et al.*, 2014; Michel *et al.*, 2015).

ATG13 folding is canonical, and it resembles the C-MAD2 (Jao *et al.*, 2013c; H. Suzuki *et al.*, 2015b; Qi *et al.*, 2015). We described already how the (homo- or hetero-) dimerization is a frequent trait and it's a marker of a possible catalyzed reaction. ATG13 and ATG101 dimerize with the canonical head-to-head interaction interface involving the same αC and the β2-β3 connector of MAD2 (H. Suzuki *et al.*, 2015b; Qi *et al.*, 2015). The structure of human ATG13 has only been published with ATG101, while Atg13 from *L. thermotolerans* could be crystallized in isolation (Atg101 is absent in most yeast strains). In yeast, Atg13 might also be homo-dimerizing, however, Jao *et al.* did not report any information regarding this aspect. In yeast Atg13 there is also an electropositive groove within the core structure and a phosphate sensor that are not conserved in human ATG13 (Jao *et al.*, 2013c; Qi *et al.*, 2015). For the folding and structure of ATG13 and ATG101 see Figure 1.5e and f.

ATG13-ATG101 is described as a constitutive dimer. Qi et al and Suzuki et al report that, given the structural features of the N-terminus and the C-terminus of ATG13 and ATG101, these are unlucky to convert topology like MAD2 (Suzuki *et al.*, 2015b; Qi *et al.*, 2015). They describe how the N-terminus of ATG101 is too long to be able to disengage without an extensive energy expenditure and that the ATG13 C-terminus might be pinned to the structure and not dislocate from β5. Also, the seatbelt appears too short to be able to embrace any binding partner. In

correlation to this, TRIP13/p31^{comet} involvement is unknown in the context of Autophagy. However, VCP/p97 is also a +AAA ATPase and is involved in Autophagy and it might have overtaken the role of TRIP13 but no study has addressed it so far (Hill *et al.*, 2021). Indeed, the lack of proper biochemical characterization regarding the potential interactors has impaired the possibility to unravel the impact of the HORMA folding within the context of autophagy.

1.6 Thesis outline and aims

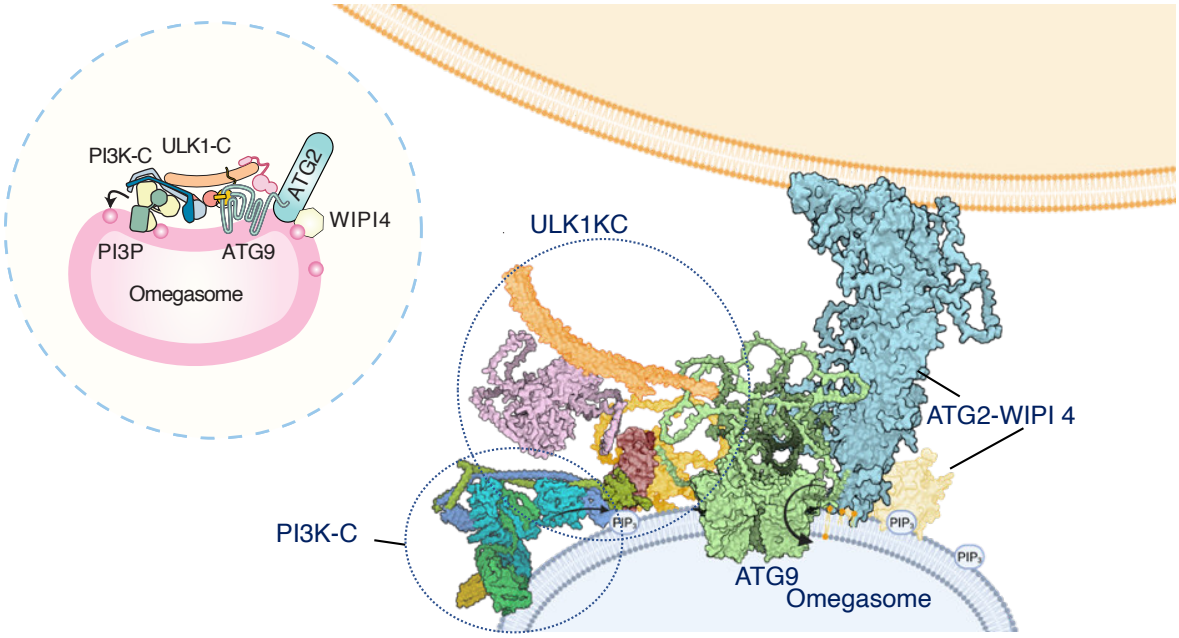

Figure 1.7 Autophagy initiation machinery

Schematic representation of Autophagy initiation machinery. The image was created with BioRender combining ATG9 structure (PDB: 7JLQ), PI3KC, FIP200, ULK1, ATG13, ATG101, ATG2, WIPI4 AlphaFold structure prediction.

In mammalian autophagy, the *de novo* formation and elongation of a membrane at the ER contact sites is an incredibly convoluted mechanism in which many cross-interacting complexes colocalize (Polson *et al.*, 2010; Karanasios *et al.*, 2013; Bakula *et al.*, 2017; Gómez-Sánchez *et al.*, 2018b; Osawa and Noda, 2019). ATG13 and ATG101 seem to be at the apex of the recruitment of all initiation complexes (Mercer, Kaliappan and Dennis, 2009; Alers *et al.*, 2011; Jao *et al.*, 2013b; Hieke *et al.*, 2015; S. W. Suzuki *et al.*, 2015b; Park *et al.*, 2016; Kim *et al.*, 2018). ATG13 and ATG101 are HORMA domain proteins (Qi *et al.*, 2015), a family of morphomeric proteins identified during the 90s (Aravind and Koonin, 1998). According to recent reconstitution studies, the considerable activation energy required for the metamorphosis of the HORMA domain creates a kinetics bottleneck for the complex formation between a HORMA and its binding partner and the rate of the activation of the pathway itself (Faesen *et al.*, 2017). Given the fact that HORMA domain proteins are often located at the apex of the processes that are associated with quality maintenance

and survival, the structural and, hence, the functional features are likely shared within the family, to some extent. ATG13 and ATG101 are also critical regulators of the autophagy process (Hosokawa, Sasaki, *et al.*, 2009; Mercer, Kaliappan and Dennis, 2009; S. W. Suzuki *et al.*, 2015b; Kaizuka and Mizushima, 2016) and their asymmetric dimerization is remarkably similar to the one shared among other HORMAs, which is a marker for a catalyzed assembly reaction. The observation that ATG101-ATG13 is located at the core of autophagy initiation and dimerization is central in preventing the complex to disassemble (Hosokawa *et al.*, 2009a; Suzuki *et al.*, 2015c; Wallot-Hieke *et al.*, 2018;), and the fact that there are few proposed binding partners for these autophagic HORMA domains that are part of the subcomplexes of autophagy initiation, supports the idea of ATG13 and ATG101 might regulate the autophagy initiation at the right place and the right time.

One of the limitations that impaired the autophagy field and the HORMA field in understanding these proteins is the lack of biochemically available protein interactors. ATG9 and ATG14 have been identified as prospective partners in cell-based research (Jao *et al.*, 2013; Kim *et al.*, 2018; Park *et al.*, 2016; Suzuki *et al.*, 2015), however, there is no direct confirmation. If the interaction exists and is mediated by a 'seatbelt interaction' or another unique conformational change, ATG101 and ATG13 would act as a link between all of the initiation complex components and master autophagy pathway regulators, determining when and where the other proteins are recruited to the omegasome (Figure 1.7).

Aims

With this project, we proposed to biochemically reconstitute part of the initiation complex of autophagy using recombinantly expressed and purified proteins, focusing on the role of ATG13 and ATG101 and in particular on their kinetics of the interaction with the yet unconfirmed interaction partners.

This work followed these steps:

1) Set up purification protocol for expression and purification of key components of autophagy initiation
2) Identify ATG13 and ATG101 putative binding partners and characterize their interaction
3) Determine the interaction kinetics by which the HORMA domain capture their BP
4) Reconstitution of the autophagy initiation machinery in collaboration with my colleague working on other components of the Autophagy initiation

2 Materials and Methods

2.1 Materials

Table 2.1: Cloning Material and Kits

Name	Company	Cathalog number
100 bp DNA Ladder	Thermo Fisher	15628019
1kb ladder	New England BioLabs	B7025
6x Loading Dye	New England BioLabs	B7021S
Agarose	Sigma Aldrich	A9539
Ampicillin	Sigma Aldrich	A9393
BamHI	New England BioLabs	R3136
beta-X-gal	ROTH	2315.3
Chloramphenicol	ROTH	3886.2
DMSO	New England BioLabs	A994.1
dNTPs	New England BioLabs	N0447S
DPNI	New England BioLabs	R0176L
EcoRI	New England BioLabs	R3101
Ethanol	Sigma Aldrich	V001229
Gel Loading Dye	BioLabs	B7024S
Gentamycin	Sigma Aldrich	PHR1077
HindIII	New England BioLabs	R3104
Isopropanol	Sigma Aldrich	I9516
Kanamycin	Sigma Aldrich	BP861
MgCl2	New England BioLabs	B9021S
NAD	New England BioLabs	M0309
PEG-8000	Promega	v3011
Phusion ® Polymerase	New England BioLabs	M0530S
Phusion HF or GC Buffer	New England BioLabs	M0532S

PmeI	New England BioLabs	R0560S
PureLink® HiPure Midiprep	Thermo Fisher	K210014
Q5® High-Fidelity DNA Polymerase	New England BioLabs	M0491S
QIAprep® Spin MiniPrep Kit	Qiagen	27104
QIAquick® PCR Purification Kit	Qiagen	28104
SERVA DNA Stain	SERVA	39804.02
Streptomycin	Sigma Aldrich	85886
SwaI	New England BioLabs	R0604S
T4 Ligase	New England BioLabs	M0202S
T5 Exonuclease	Epicentre	T5E4111K
Taq DNA-Ligase	New England BioLabs	M0208S
Taq Polymerase	New England BioLabs	M0273S
Tetracycline	Sigma Aldrich	T3258
Tris-HCl	Sigma Aldrich	10812846001
X-tremeGENE transfection	SIGMA	6365787001

Table 2.2 Cell lines and media

Name	**Company**	**Cathalog number**
NEB5alpha	NEB	C2987H
LOBSTR-BL21(DE3)-RIL	Kerafast Lcc	NC1789768
Rosetta2™	Novagen	71402
XL10-Gold® Ultracompetent Cells	Agilent	200314
DH10Bac Competent Cells	Gibco	10361012
Hi5 cells	Gibco	10361012

Sf9 cells	Gibco	11496015
Sf-900 III SFM-500ml	Gibco	12658019
ESF 921 Insect Cell Culture Medium 1L	Expression System	96-001-01
LB-Agar	SigmaAldrich	L3022
SOC Medium	ThermoFisher	15544034
LB Medium	MP Biochemicals	113002022-CF

Table 2.3 Protein Purification materials

Name	Company	Cathalog number
Strep-Tactin® column	IBA	2-1239-001
0,8µm Filters	Sartorius	1AY0.1
1ml/5ml GST column	Cytiva	GE28-4017-48
1ml/5ml MBP column	Cytiva	GE28-9187-80
5ml His column	Cytiva	GE17-3712-05
Acetic Acid	Sigma-Aldrich	695092-500ML
Acrylamid	Sigma-Aldrich	A3574
Amicon 15 100k	Merck Millipore	UFC910008
Amicon 15 30k	Merck Millipore	UFC903024
Amicon 15 3k	Merck Millipore	UFC900308
Amicon 15 50k	Merck Millipore	UFC905008
Amicon 4 100k	Merck Millipore	UFC801008
Amicon 4 30k	Merck Millipore	UFC803024
Amicon 4 3k	Merck Millipore	UFC800324
Amicon 4 50k	Merck Millipore	UFC805008

Amphipol A8-35	Jena Biosciences	X-A835
Commassie Brillian Blue-G	ThermoFisher	20279
Commassie Brillian Blue-R	ThermoFisher	20278
d-Desthiobiotin	Merck Millipore	D1411-500MG
DNAseI	Sigma-Aldrich	10104159001
Glycerol	Sigma-Aldrich	G5516
GSH	Sigma-Aldrich	G4251-10MG
GST beads	Sigma-Aldrich	GE17-0756-01
Hepes	Merck Millipore	H3375-25G
HiLoad® 16/600 Supeose® 6	Cytiva	GE29-3239-52
HiLoad® 16/600 Superdex® 200 pg	Cytiva	GE28-9893-35
HiLoad® 16/600 Superdex® 75 pg	Cytiva	GE28-9893-33
His pure NiTA resin	ThermoFischer	88221
Imidazole	Sigma-Aldrich	I5513
IPTG	Sigma-Aldrich	I6758-1G
Maltose	Merck Millipore	63418
Maltose Binding Protein AB	Biolabs	E8021L
n-Dodecyl-beta-Maltoside Detergent	Merck Millipore	D4641-25G

NaCl	Sigma-Aldrich	S9888-25G
Ph.D.™-7 Phage Display Peptide Library Kit	BioLabs	E8100S
PMSF	ROtH	6367.2
precast gels	BioRad	4561084DC
Protease Inhibitor Cocktail	CellSignaling	5871
Proteinmarker	BioRad	1610374
ResQ column 1ml/6ml	Cytiva	GE71-7146-00
Strep beads	IBA	2-1201-002
Strep-Tactin® regeneration buffer with HABA	IBA	2-1002-100
Superdex™ columns s200 10/300 GL	Cytiva	GE17-5175-01
Superdex™ columns s75 10/300 GL	Cytiva	GE17-5174-01
Superose columns s6 10/300 GL	Cytiva	GE17-5172-01
TCEP	Sigma-Aldrich	C4706
TEMED	Roth	110-18-9
Triton™ X-100	Sigma-Aldrich	X100-100ML

Table 2.4 Software and tools

Name	Version
Jalview	2.11.1.5
Clustal W	2
Fiji	1.53

GraphPad Prism	9
Jpred	/
PhosphoSitePlus®	/
Affinity Designer	1.1
Affinity Photo	1.1
PrimerX	/
Expasy ProtParam Tool	/
Aliview	1.28
PyMOL	2.5
Scaffold	5
SnapGene	6
Chimera/ Chimera X	1.16

2.2 Constructs and cloning

2.2.1 Genes amplification or site-directed mutagenesis by Polymerase Chain Reaction (PCR)

Genes of human ATG13, ATG101, ATG14, BECN1 and ATG9 were obtained from AddGene plasmid repository. The vectors were expanded in XL10Gold and purified by QIAprep® Spin MiniPrep Kit (See Table 2.6).

The genes were then amplified by using overlapping primers designed manually by adding part of the gene sequence to the Gibson-specific overlapping sequence. The site-directed mutagenesis primers were also designed manually or through the PrimerX online tool. Q5 High-Fidelity Polymerase or Phusion in a 25ul reaction is used to amplify the gene of interest with primers described by manufacturer protocols for each specific Polymerase. The major modifications were applied to the final extension time depending on the length of the gene of interest.

Table 2.5 general PCR conditions

	Temperatures	**Time**
Denaturation step	98ºC	30 seconds
	98ºC	5-10 seconds

35-40 cycles	*50-72ºC	10-30 seconds
Extension step	72ºC	20-30seconds/kb
Hold step	4ºC	∞

For the generation of site-directed mutations, a single PCR was performed from the WT gene inserted in the vector of interest, by prolonging further the extension step taking in account the whole length of the vector. All the PCR products were subsequently digested with DPNI enzyme to select for the PCR product with an overnight incubation at 37ºC. The QIAquick® PCR Purification Kit was then used in the purification procedure.

Table 2.6 Vector Sources

Name	Source
ATG13	https://www.addgene.org/54987/
ATG101	https://www.addgene.org/22876/
ATG9	https://www.addgene.org/60609/
ATG14	https://www.addgene.org/21635/
BECN1	https://www.addgene.org/24388/

2.2.2 General cloning procedure

Gibson assembly was used for the majority of cloning processes. The Gibson master mix is produced in-house by following Gibson *et al.* (2009). The vectors chosen for the gene insertion were either pLIB for insects or pColi (derived from a pET43) for *E. coli* expression with different N-terminus or C-terminus tags. Prior to the usage in the Gibson assembly, the vectors were linearized by digestion with the enzymes HindIII, BamHI and EcoRI and subsequently purified by QIAquick® PCR Purification Kit.

A moral ratio of 1:5 was kept while mixing the chosen vector and the gene of interest for the one-step isothermal Gibson reaction. 15µl of Gibson master mix are transferred with 5µl of the vector combined with the gene of interest and immediately incubated at 50ºC for 15-60 minutes.

Table 2.7 Gibson Master Mix

Volume	Buffer and Enzymes

320µl	5X ISO buffer*
0.64µl of 10 U/µl	T5 exonuclease
20µl of 2 U/µl	Phusion Polymerase
160µl of 40 U/µl	Taq ligase
Up to 1.2 ml	ddH_20

*1M $MgCl_2$, 80mg PEG-8000, 1M Tris-HCl pH=7.5, 100mM dNTPs, 1M DTT, 100mM NAD, ddH_20 to 320µl

2.2.3 Transformation in NEB5a and positive colony isolation

15µl of *E. coli* strain NEB5 cells are mixed on ice with 2µl of Gibson reaction containing the vector with the inserted gene of interest. The mixture of cells and vectors are then heated for one minute at 42°C for DNA uptake. The cells are then immediately transferred on ice for a 10 minutes incubation and subsequently diluted with room temperature SOC media for 30 minutes. After the cells are evenly spread on plate with LB-agar containing the specific antibiotics, the plates are incubated overnight at 37°C.

The identification of the positive colonies is performed in-house by using a 25µl Taq Polymerase reaction following manufacturer protocol, and choosing forward gene-specific primers and reverse vector-specific primers. The individual transformants are select casually and diluted in 100µl H_20, followed by a brief heating step at 95°C and finally combined with the Taq Polymerase reaction mix. The screen for the positive colony is this case is performed by an agarose gel electrophoresis (usually at 1%).

The second method used for the identification of positive colonies is the Microsinth AG Company service *E.coli* NightSeq®. In both cases, the positivity of a colony is confirmed by manual sequence alignment using the Clustal W online tool, Gene Compiler or SnapGene software.

Successful identification is followed by inoculation of 5ml of LB media combined with specific antibiotics and subsequent overnight incubation at 37°C (shaker). The culture is harvested by centrifugation at 4000 x g for 15 minutes and isolated by QIAprep® Spin MiniPrep Kit according Qiagen protocol. Absorbance at A260nm with a Thermo Scientific NanoDrop is used to measure concentration and purity of the isolated plasmid DNA. In case of in-house positive colonies isolation or in case of inconclusive results from the *E. coli* NightSeq®, an additional sequencing step is added ("Economy Run" service from Microsinth) to confirm positivity and identify eventual mutations inside the plasmid.

If the vector chosen is a pColi, the next step is directly transformation in expression *E. coli* cell lines like *Rosetta2™* or LOBSTR. In case of expression in insect cells, an additional passage of

cloning might be necessary for proteins which require coexpression to stabilize eachother (see paragraph. 2.3.2).

2.2.4 Cloning for pBIG expression vectors

In order to assemble multiple genes in a single vector for insect cells coexpression, Weissmann *et al.* developed an elegant system that allows the insertion, in only two steps of up to 25 different cDNAs is a single baculoviral expression vector (pBIG2). In order to do this, a 'GEC' is generated by amplification from pLIBs with predefined primers (α, β, γ, δ, and ώ from I to V, frw and rew). Each amplified GEC will contain a polh (polyhedrin promoter), a cDNA with a (un-)tagged GOI and a terminator (SV-40) thanks to the Cas optimized primers. Up to 5 GECs are then inserted by a Gibson reaction in a pBig1 (either a, b, c, d or e) as a polygene cassette (PGCs). Each pBig1 has to be predigested for linearization with PmeI enzyme following manufacturer protocol before Gibson assembly. Each GEC is flanked by an additional restriction site for SwaI enzyme that can be used for identification of the GECs correct insertion, together with the PmeI digestion. Different pBIG1s can be then combined in an additional passage of PCR with predesigned primers (in this case termed from "A" to "F") and inserted in a pBIG2 through a second Gibson assembly reaction.

We decided to use this system to combine to 2 genes for optimal coexpression in insect cells. In order to assemble ATG13 with ATG101, for example, a PmeI-linearized pBig1a was mixed in a Gibson assembly reaction with two PCR-derived GECs from pLIBs containing a GST N-terminus tagged ATG13 and untagged-ATG101. The PCR amplified GECs are kept at a two/three-fold molar excess over the pBIG1 for an optimal insertion. After plating in Streptomycin-containing plates, the positive transformants were identified as described in section 2.3.1 (colony PCR or Ecoli NightSeq®) or by restriction digestion, taking advantage of the SwaI and PmeI restriction sites.

2.2.5 Integration of GOI into DH10aBacY

E. coli is an excellent machine for the production of recombinant proteins, however big protein complexes or proteins that need post-translational modifications, or membrane proteins, require a different approach. From this point of view, the BEVS (Baculovirus Expression Vector System) represents a huge advantage. The most common viruses that infect insect populations are indeed baculoviruses. Combining the BEVS and the insect cells culture system enables high-quality protein expression circumventing *E. coli* system limitations (Luckow *et al.*, 1993; Berger, Fitzgerald and Richmond, 2004; Abdulrahman *et al.*, 2015; Gecchele *et al.*, 2015).

In particular, the BEVS employs an engineered Bacmid derived from the genome of a baculovirus and termed AcMNPV (*Autographa californica multicapsid nucleopolyhedrovirus*). A recombinant gene (GOI) gets inserted into the AcMNPV to generate recombinant virions. The P10 and PolH promoters of the AcMNPV regulate the GOI transcription (see section 2.3.2 for further information). The AcMNPV bacmid, a helper plasmid containing the Tn7 transposase, a *YFP* gene under the control of the PolH promoter, and a *LacZ* gene are all found in DH10BacY cells (Gradia *et al.*, 2017).

To allow recombination, the pLib containing the GOI (identified, amplified and isolated) was mixed with DH10EMBacY *E. coli* competent cells and a heat shock treatment is performed as described previously in section 2.2.2 and 2.2.3. In this case, the incubation at 37°C was prolonged to 4h. The cells DH10EMBacY were plated on LB-agar plates for white-blue colonies selection. The plates contain kanamycin, tetracycline, and gentamycin, Xgal 100 g/ml and 0.5mM IPTG. The positive colonies could be identified by the white color because, upon recombination with the pLIB mediated by the Tn7 transposase, the *lacZ* gene in the genome of DH10EMBacY is disrupted. A proper recombined colony with inserted GOI is not able to metabolize Xgal in a blue bioproduct, therefore only negative colonies will appear blue (Gradia *et al.*, 2017; Luckow *et al.*, 1993).

Positive colonies were amplified in 5ml LB-media with proper antibiotics and the DNA isolated by alkaline lysis with a sequential isopropanol precipitation and ethanol 70% wash.

2.3 Recombinant protein expression

2.3.1 Protein expression in E. coli

As indicated in section 2.2.2 and 2.2.3, the GOI was inserted in the pColi vector and subsequently amplified and purified . Competent cells like *Rosetta2*™ or LOBSTR were employed for protein expression. The transformation was performed as described in (Miller, 1992). The cells were then inoculated in a flask with 25ml LB-medium with antibiotics for proper selection and let to grow overnight in a shaker at 37°C. Subsequently, a large amount of LB-medium (up to 6 l) was inoculated with the growth culture and let to reach mid-log phase. The inoculated cultures were then immediately transferred at 16°C and the protein expression was induced with 0.5mM of IPTG at late log phase. The growth state was assessed by measuring OD600 every 45-60 minutes. The inoculated flasks were cultivated for an additional 12-18h at 16°C in a shaker mode and finally harvested by centrifugation at 3500 x g for 15 minutes, washed with PBS 1X, and stored at -20°C until further use.

2.3.2 Transfection of Bacmid DNA, virus expansion and protein expression in insect cells

The Sf9 insect cell line, from *Spodoptera frugiperda*, is the most frequently used for BEVS. It is employed for recombinant virus generation, transfection, creating viral stocks, and recombinant protein production. Hi5 cells, differently, are exceptionally effective protein machine, producing up to 10 times more protein than Sf9 cells and therefore are used for the later step of the protein expression.

The recombined Bacmid DNA was purified in sterile ambient (see section 2.2.5) was resuspended in water and mixed with transfection agent, which contains lipids that mediate the incorporation into the membrane of insect cells (SF9). The mixture was gently dropped over adherent Sf9 in 6-well plates (1 million cells and 3 ml of Sf9 media). Roughly after 48h after transfection, the GOI is transcribed and translated together with the YFP gene of the AcMNPV. The YFP gene is a marker for relative transfection efficacy and is used to monitor various parameters (proper virus amplification, cell state and harvesting conditions). After most the Sf9 cells appeared green at a fluorescence light microscope (~4 days), the 3 ml of the supernatant (V0) could be used to infect a 10 cm plate containing 10 million Sf9 adherent cells and 10 ml of Sf9 media. After 3-4 days, the 10 ml of media were harvested and used to infect 50ml of Sf9 to amplify the virus (V1) (250µl V0 in 25ml Sf9 at 1million/ml). After 4 days, the V1 could be pelleted to isolate enough cells to do test pull-down and use the V1 for additional expansion (V2, 250µl V1 in 25ml Sf9 at 1million/ml). After 4 days, the 25ml V2 was all used to inoculate a culture of 500ml of Hi5 at 2 million/ml, then was then harvested 3 days later by centrifugation at 500 x g for 15'. The pellet obtained was then washed with PBS 1x and stored at -20°C until further use.

2.4 Protein purifications

All soluble proteins containing GST- or HisMBP-tags expressed in insect cells were purified as follows.

A maximal temperature of 4°C was matained along all the steps of purification. 5ml of pellet was resuspended in Buffer A 50ml (25mM HEPES (pH=8), 150mM NaCl, 5% Glycerol, 0.5mM TCEP, 1mM PMSF, 1% Triton) and lysed by detergent incubation for 1h (ATG13 and mutants were incubated for up to 4h). The samples were then centrifugated at 15000g at 4°C for 15 minutes and filtered with a 0.8um filter (Sartorius). The sample was then loaded subjected to Affinity chromatography with the appropriate column. The ÄKTA START system was used to purify proteins by affinity or IMAC. The column was pre-equilibrated with Buffer A without PMSF and Triton. After an extensive wash, the column-bound protein was eluted with Buffer B (25mM

HEPES (pH=8), 150mM NaCl, 5% Glycerol, 0.5mM TCEP, 10mM Gluthathione or 5mM Maltose).

Transmembrane protein $^{MBP-}$ATG9 and its truncations were purified in the exact same way as described previously but, in this case, 1% Triton was substituted with 1% DDM. Buffer A contained an additional 0.03% of DDM, as well as Buffer B. In a similar way, Strep-ATG2 necessitated 1% DDM during all the purification steps (Protolocol Anh Nguyen). $^{Strep-}$ATG2 was purified using a Strep-Tactin® Superflow® column and eluted with 2.5 mM of *d*-Desthiobiotin.

ATG14/BECN1 complex is His-GFP tagged was also solubilized in a similar manner then the soluble proteins. However, it was purified by imidazole gradient with Buffer A (25mM HEPES (pH=7.4), 400mM NaCl, 5% Glycerol, 0.5mM TCEP, 1mM PMSF, 1% Triton, 5mM Imidazole) and Buffer B (25mM HEPES (pH=8), 400mM NaCl, 5% Glycerol, 0.5mM TCEP, 300mM Imidazole). In addition, ATG14/BECN1 was also subjected to an additional step of Anion Exchange Chromatography with Buffer 0 (25mM HEPES (pH=8) 5% Glycerol, 0.5mM TCEP) and Buffer 100 (25mM HEPES (pH=8) 5% Glycerol, 0.5mM TCEP). The dilution before AE was 100mM NaCl. The complex always elutes at 400mM NaCl. $^{HisGFP-}$WIPI4 was also purified by imidazole gradient but without AE.

ATG9^{N} and ATG101 were the only proteins expressed and purified from E. coli and followed the same protocol of the soluble proteins with the substitution of the detergent solubilization with sonication lysis.

Tags were cleaved with an overnight incubation with 1:1000μg/mg PreScission Protease (His-tag PreScission for His-GFP or His-MBP proteins; GST- PreScission with GST-tagged proteins). In most of the cases, where the protein was tagged with MBP, a reverse affinity purification step was added in order to reduce the amount of MBP in the sample. SDS-PAGE is used to determine whether the tagged protein was successfully cleaved and/or removed.

Before SEC or concentration, all the samples were centrifugated at 15000g for 10 minutes to remove aggregates. Amicon® Ultra-15 or -4 Centrifugal Filter Tube with an appropriate molecular weight cut-off was used to concentrate the eluted fractions.

ATG101 and mutants were mainly purified with Superdex 200 (10/300 GL or 16/600 High Load) or Superdex 75 (10/300 GL or 16/600 High Load). ATG14/BECN1 was mainly purified with Superdex 200 (10/300 GL or 16/600 High Load) or Superose 6 (10/300 GL or 16/600 High Load). ATG9 and truncations, ATG13 mutants, ATG2 were all purified with Superose 6 (10/300 GL or 16/600 High Load). Gel filtration Buffers were composed by 25mM HEPES (pH=8), 150mM NaCl, 5% Glycerol, 0.5mM TCEP. The only exceptions were ATG9 with 0.03% DDM and ATG2 with 1% DDM. Elution profiles were all assessed by SDS-PAGE. The protein was then

concentrated again with appropriate Amicon® Ultra-15 or -4 Tube Proteins, quantified at Nanodrop, aliquoted, snap frizzed in liquid nitrogen, and stored at -80°C until future usage.

2.5 XL-MS of ATG13-ATG101-ATG9 complex

For the three-dimensional study of proteins, chemical cross-linking Mass Spectrometry (XLMS) has emerged as a successful approach. Each cross-linker has a specific length and purpose. We used BS^3 (11.4 Å). Different amounts of cross-linker were added to 1mg/ml of sample to create a concentration series (0.5mg/ml to 2mg/ml). After incubation at room temperature for 1h, the samples were loaded on SDS-gels electrophoresis gels to separate the cross-linked complex from uncross-linked ones. The gel was then handled to Iwan Parfentev (Urlaub Lab).

2.6 Pull-downs

The buffer A was used for pull-downs is 25mM HEPES (pH=8), 150mM NaCl, 5% Glycerol, 0.5mM TCEP, 0.03 % DDM.

Figure 3.1a; Figure 3.4c 30ul pre-equilibrated MBP-beads were incubated with 0.1µM MBP-tagged bait for 10 minutes. After a brief wash with 500ul buffer, the pray was added at a 0.3µM concentration for 1h on ice. After 3x500ul washes with buffer A, 10ul of 4xloading buffer were added to the samples and run on SDS-PAGE gel for electrophoresis.

Figure 3.1d and e. 1µM of bait was incubated overnight at 20 °C with 3µM of pray in 20ul of buffer. Subsequently, the samples were incubated on pre-equilibrated MBP beads for 10 minutes, followed by 3x500ul washes with buffer A. 10ul of 4xloading buffer were added to the samples and subsequently run on an SDS-PAGE gel for electrophoresis.

Figure 3.3a; Figure 3.4b. 30ul pre-equilibrated GST beads were incubated with 0.1µM $^{GST-}$ATG13-ATG101 for 10 minutes. After a brief wash with 500ul buffer, the prays were added at a 0.3µM concentration for 1h on ice. After 3x500ul washes with buffer A, 10ul of 4xloading buffer were added to the samples and loaded on an SDS-PAGE gel for electrophoresis.

Figure 3.4d 0.1µM $^{GST-}$ATG13-ATG101 was incubated on ice for 1h with or without 0.3µM of ATG14/BECN1. On a side, $^{GST-}$ATG13-ATG101 was incubated on ice for 1h with or without 0.3µM of ATG9. The samples were incubated with 30ul pre-equilibrated GST beads for 10 minutes and washed 1x500ul of the buffer. ATG14-BECN1 was added to the ATG9-ATG13-ATG101 complex and *vice versa* and incubated for an additional 1h on ice. The additional pray was added at

0.3μM concentration to the samples as indicated. In the controls, only the buffer was added. The samples were then washed 3x500ul with buffer A, eluted with 10ul of 4xloading buffer and run on an SDS-PAGE gel for electrophoresis.

Figure 3.6b 0.1μM of bait was incubated for 18h on ice with 0.3μM of pray in 20ul of buffer. Subsequently, the samples were incubated on pre-equilibrated GST beads for 10 minutes, followed by 3x500ul washes with buffer A. 10ul of 4xloading buffer were added to the samples and subsequently run on an SDS-PAGE gel for electrophoresis.

Figure 3.8c. 30ul pre-equilibrated GST beads were incubated with 0.1μM $^{GST-}$ATG101 for 10 minutes. After a brief wash with 500ul buffer, the prays were added at a 0.3μM concentration for 1h on ice. After 3x500ul washes with buffer A, 10ul of 4xloading buffer were added to the samples and loaded on an SDS-PAGE gel for electrophoresis.

Figure 3.8g. 30ul pre-equilibrated GST beads were incubated with 0.1μM $^{GST-}$ATG13 for 10 minutes. After a brief wash with 500ul buffer, the prays were added at a 0.3μM concentration for 1h on ice. After 3x500ul washes with buffer A, 10ul of 4xloading buffer were added to the samples and loaded on an SDS-PAGE gel for electrophoresis.

2.7 Pull-downs kinetics

Figure 3.5a; Figure 3.6c 30ul pre-equilibrated GST beads were incubated with 0.1μM GST-ATG13-ATG101 for 10 minutes. After a brief wash with 500ul buffer, the prays were added for the time indicated at a 0.3μM concentration on ice. After 3x500ul washes with buffer A, 10ul of 4xloading buffer were added to the samples and loaded on an SDS-PAGE gel for electrophoresis.

Figure 3.5c; Figure 3.7a 1μM of bait was incubated for the time indicated at 20°C with 3μM of pray in 20ul of buffer. Subsequently, the samples were incubated on pre-equilibrated MBP beads for 10 minutes, followed by 3x500ul washes with buffer A. 10ul of 4xloading buffer were added to the samples and subsequently run on an SDS-PAGE gel for electrophoresis.

Figure 3.8e 0.1μM of bait was incubated for the time indicated at 20°C with 0.3μM of pray in 20ul of buffer. Subsequently, the samples were incubated on pre-equilibrated MBP beads for 10 minutes, followed by 3x500ul washes with buffer A. 10ul of 4xloading buffer were added to the samples and subsequently run on an SDS-PAGE gel for electrophoresis.

Figure 3.9c. *Fresh pull* 1μM $^{GST-}$ATG9N and $^{GST-}$ATG101 were incubated with 30ul pre-equilibrated GST beads for 10 minutes. After a brief wash with 500ul buffer, fresh 3μM of $ATG13^{WT}$ and mutants were added at a 0.3μM concentration for 1h on ice. After 3x500ul washes with buffer A, 10ul of 4xloading buffer were added to the samples and loaded on an SDS-PAGE gel for electrophoresis. *Overnight pull* $ATG13^{WT}$ and mutants were incubated overnight at 20°C and the pull-down was repeated as previously

3 Results

Figure 3.0

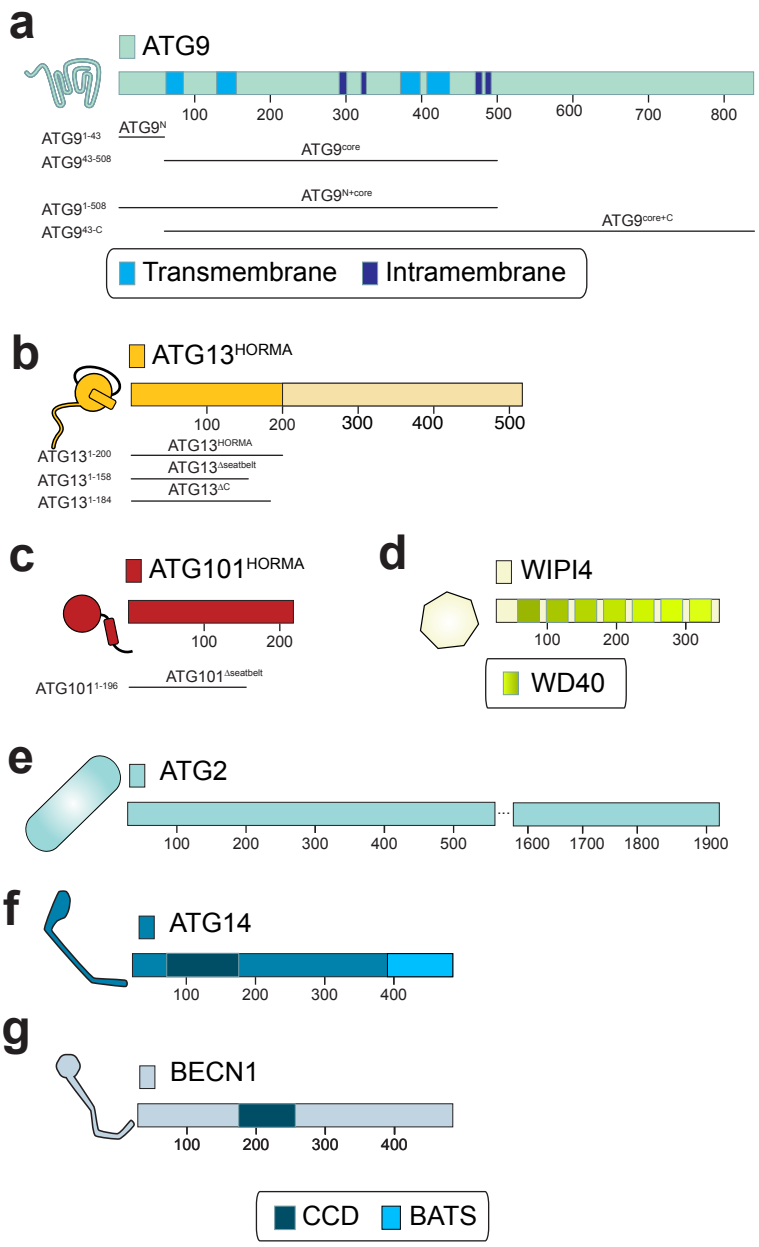

Figure 3.0 Proteins and truncations used in this work

(a) ATG9 **(b)** ATG13 **(c)** ATG101 **(d)** ATG2 **(e)**WIPI4 **(f)** ATG14 **(g)** BECN1. The truncations used in this work are indicated below every panel.

3.1 Purification of ATG101 and ATG13 and potential interactors

3.1.1 Purification of ATG13 and ATG101

One of the limitations that impaired the possibility to address biochemically the autophagy initiation in mammals, is the lack of available recombinant proteins for dissecting direct protein-protein interaction and characterizing their structure and kinetics. Most of the components of autophagy can be considered challenging to purify: they are non-globular extended, mostly unstructured (with the exception of ATG101). Some also bind lipids and tether membranes. In some cases, the structure contains a high percentage of IDRs (intrinsically disordered regions), involved in critical steps of early autophagy.

All of the proteins mentioned in the two following sections were expressed with either GST- (glutathione S-transferase) or 6XHis-MBP -tag (Maltose binding protein) and purified by affinity using a SigmaAldrich MBPTrap™ HP column or a GST HiTrap™ column. The eluted sample was then concentrated with AMICON ® Ultra Centrifugal Filters, and the concentrated protein was subjected to size exclusion chromatography (SEC) (Figure 3.0).

Out of all the human proteins purified in this work, only the ATG101 (25kDa) purification protocol was already established and published (Michel *et al.*, 2015). ATG101 presents a HORMA fold for its whole length and it can easily be expressed both in *E. coli* and insect cells with high yields (Figure 3.1a). It elutes at an apparent molecular weight of ~25kDa in SEC.

The ATG13^{HORMA} has been published, but only in co-expression with ATG101 (Qi *et al.*, 2015). Hurley and colleagues claimed in their study that ATG13^{HORMA} could not be expressed in isolation (without ATG101), stating that ATG13 ^{HORMA} is unstable in the absence of ATG101. However, we succeeded in expressing and purifying isolated ATG13^{HORMA} from insect cells. ATG13 ^{HORMA} (22kDa) expression was stabilized by the presence of either GST- or 6XHis-MBP-fused tags (Figure 3.1b). ATG13^{HORMA} purification was not straightforward. One of the issues that we faced during purifications was degradation (3.1b, second peak on the right, not shown in gel). Also, ATG13^{HORMA} is often not pure after the initial affinity purification. Therefore, in order to remove aggregates and membranes, we added 1% Triton X-100 detergent for 3h-4h to the first step which yielded a cleaner ATG13 ^{HORMA} sample. However, we noted that despite eluting in a sharp peak, ATG13^{HORMA} elutes at a higher apparent molecular weight than expected (Figure 3.1b).

Few purifications also shown elution at a smaller molecular weight (data not shown). We did not detect any functional difference between the ATG13^{HORMA} eluted at different volumes, therefore we suppose that ATG13 might have some affinity for the Superose column, lipids and/or exposing some charged/hydrophobic patches accessible to cell debris when expressed without ATG101. In addition, we noticed that purified ATG13^{FL} and ATG13^{HORMA} are stable and well

behaved for several days at room temperature without any obvious precipitation, aggregation, or loss of function. Unfortunately, the affinity tag of ATG13^{HORMA} could not be removed without severely impacting protein stability, which largely prevented its use in this project.

Purification of co-expressed ATG13 ^{HORMA}-101 was straightforward and did not require detergent. In order to maintain a stable 1:1 ratio, we used the BigBac expression system where ATG101 and ATG13 were expressed from a single vector (see Materials and Methods section 2.2.4). Differently from Qi *et al.*, 2015 we expressed full-length ATG101 and maintained the full N-terminus of ATG13^{HORMA} (1-200). ATG101 and ATG13^{HORMA} form a stable protein with a monodisperse peak in SEC. The protein eluted at around 44Da (~47kDa predicted) (Figure 3.1c), indicating a dimer. The stoichiometry ratio is always 1:1 and was also assessed by SLS, MALS, mass spectrometry and gel-based quantifications.

3.1.2 Purification of ATG9

Although ATG9 and ATG14 are both putative ATG13 and ATG101 interactors (Jao *et al.*, 2013; S. W. Suzuki *et al.*, 2015; Kim *et al.*, 2018; Park *et al.*, 2019; Kannangara *et al.*, 2021), no direct interaction has been proven so far. To assess whether these interactions are indeed happening we decided to purify both human proteins using over-expression in insect cells. The structure of ATG9 was determined during this project (Guardia *et al.*, 2020; Maeda *et al.*, 2020) and shows that ATG9 is a homotrimer and acts as a lipid scramblase. ATG9 is a transmembrane protein that presents six transmembrane domains, two of which are only half embedded inside the membrane (TM, Figure 3.0a and Figure 3.6a). The N- and C-terminus of ATG9 (the two main cytosolic regions) are probably largely unstructured, aside from potentially a few α-helices (Figure 3.6a and Supplementary Figure 2b and c).

The purification protocol of ATG9 full-length (~94 kDa) is similar to the protocol for ATG13 ^{HORMA}, but we typically used a lysis step of just 1h in the presence of 1% DDM for solubilization, which was subsequently reduced to 0.015-0.030% during later stages of the purification process. As expected, the trimer ATG9 elutes early in SEC. The peak is larger broad, which we hypothesize is due to either the incorporation and presence of DDM micelles (~70kDa, (Oliver *et al.*, 2013)), the large unstructured regions or due to weak transient dimerization of the ATG9 trimers that has been observed before by others (Lai *et al.*, 2020; Matoba *et al.*, 2020). (Figure 3.1e). The first option seems the most likely, as replacing DDM with amphipols, the peak became more defined. Amphipols are amphiphilic polymers that wrap around the transmembrane protein and are less dynamic than DDM, therefore highly helpful in situations when DDM cannot be employed (Bowie, 2001).

The apparent polydisperse behaviors ATG9 was also observed by Lai and Matoba while purifying ATG9 from *A. thaliana* (with glycerol gradient) and yeast (with SEC), respectively (Lai *et al.*, 2020; Matoba *et al.*, 2020). Lai observed the presence of trimers of ATG9 facing each other (hexamer) causing a polydisperse sample(Lai *et al.*, 2020). This was also observed by Guardia and colleagues using human ATG9 purified from HEK cells lysate (Guardia, *et al.*, 2020). However, these groups were working with truncated versions of ATG9 lacking the unstructured regions at the termini. Indeed, we have not observed any hexamers in CryoEM grids, which suggests that the hexamer might not happen in the full-length protein.

ATG9 truncations were initially designed using JPRED to estimate secondary structure boundaries, and later using the published structure. These constructs were purified using the same protocol as the full-length protein. See figure 3.0 for full details of all constructs. For most constructs, we had to include the transmembrane domains for stability.

3.1.3 Purification of ATG14/BECN1

The other possible interactor of ATG13 and ATG101 are two components of the PI3KC1: ATG14 and BECN1. Because ATG14 and BECN1 are both coiled-coil proteins with extensive interaction interfaces, we opted to co-express them for stability. The complex could be expressed by fusing a His-GFP tag on ATG14 and co-expressing it with untagged BECN1. This complex was then purified using HisPur™ Ni-NTA columns using an imidazole gradient (see Methods for further information). A passage on a ResQ column was added for cleaning the sample before loading onto a gel filtration column for SEC (Figure 3.1f). The ResQ is a column that allows the separation of species by surface charge but is also very useful for removing protein impurities. During SEC, the peak of the ATG14-BECN1 elutes earlier than expected, which is probably due an extended protein shape. See the Materials and Methods section for more information on the purification (section 2.4.1). For further details of proteins and truncations used in this work, refer to Figure 3.0.

Figure 3.1 **Autophagy initiation proteins can be purified separately and in sub-complexes**

(a) SEC of untagged ATG101 on S75 60/600 HighLoad column; **(b)**SEC of $^{GST-}$ATG13^{HORMA} on Superose 6 10/300 GL column; **(c)** SEC of co-expressed $^{GST-}$ATG13^{HORMA}-ATG101 complex on Superdex 75 10/300 GL column; **(d)** SEC of $^{GST-}$ATG9 N-terminus (1-60) on Superdex 200 10/300 GL column; **(e)** SEC of untagged ATG9 Superose 6 10/300 GL column; **(f)** SEC of co-expressed $^{His-GFP-}$ATG14-BECN1 on S200 60/600 HighLoad column. The elution profiles of molecular weight standards are shown as a gray line with the native molecular mass of the standard

indicated. Coomassie blue-stained SDS-PAGE of fractions with elution volumes are shown in the bottom panels

Figure 3.1

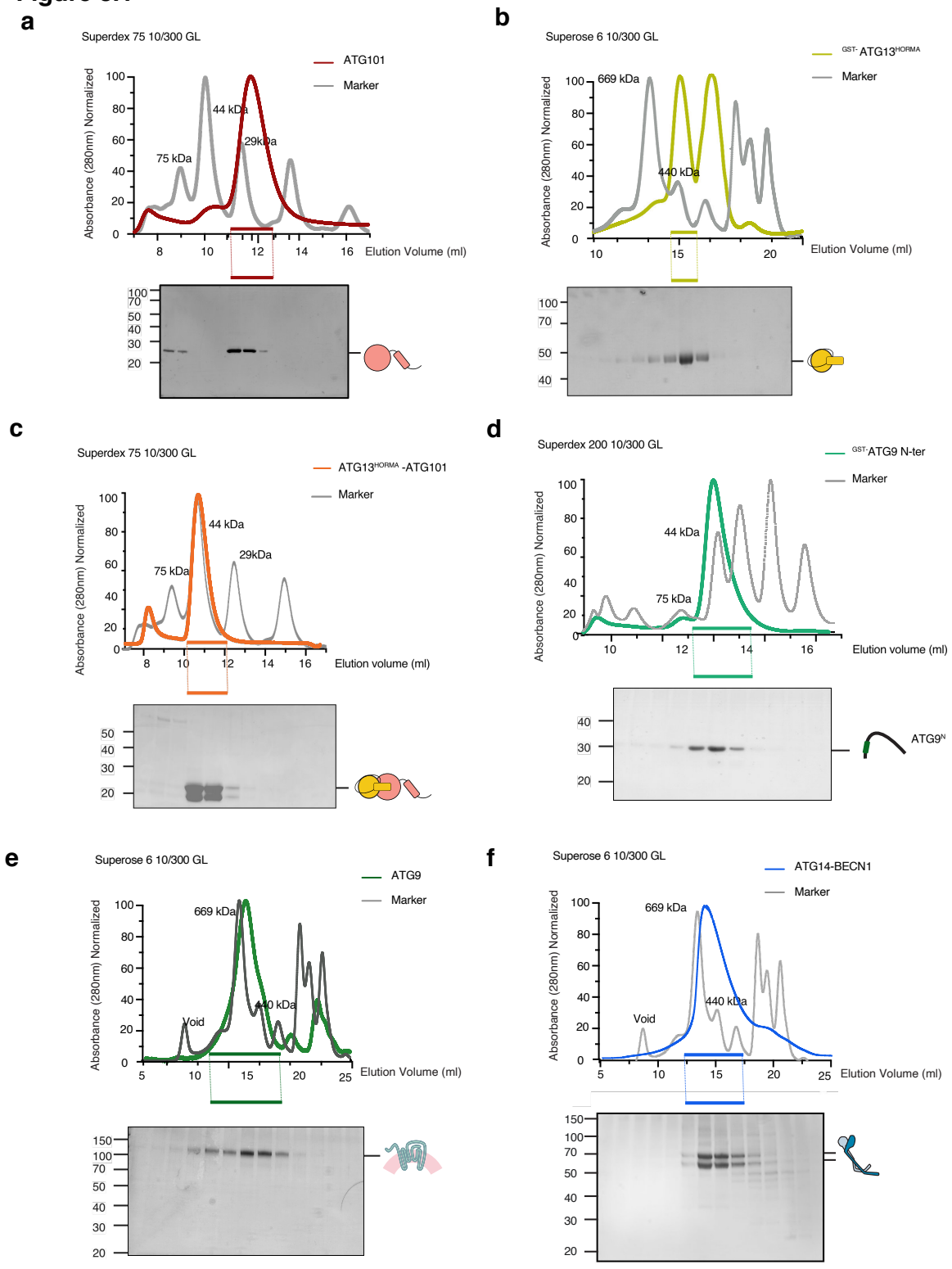

3.2 ATG13 and ATG101 directly bind to ATG9

ATG9 has been proposed as a possible ATG13 interactor in yeast (S. W. Suzuki *et al.*, 2015; Kannangara *et al.*, 2021). ATG101 is not present in budding yeast. To directly assess the binding between ATG9 and the complex of ATG13-ATG101, we performed a pull-down assay with purified proteins. $^{MBP-}$ATG13^{HORMA}-ATG101 was bound to Maltose Binding Protein (termed "MBP beads" from now on). We used purified MBP as a control. After 1h incubation on ice, ATG9 was only pulled down by the beads in the presence of the ATG13^{HORMA}-ATG101 complex (lane 4 compared to lanes 5 and 6), showing a direct interaction between the ATG13^{HORMA}-101 complex and ATG9.

The direct binding between the ATG13^{HORMA}-ATG101 complex and ATG9 was also confirmed by size-exclusion chromatography. ATG13^{HORMA}-ATG101 co-eluted with ATG9, indicating that ATG13^{HORMA}-ATG101-ATG9 forms a stable complex in solution. The excess of the ATG13^{HORMA}-ATG101 complex eluted later from the column (figure 3.2b). A sample isolated from the peak of the co-eluted three-protein complex was cross-linked with BS^3 (Bissulfosuccinimidyl suberate) by Anh Nguyen and subsequently subjected to cross-linking mass-spectrometry (XL-MS) performed by Iwan Parfentev (Urlaub lab). The two-dimensional map connecting the residues between the three proteins is shown in figure 3.2c. All the cross-linked residues that were identified on ATG9 are localized on the cytosolic interface (data not shown). Cross-links within ATG9 can be explained by the ability of ATG9 to trimerize and agree with the published structure.

Suzuki *et al.* used yeast-two-hybrid experiments to show that only the N-terminal 300 residues (up to the first transmembrane region) of yeast Atg9 binds to ATG13. This region is poorly conserved, and the human ATG9 has a relatively short N-terminus (60 residues). The cross-linking data shows no cross-links between ATG13-ATG101 and the N-terminal region of ATG9. In fact, most of the cross-links were localized at the C-terminus, a region proposed as an interaction hub for the recruitment of downstream autophagy effectors like LC3 or DFCP1 (S. W. Suzuki et al, 2015; Kannangara *et al.*, 2021). Interestingly, of the fourteen intermolecular crosslinks, eleven were between ATG9 and ATG101.

Therefore, to prove that either ATG13 or ATG101 are directly binding to ATG9, we performed two pull-down assays (Fig.3.2d and e). In panel d, ATG9 was incubated with either ^{MBP} ATG13 full-length (FL), ^{MBP}ATG13^{HORMA,} or purified MBP for 24h at 20ºC (for further information about why we selected this temperature and time, refer to figure 3.5c and discussion). ATG9 could be pulled down by the beads only when the HORMA domain of ATG13 was present (lanes 5 and 6 compared to lanes 7 and 8), indicating that the HORMA domain of ATG13 is sufficient for the

binding to ATG9. Next, we tested for the interaction between ATG9 and ATG101. Using size exclusion chromatography, XL-MS, and pull-downs (Figure 3.2e) we could confirm the surprising direct interaction between ATG9 and ATG101.

We wondered what the stoichiometry could be and tried to also determine the stoichiometry of the complex using different approaches: MALS (Multi-Angle Light Scattering) (performed by Anh Nguyen), mass photometry (MS) (performed by Anh Nguyen and Anoshi Patel), and also gel-based quantification like Commassie Blue-stain gel and stain-free gel quantifications (performed by Anh Nguyen). All these techniques were required to deconvolute that the ATG-ATG13-ATG101 complex assumes an unusual 3:6:3 stoichiometry: for each monomer of ATG9, there are two ATG13 and one ATG101 (Figure 3.2e). Most of our samples eluted from SEC in S6 columns appeared heterogeneous in their stoichiometry and in many of the techniques used. Probably they contained multiple species or intermediates of the complex that complicated the determination of the stoichiometry of this three-protein complex.

We summarized the results in Figure 3.2g. Our results indicate that ATG13 and, surprisingly, ATG101 can bind ATG9 directly. In addition, the three proteins can also form a stable complex. However, we could not resolve whether ATG101 and ATG13 still interact with each after binding to ATG9.

Figure 3.2 ATG13-ATG101 complex directly interacts with ATG9 as a complex and in isolation

(a) *In vitro* pull-down assay between recombinantly purified $^{6XHis\text{-}MBP}$-ATG13^{HORMA}-ATG101 co-expressed complex and ATG9. The samples were incubated with MBP beads after 1h incubation on ice. The results were analyzed by SDS-PAGE; **(b)** SEC of co-expressed $^{6XHis\text{-}MBP}$-ATG13^{HORMA}-ATG101 complex with $^{6XHis\text{-}MBP}$-ATG9 on S200 60/600 column. The elution profile of molecular weight standards is shown as a gray line with the native molecular mass of each standard indicated. Coomassie blue-stained SDS-PAGE of fractions with elution volumes from 50 to 80 ml is shown in the bottom panel; **(c)** Two-dimensional mapping of the intra- and inter-protein cross-links identified by XL-MS (Anh Nguyen, Iwan Parfentev) in the ATG13^{HORMA}-ATG101 complex coeluted with ATG9 in panel (b); **(d)** *In vitro* pull-down assay between $^{6XHis\text{-}MBP}$-ATG13^{HORMA} or $^{6XHis\text{-}MBP}$-ATG13^{FL} with ATG9. The samples were incubated with MBP beads after 24h incubation at 20ºC. The results were analyzed by SDS-PAGE; **(e)** *In vitro* pull-down assay between recombinantly purified $^{6XHis\text{-}MBP}$-ATG101 with ATG9. The samples were incubated with MBP beads after 24h incubation at 20ºC. The results were analyzed by SDS-PAGE; **(f)** quantification of unstained gel-based stoichiometry determination (Anh Nguyen) **(g)** schematic representation of the direct interactions determined in (a), (b), (c), and (d);

Figure 3.2

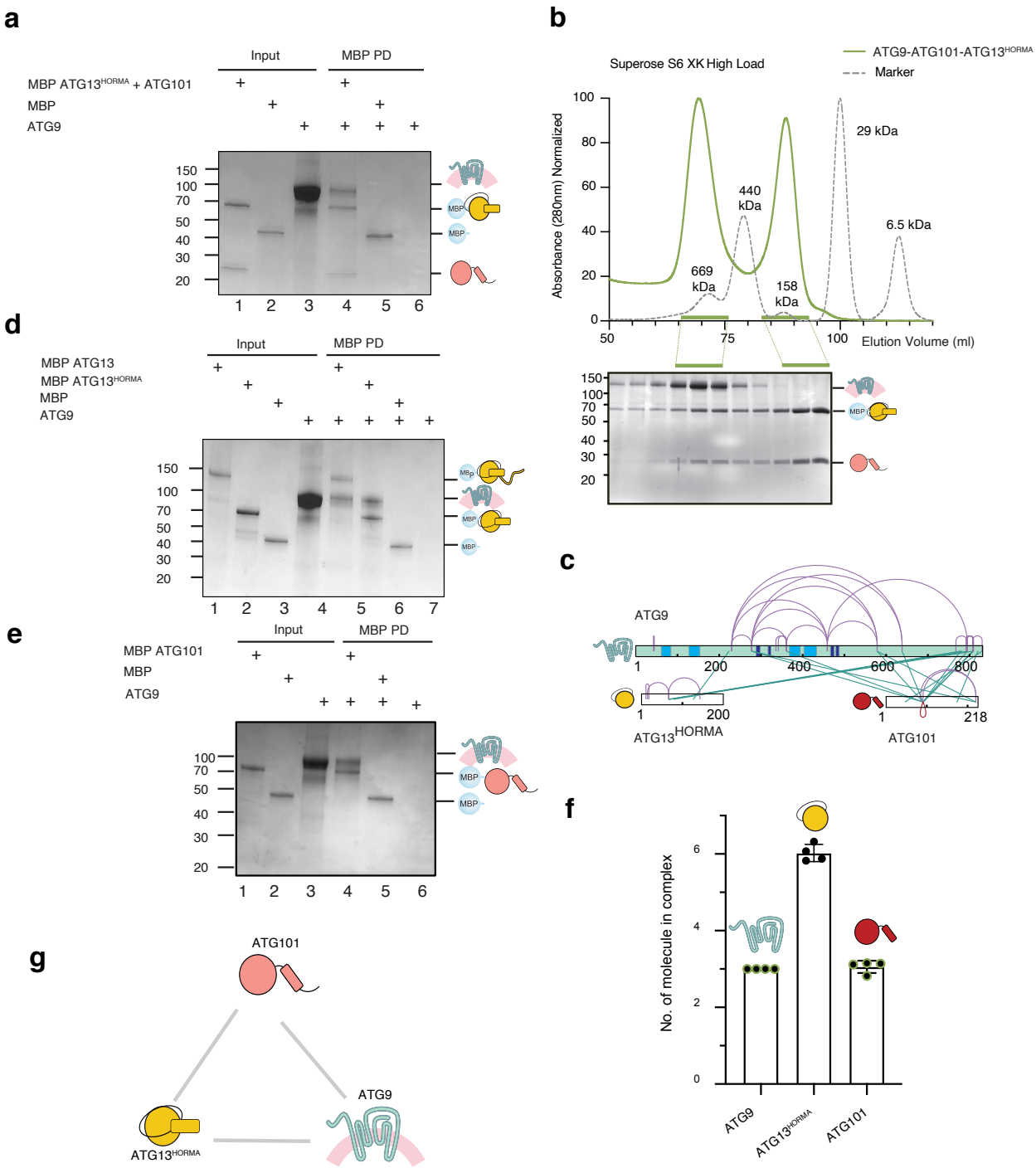
a
Input
MBP PD
MBP ATG13HORMA + ATG101
MBP
ATG9
150
100
70
50
40
30
20
1 2 3 4 5 6
MBP
MBP
b
Superose S6 XK High Load
ATG9-ATG101-ATG13HORMA
Marker
Absorbance (280nm) Normalized
100
80
60
40
20
0
29 kDa
440 kDa
6.5 kDa
669 kDa
158 kDa
50
75
100
Elution Volume (ml)
150
100
70
50
40
30
20
MBP
d
Input
MBP PD
MBP ATG13
MBP ATG13HORMA
MBP
ATG9
150
100
70
50
40
30
20
1 2 3 4 5 6 7
MBP
MBP
MBP
c
ATG9
1
200
400
600
800
1
200
ATG13HORMA
1
218
ATG101
e
Input
MBP PD
MBP ATG101
MBP
ATG9
100
70
50
40
30
20
1 2 3 4 5 6
MBP
MBP
f
No. of molecule in complex
6
4
2
0
ATG9
ATG13HORMA
ATG101
g
ATG101
ATG9
ATG13HORMA

3.3 ATG13-ATG101-ATG9-ATG2-WIPI4 form a stable complex

The IM expanding edge interacts with the ER at specific contacts sites (ERES), where also the ATG2, Atg8/WIPI, and ATG9 colocalize (Graef *et al.*, 2013; Suzuki *et al.*, 2013; Chowdhury *et al.*, 2018; Gómez-Sánchez et al, 2018). This has been mainly studied in yeast, although there are some indications that it may also occur in mammals (Graef *et al.*, 2013; Suzuki *et al.*, 2013; Valverde *et al.*, 2019). ATG2 and ATG9 have been found to function as intermembrane and interleaflet lipid transporters (Guardia *et al.*, 2020; Maeda *et al.*, 2020; Gómez-Sánchez *et al.*, 2018; Osawa and Noda, 2019; Valverde *et al.*, 2019; Orii *et al.*, 2020; Noda, 2021). ATG2 is a rod-shaped lipid channel that can tether vesicles without inducing fusion and can also transport lipids (Chowdhury *et al.*, 2017, 2018; Otomo, Chowdhury, and Lander, 2018; Maeda, Otomo and Otomo, 2019; Osawa and Noda, 2019; Valverde *et al.*, 2019; Osawa, Ishii and Noda, 2020; Noda, 2021), while ATG9 is a scramblase, whose active unit is a trimer. ATG9 flips lipids from the outer leaflet to the inner leaflet of a vesicle (Maeda *et al.*,2020; Matoba *et al.*, 2020). ATG2 and ATG9 are likely to form a tandem unit for the delivery of lipids from the ER to the IM (Noda, 2021b).

Anh Nguyen's unpublished work shows that ATG9-ATG2-WIPI4 forms a complex. He also showed that ATG2 transfers lipids between two vesicles and that ATG9 accelerate the process. We sought to see if the ATG13-ATG101 complex could also interact with ATG9 in presence of ATG2 and WIPI4. Therefore, we performed a pull-down as shown in figure 3.4a, using purified ^{Strep}ATG2 and ^{GFP}-WIPI4 and the three-protein complex composed of ATG9, ATG101, and ATG13^{HORMA}. Following the incubation of the ATG13-ATG101 complex to GST beads, we added ATG9, ATG2, and WIPI4 as specified. Although some ATG2 was unspecifically bound to the beads (lane 9), additional ATG2 was pulled down in the presence of ATG9 compared to the control (lane 2 compared to lane 4). WIPI4 does not interact with the ATG101-ATG13^{HORMA} complex by itself (lane 3) or with the addition of ATG9 (lane 5), but it can be observed when ATG2 is present (lane 6). Unfortunately, ATG2-WIPI4 is bound to the beads in lane 7. The quantification is shown in figure 3.3b. The data are normalized on the binding between ATG9 and ATG13 (lane 1), and also the ATG2 unspecific binding to the beads is taken into consideration. Although a gel-based quantification is not optimal to detect stoichiometry of complexes, we estimate that indicatively one ATG2 and one WIPI4 interact with one complex of ATG9-ATG13-ATG101. This was confirmed by Anh's experiments supporting a stoichiometry of 3:6:3:1:1 for the ATG9-ATG13-ATG101-ATG2-WIPI4 complex (data not shown).

Therefore, we can conclude that ATG13-ATG101-ATG9-ATG2-WIPI4 forms a stable complex, with ATG9 mediating the interaction between ATG13-ATG101 and ATG2-WIPI4 (Figure 3.4c). We hypothesize that ATG13^{HORMA} and ATG101 create a module that localizes to the

ERES, where it joins forces with ATG9-ATG2 and the PI3P sensor WIPI4 to form a single stable complex (Figure 3.4d) and probably promote the lipid transfer activity of ATG9 and ATG2 (Supplementary Figure 1). Indeed, Anh observed that upon the addition of the ATG13-ATG101 complex to its lipid transfer assay, the basal speed of lipid transfer activity of the active unit of WIPI4-ATG2-ATG9 accelerated up to 6 times.

Figure 3.3

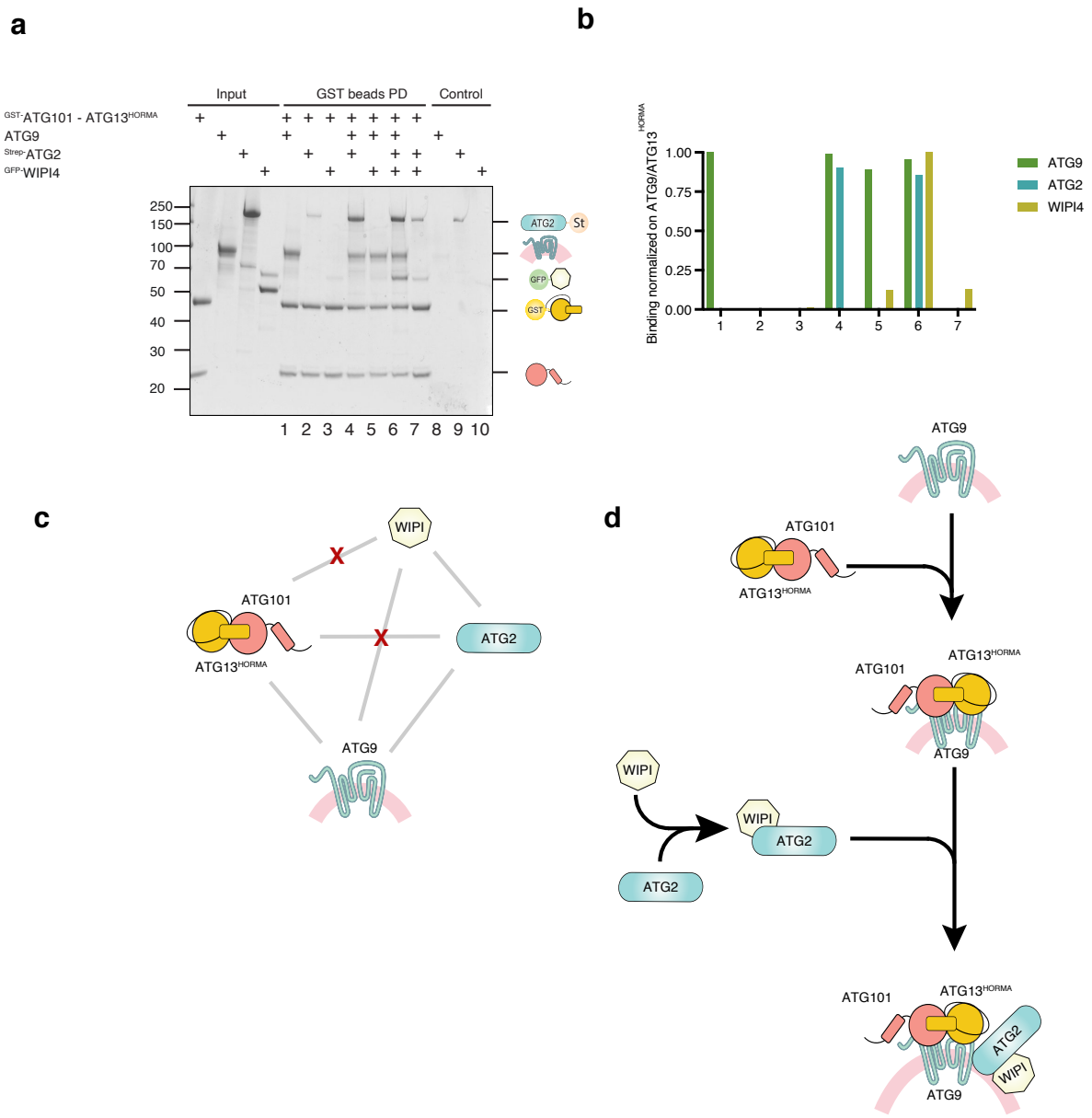

Figure 3.3 **ATG9-ATG13-ATG101 complex interacts with lipid transferase ATG2-WIPI4 complex**

(a) *In vitro* affinity PD assay between recombinantly purified $^{GST-}$ATG13^{HORMA}-ATG101 complex with ATG9, $^{His-GFP-}$WIPI4, $^{Strep-}$ATG2. $^{GST-}$ATG13^{HORMA}-ATG101 was preincubated on GST beads.

All the proteins were incubated for 1h on ice. The results were analyzed by SDS-PAGE; **(b)** quantification of (a) normalized over the binding of ATG9 to $^{GST-}$ATG13^{HORMA}-ATG101 complex in lane 1; **(c)** schematic representation of the direct interactions determined in (a); **(d)** proposed model of subcomplexes formation and binding

3.4 The ATG13^{HORMA}-ATG101 complex interacts with the ATG14-BECN1

Three different papers propose a potential interaction between ATG13 and ATG101 with ATG14. However, just as in the case of ATG9, there is no evidence that the interaction is direct (Jao *et al.*, 2013; Kim *et al.*, 2018; Park *et al.*, 2019). ATG14 is part of the PI3KC1, which is involved in the conversion of PI in PI3P at ER subdomains (omegasomes) (Obara, Sekito, and Ohsumi, 2006; Obara, Noda, *et al.*, 2008; Obara and Ohsumi, 2011). In particular, ATG14 is required to target the PI3KC1 at the location(Obara, Noda, *et al.*, 2008) and this recruitment is essential for autophagy (Matsunaga *et al.*, 2009). ATG14 contains a BATS domain specifically interacting with highly-curved PI3P-containing membranes onto the IM (Obara and Ohsumi, 2011). Since ATG2-interacting WIPI4 is a PI3P sensor (Maeda, Otomo, and Otomo, 2019), is reasonable to suppose that PI3KC1 is needed nearby this complex to ensure the proper enrichment of PI3P for the overall of the autophagosome formation to maintain ATG2 and WIPI on the site.

Therefore, we try to determine the direct binding between the ATG13^{HORMA}-ATG101 complex and the ATG14-BECN1 complex. After purifying the ATG14-BECN1 complex (Figure 3.4a), we performed an *in vitro* pull-down with the co-expressed ATG13^{HORMA}-ATG101 complex (Figure 3.4b). ATG14-BECN1 complex was pulled down in presence of ATG13^{HORMA}-ATG101 (lane 6 compared to lane 3). ATG9 doesn't interact with ATG14/BECN1 complex directly (or the binding is weak) (Figure 3.4c, lane 4 compared to lane 5), therefore we could conclude that the binding between ATG9 and ATG14-BECN1 complex is mediated by the presence of the ATG13^{HORMA}-ATG101 complex.

We also wondered if ATG13-ATG101 could interact with both ATG14-BECN1 and ATG9 and form a five-component complex (Figure 3.4d). In this pull-down, we first assessed that the $^{GST-}$ATG13-ATG101 complex interacts with both ATG9 (lane 4) and the ATG14-BECN1 (lane 5) complex when incubated for 1h on ice and then pulled for GST. This confirmed the findings shown in Figure 3.1a and Figure 3.4b. In the same pull-down, we checked if the order of assembly would matter for the formation of the five-component complex. We preformed the complexes between $^{GST-}$ATG13-ATG101 with ATG9 (lane 6) or ATG14-BECN1 (lane 7) by incubation for 1h on ice. After binding these samples to GST beads, ATG14-BECN1 was added to the ATG9-ATG13-ATG101 complex (lane 6) and *vice versa* (lane 7) and incubated for an additional 1h on ice.

The prays were added in large excess compared to the bait and all the unbound was washed away after incubation on beads. No discernable difference was observed between the pulldowns, so we concluded that there is no obvious order of assembly and that the binding of ATG14-BECN1 and ATG9 to ATG13-ATG101 is not mutually exclusive.

In lane with this data, Anh Nguyen also performed a preliminary SEC and XL-MS (in collaboration with Iwan Parfentev) showed that ATG14-BECN1, ATG13^{HORMA}-ATG101, ATG9, ATG2-WIPI4 form a stable 7-component complex, supporting the hypothesis that they can form a super-complex.

Taken together, we can now propose an updated model where ATG14-BECN1 interacts directly with the ATG13-ATG101 complex (this work). They all might congregate at the IM (Matsunaga *et al.*, 2010), where the PI3KC1 kinase converts PI to PI3P (Choi, Houdek, and Anderson, 2018). WIPI4 binds to PI3P and ATG2, enhancing lipid transport from the ER to the omegasome mediated by the lipid transferase activity of ATG2 (Maeda, Otomo, and Otomo, 2019). ATG9 vesicle is recruited to the phagophore and fuses, probably temporarily (Yamamoto *et al.*, 2012; Karanasios *et al.*, 2016). The lipid scramblase flips lipids from the outer leaflet to the inner leaflet of the IM to re-equilibrate lipid distribution (Maeda *et al.*,2020; Matoba *et al.*, 2020). ATG13-ATG101 colocalize with ATG9 at the ERES (Karanasios *et al.*, 2016) and interact with it (this work) and accelerate the lipid transfer activity of ATG2 (Anh Nguyen, unpublished data) (Figure 3.4e). Therefore, the ATG13-ATG101 complex forms an interaction hub for bridging the PI-to PI3P converting-complex PI3KC1 to PI3P-sensor WIPI4 and actively accelerates the lipid transfer activity of ATG2 (Supplementary Figure 1).

Figure 3.4 The ATG13^{HORMA}-ATG101 complex bridges ATG9 to ATG14-BECN1 complex

(a) SEC of co-expressed $^{GFP-}$ATG14-BECN1 complex on s200 60/600 High Load column. The elution profile of molecular weight standards is shown as a gray line with the native molecular mass of each standard indicated. Coomassie blue-stained SDS-PAGE of fractions with elution volumes from 10 to 20 ml is shown in the bottom panel; **(b)** *In vitro* affinity PD assay between recombinantly purified $^{GST-}$ATG13^{HORMA}-ATG101 co-expressed complex and $^{GFP-}$ATG14-BECN1 co-expressed complex. The samples were incubated with GST or Ni-NTA agarose beads for 1h on ice. The results were analyzed by SDS-PAGE; **(c)** *In vitro* affinity PD assay between recombinantly purified $^{MBP-}$ATG9 and $^{GFP-}$ATG14-BECN1 co-expressed complex. The samples were incubated with MBP agarose beads for 1h on ice. The results were analyzed by SDS-PAGE; **(d)** *In vitro* affinity PD assay between recombinantly purified $^{GST-}$ATG13^{HORMA}-ATG101 complex and $^{GFP-}$ATG14-BECN1 co-expressed complex (lanes 5 and 7) and/or ATG9 (lanes 6 and 8). After incubation for 1h on ice, the samples were incubated with beads for 10 minutes and then washed to remove excess pray. In

lanes 5 and 6 were added 30ul of buffer, while in lanes 7 and 8 were added an excess of ATG14/BECN1 and ATG9, respectively, in a volume of 30ul for an additional 1h on ice. The results were analyzed by SDS-PAGE; **(e)** schematic representation of the direct interactions determined in (b) and (c); **(f)** proposed model of subcomplexes formation and binding.

Figure 3.4

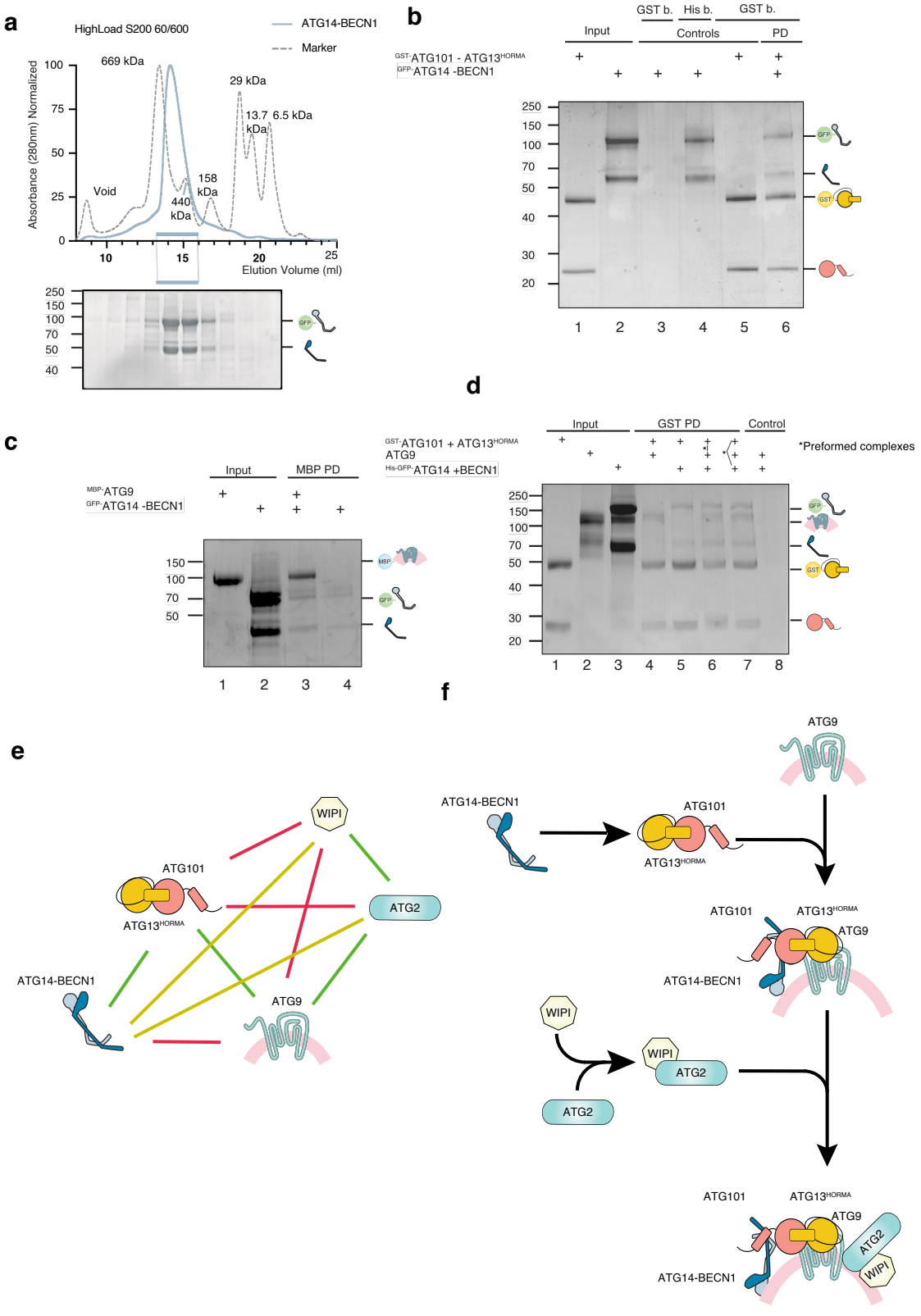

3.5 ATG13 and ATG101 interaction to ATG9 is slow but is accelerated by dimerization

As previously stated, both ATG13 and ATG101are HORMA domain proteins (Jao *et al.*, 2013a, 2013b; Michel *et al.*, 2015; Qi *et al.*, 2015; Suzuki *et al.*, 2015a). HORMA domains proteins are known for their metamorphic behavior. A metamorphic protein is a single amino acid sequence that spontaneously adopts various folded conformations and interconverts reversibly between them (Murzin, 2008). MAD2 is the most studied HORMA. It is part of the MCC (mitotic checkpoint complex), a regulator of the spindle assembly checkpoint (SAC) which delays chromosomal segregation to ensure genome stability. MAD2 converts between two different topologies (open -O- and closed -C-) depending on the change of topology. Two regions of the proteins are involved: the N-terminus and the C-terminus. The energy necessary for a topological change of these two regions within MAD2 itself is a rate-limiting step for the binding to CDC20 and the MCC complex assembly (Mapelli *et al.*, 2006, 2007; Simonetta *et al.*, 2009; Faesen *et al.*, 2017). The conversion C to O is spontaneous but the speed at which this conversion happens is not sufficient to ensure an appropriate rate of MCC complex assembly. Indeed, catalytic activation of the SAC is dependent on controlled protein-protein interactions, which speed up the spontaneous but MAD2 rate-limiting conversion necessary for MCC assembly (Faesen *et al.*, 2017). An asymmetric dimerization between O-MAD2 and C-MAD2 is part of the essential interactions that need to happen to accelerate the conversion from O to C and ensure an optimal response in an appropriate time frame.

The ATG13^{HORMA}-ATG101 dimer is structurally comparable to the MAD2 asymmetric dimer, where ATG13 resembles the C-MAD2 conformer, while ATG101 has structural features more similar to the O-MAD2 (Luo *et al.*, 2002; Sironi *et al.*, 2002; Qi *et al.*, 2015; Suzuki *et al.*, 2015a). Therefore, we questioned whether the dimerization of ATG13^{HORMA} with ATG101 could also accelerate the association between the two HORMA domain proteins to ATG9. We set up a time course pull-down for this purpose. When 0.3 μM of ATG9 was incubated with 0.1μM concentration of ATG13^{HORMA}-ATG101 complex fused to glutathione S-transferase (GST), it reached maximal binding in roughly 30~60 minutes on ice (Figure 3.5a). The ATG9 is in excess to prevent concentration-dependent variations in the binding rate. The quantification shows how the reaction slowly reached equilibrium, plateauing around 30~60 minutes on ice (Figure 3.5b). However, when ATG9 was incubated with an isolated ATG13^{HORMA} or ATG101, the reaction took almost 24h at 20ºC (Figure 3.5c). ATG13 and ATG101 interact extremely slowly with ATG9, but the dimerization between the two HORMAs accelerates the binding rate.

A similar experiment was performed by Simonetta and colleagues using MAD2^{WT} and a MAD2 mutated on the dimerization interface (Simonetta *et al.*, 2009). The main difference is that we have two different HORMA domain proteins and therefore we have the advantage we can isolate the two proteins and perform the kinetics experiment without mutations. However, a perfect control for our experiments would have also been a dimer interface mutant (I131, R133, V134, Y138; Qi *et al.*, 2015; Wallot-Hieke *et al.*, 2018). Unfortunately, the binding between ATG101 and ATG13^{HD} was not completely abrogated *in vitro* as expected.

Figure 3.5

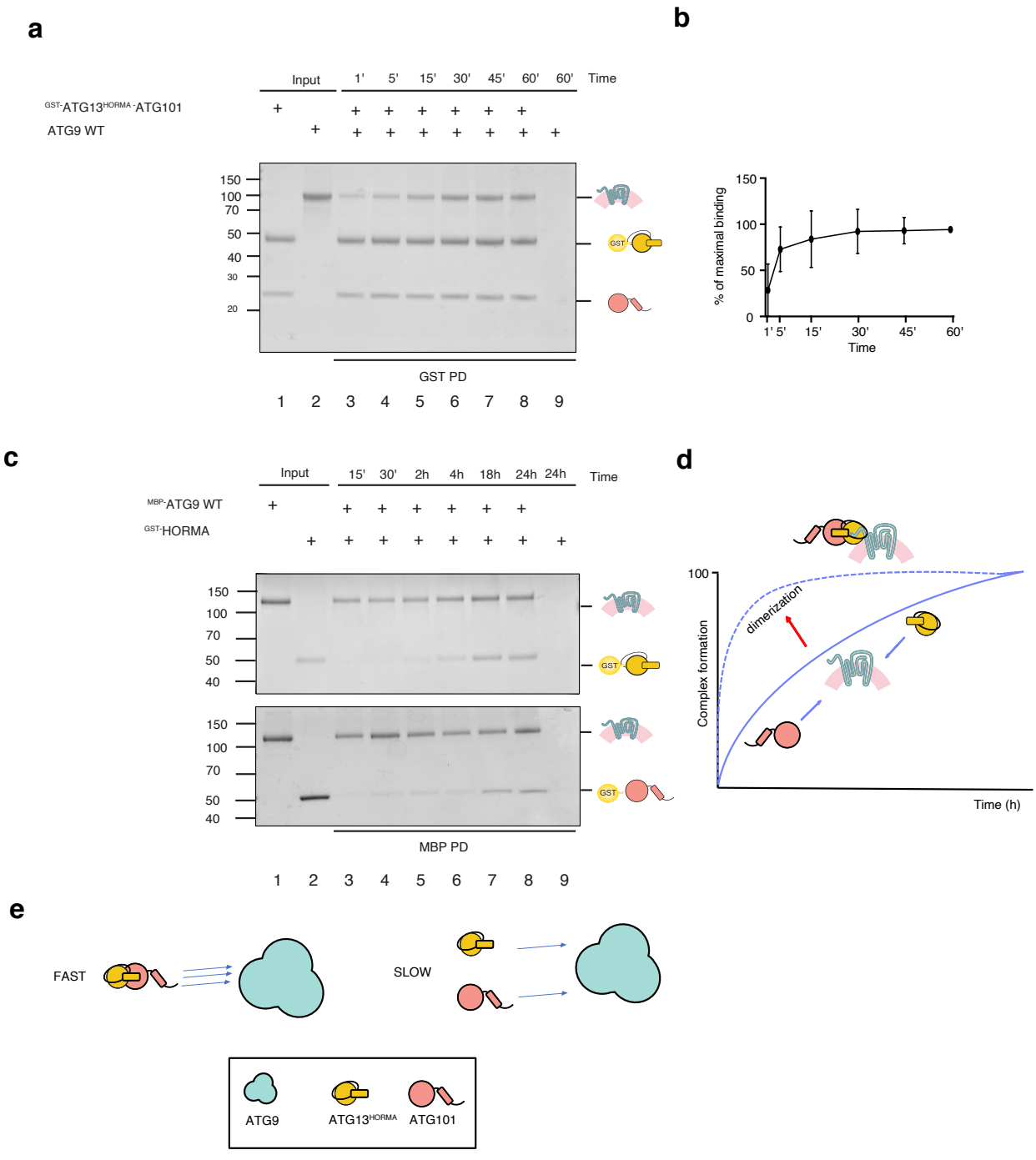

Figure 3.5 ATG13-ATG101 dimer formation accelerates the binding to ATG9

(a) *In vitro* PD kinetics assay performed with $^{GST-}$ATG13^{HORMA}-ATG101 co-expressed complex and ATG9. ATG13-ATG101 were preincubated with the GST beads. ATG9 was incubated with ATG13-ATG101 for the time indicated on ice. The results were analyzed by SDS-PAGE; **(b)** quantification of (a) **(c)** *In vitro* PD kinetics assay performed using $^{GST-}$ATG13^{HORMA} or $^{GST-}$ATG101 with $^{6XHis-MBP-}$ATG9. ATG9 was incubated with ATG13 or ATG101 for the time indicated at 20ºC and subsequently incubated with the beads MBP beads. The results were analyzed by SDS-PAGE; **(d)** schematic representation of the kinetics profile determined in (a) and (b); **(e)** proposed model of complexes formation and binding speed.

Overall, these data suggest that, in a typical HORMA-manner, ATG13 and ATG101 interaction to ATG9 is slow, but the dimerization accelerates the complex formation. We suspect that this might be relevant for the autophagy initiation where ATG13-ATG101 has an important role in accelerating the complex formation with ATG9.

3.6 ATG13-ATG101 interacts with the N-terminus and the C-terminus of ATG9 with a different kinetics

After establishing that ATG9 binds ATG13 and ATG101 we were interested in determining the binding region(s) in ATG9. HORMAs usually bind specific motifs within unstructured regions of their binding partners (Sironi *et al.*, 2002b; Hanafusa *et al.*, 2010). Yeast Atg9 is structurally similar to ATG9 from mammals(Guardia, Christenson, *et al.*, 2020; Guardia, Tan, *et al.*, 2020; Maeda *et al.*, 2020; Matoba *et al.*, 2020). They differ however in the length of the N-terminus (~318 for Atg9^{N} and ~60 for ATG9^{N}), and the C-terminus of human ATG9 is slightly longer than the yeast one (509-839 for ATG9 and 747-997 in Atg9). Before the publication of the structure, we used an online tool, IUPred, to identify Intrinsically Disordered Proteins Regions (IDPR) and design truncations of the cytosolic regions (Erdos, Pajkos and Dosztányi, 2021) (Supplementary Figure 2a and Figure 3.6a). Like the N-terminus (Supplementary Figure 2c), the C-terminus of ATG9 is mostly unstructured with a few predicted helices by AlphaFold (Supplementary Figure 2b). A sequence alignment of the N-terminus of ATG9 of different organisms (Figure 3.9a) shows that residues ~17 to 43 of the human ATG9 are conserved (the residues after 43 until 60 form an α-helix and also conserved, Supplementary Figure 2). We designed three different truncations of ATG9 which include the transmembrane domains for stability. Indeed, we could express and purify these truncations with good yields: ATG9^{core+C} (43-839), ATG9^{N+core} (1-509), and ATG9^{core} (43-509). The 'core' comprises the transmembrane domains

(see Figure 3. for more details). Anh Nguyen confirmed that the shortest of the truncations, $ATG9^{core}$, could be inserted into liposomes like $ATG9^{WT}$.

Next, we performed pull-down experiments with these ATG9 truncations and ATG13-ATG101. In order to prevent unclear/intermediate results which would interfere with the interpretation of the data in case of kinetics variations caused by the use of truncations, we prolonged the incubation of the ATG13-ATG101 complex up to 18h on ice. After incubation, the proteins were pulled for GST and analyzed by SDS-PAGE (Figure 3.6b). $ATG9^{core+C}$, $ATG9^{N+core}$, and $ATG9^{WT}$ (lanes 6, 7, and 8) were all pulled down in presence of the HORMA dimer, while the $ATG9^{core}$ was not (lane 9). This indicates that both the N-terminus and the C-terminus are directly interacting with ATG13-101. This result agrees with the XL-MS shown in Figure 3.2c, where most of the crosslinks were localized at the $ATG9^{C}$.

In order to deconvolute how ATG13 and ATG101 bind to these specific regions, we assessed the kinetics of the interaction between the truncations and the dimer of ATG13-ATG101. Surprisingly, the binding kinetics between the $ATG13^{HORMA}$-ATG101 complex and the N-terminus or C-terminus of ATG9 were not identical (Figure 3.6c). Using the same setup as in figure 3.5a, we could notice how the $ATG9^{N+core}$ binding to $ATG13^{HORMA}$-ATG101 complex could not be completed in 1h on ice (Figure 3.6c, yellow panel) compared to $ATG9^{WT}$ and $ATG9^{core+C}$ (Figure 3.6c, green and blue panel). We concluded that the binding of the HORMAs to the $ATG9^{N}$ is slow, similar to the binding kinetics of the individual monomers and that the dimer formation is insufficient to accelerate the interaction to a speed comparable to the one observed with WT or the C-terminus. This data suggests that associating the ATG13-ATG101 complex to $ATG9^{N}$ requires higher activation energy compared to the C-terminus. One probable hypothesis is that either ATG13 or ATG101 has easier access at the C-terminus rather than at the N-terminus. If this is true, it would also suggest that the interaction at the N-terminus might be the rate-limiting step of the assembly and, possibly, the C-terminus interaction might aid in the association to the N-terminus.

We could summarize this data as follows (Figure 3.6e). There are two bindings sites for the $ATG13^{HORMA}$-ATG101 complex: one at the N-terminus and one at the C-terminus of ATG9. However, a difference was observed in the binding kinetics: whereas the binding speed at the C-terminus is equivalent to that of the full-length protein, the binding of $ATG13^{HORMA}$-ATG101 at the N-terminus of ATG9 is substantially slower, equivalent to that of the HORMA monomers binding to the full-length protein. The interaction between ATG9 and ATG13-ATG101 is completely impaired upon deletion of both regions.

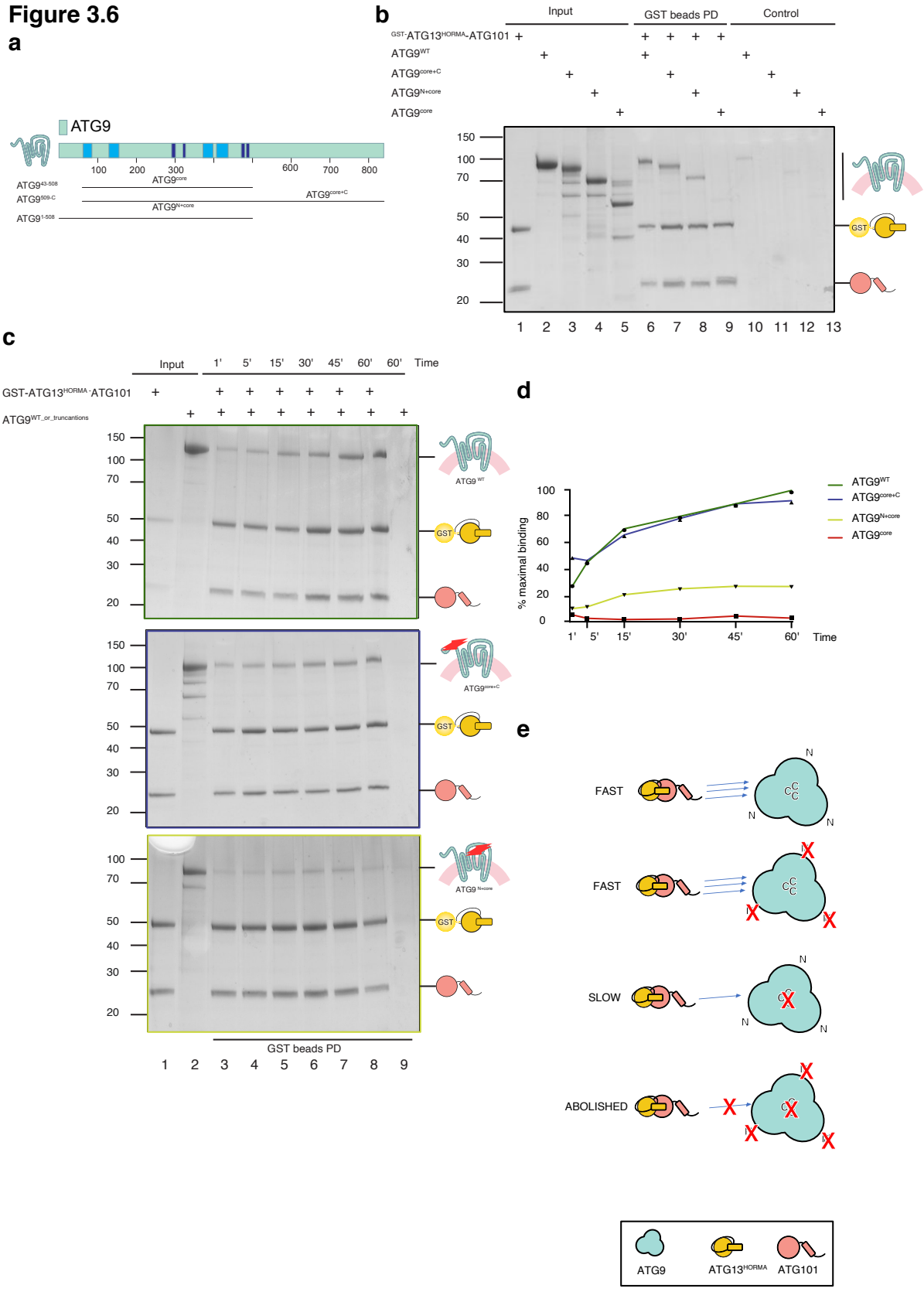

Figure 3.6 ATG13-ATG101 dimer binds the N-terminus and the C-terminus of ATG9 with a different kinetics

(a) Schematic representation of the truncations of ATG9 used in this figure **(b)***In vitro* affinity PD assay performed with $^{GST-}$ATG13^{HORMA}-ATG101 complex and ATG9$^{\Delta WT}$, ATG9^{core+C} (43-839), ATG9^{N+core} (1-509), or ATG9^{core} (43-509). ATG9 was incubated with ATG13-ATG101 for 18h on ice and subsequently incubated with beads. The results were analyzed by SDS-PAGE; **(c)** *In vitro* PD kinetics assay performed with $^{GST-}$ATG13^{HORMA}-ATG101 co-expressed complex and ATG9$^{\Delta WT}$, ATG9^{core+C} (43-839), ATG9^{N+core} (1-509), or ATG9^{core} (43-509). ATG13-ATG101 were preincubated with the GST beads. ATG9 was incubated to ATG13-ATG101 for the time indicated on ice. The results were analyzed by SDS-PAGE; **(d)** quantification of (c) **(e)** schematic representation of the kinetics profile determined in (c).

3.7 ATG13 and ATG101 are different from MAD2

The fact that ATG13 and ATG101 can form interaction to ATG9 at an incredibly slow speed when in isolation, indicates that they undergo a topological change of their unstructured regions (Figure 3.2c), similarly to MAD2 and REV7. In MAD2 and REV7, the conformational change of the unstructured regions implies a rearrangement of the N-terminus and the C-terminus (Figure 1.5a and b). The C-terminus, through this rearrangement, can interact with the HORMA binding partner (CDC20 for MAD2 and SHLD3 for REV 7) (Lou *et al.*, 2000; Liang *et al.*, 2020). The 'seatbelt' is the region within the C-terminus that forms this interaction(Sironi *et al.*, 2002b). There are different mutants in MAD2 that have been created to trap the protein in either the O or C conformer. A summary of the specific mutant and the topology associated are listed in Figure 3.8a. We wanted to characterize the autophagy HORMAs conversion by evaluating the effect of mutations using MAD2 as a starting model. The first mutants that we developed are termed HORMA$^{\Delta C}$. One elegant way to establish the topology of a mutant is to use an anion exchange (AE) column which allows the separation of proteins depending on their surface charge (Luo *et al.*, 2002; Mapelli *et al.*, 2007). When a protein undergoes extensive topology change, it might have two different elution profiles. This approach requires to be combined with a binding test of the eluted fractions with the binding partner to determine which of the two conformations is the 'active' one, that is the one that interacts with the binding partner. It is also possible that a conformational change doesn't alter the overall charge of the protein so extensively to be able to detect a peak separation of the conformers and therefore it is very important to combine these two techniques. Various studies show that MAD2$^{\Delta C}$ mutant elutes as O-MAD2 and it is incapable of interacting with CDC20. In this mutation, part of the region following the 'seatbelt' is removed and, therefore, the MAD2 closure is impaired by a weakened 'seatbelt' docking.

We wanted to assess whether the seatbelt of ATG13 and ATG101 is involved in this conformational change and, in particular, directly interacting with ATG9. Therefore, the first mutants we used are two different versions of the ΔC mutants: ΔC (weakened docking) and Δseatbelt (Figure 3.7c), where the complete seatbelt is removed. We tested the interaction between ATG9 and the HORMA$^{\Delta seatbelt}$ mutants by a kinetics pull-down experiment. However, contrarily to MAD2, where the interaction between MAD2$^{\Delta C}$ mutant and CDC20 is abolished, the HORMA $^{\Delta seatbelt}$ mutants were still able to bind ATG9 and we were unable to detect any discernible change between the kinetics of HORMA^{WT} or HORMA$^{\Delta seatbelt}$ (Figure 3.7a). The trends are shown in Figure 3.7b. This data indicates that the seatbelt of ATG13 and ATG101 is not directly supporting the interaction with ATG9 and are not the factor that creates the energy barrier.

Figure 3.7

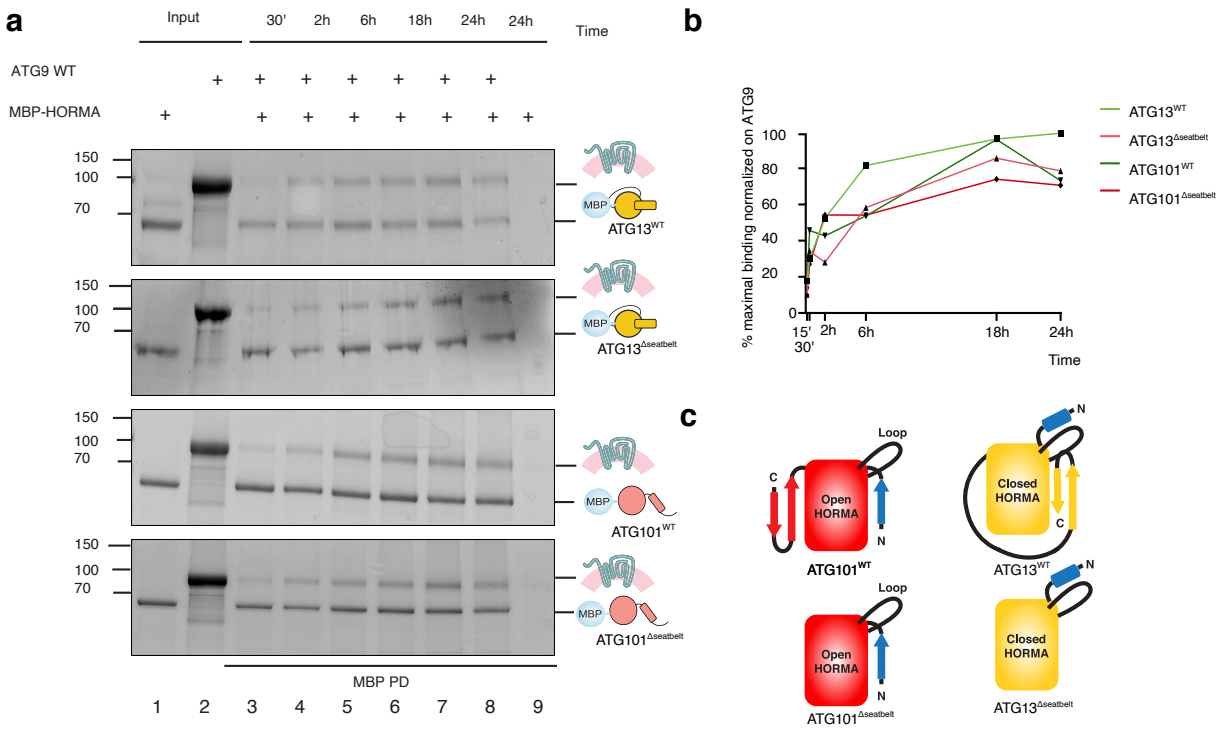

Figure 3.7 Autophagy HORMAs$^{\Delta seatbelt}$ mutants can still interact with ATG9

(a) *In vitro* PD kinetics assay performed with $^{6XHis\text{-}MBP}$-ATG13^{WT}, $^{6XHis\text{-}MBP}$-ATG13$^{\Delta seatbelt}$, $^{6XHis\text{-}MBP}$-ATG101^{WT} or $^{6XHis\text{-}MBP}$-ATG101$^{\Delta seatbelt}$ and ATG9. ATG9 was incubated to ATG13 and ATG101 for the time indicated at 20°C. The results were analyzed by SDS-PAGE; **(b)** quantification of (a); **(c)** Schematic representation of the mutants used in this assay

3.8 The dimerization of ATG13-ATG101 is regulated by the conformation of ATG13

One important aspect of HORMAs is that their dimerization is restricted to opposite conformers (DeAntoni *et al.*, 2005; Mapelli *et al.*, 2006) (Figure 3.8b). If two HORMA can interact, they have an opposite conformation, with the only exception of $p31^{comet}$ which is unique (See introduction and discussion for more information). Different MAD2 mutants have different conformations, therefore they would only bind to form an asymmetric dimer.

We decided to test the autophagic HORMA domain proteins for the dimerization of opposite conformers and used different mutants for this purpose modeled on MAD2 known mutants. We performed a pull-down (Figure 3.8c) where $^{GST}ATG101^{WT}$ was first bound to GST beads and then incubated with three different mutants of $ATG13^{HORMA}$ for 1h on ice: $ATG13^{\Delta seatbelt}$, $ATG13^{\Delta N,}$ or $ATG13^{LL}$. This showed that the $ATG13^{WT}$-$ATG101^{WT}$ dimer is formed in 1h on ice (Figure 3.8c, lane 7). We also noticed that the $ATG13^{\Delta seatbelt}$ -$ATG101^{WT}$ binding was impaired (Figure 3.8c, lane 9) and $ATG13^{\Delta N}$ -$ATG101^{WT}$ and $ATG13^{LL}$ -$ATG101^{WT}$ were completely abrogated (Figure 3.8c, lanes 8 and 10). One possible explanation of this behavior would be that the Δseatbelt mutation might have altered the conformational state of ATG13 and, consequently, affected the dimerization capacity with fresh ATG101. We supposed that the $ATG13^{\Delta seatbelt}$, used in Figure 3.8c, was potentially a mixture of O and C topologies, while $ATG13^{WT}$ equilibrium was more shifted towards just one. This could explain why ATG101 could readily interact with $ATG13^{WT}$ and not with $ATG13^{\Delta seatbelt}$. We performed a kinetics assay to assess if $ATG13^{\Delta seatbelt}$ would shift the equilibrium among the conformers over time. $ATG13^{WT}$ or $ATG13^{\Delta seatbelt}$ were incubated at 20ºC to aid in the conversion (Figure 3.8e) before adding to $^{GST}ATG101^{WT}$ pre-incubated beads. The samples were loaded on SDS-PAGE gel and visualized with Coomassie-Blue stain. From the quantification in Figure 3.8f, it is clear how the $ATG13^{WT}$ completed its binding to $ATG101^{WT}$ almost immediately, while the $ATG13^{\Delta seatbelt}$ required roughly 6h to do the same.

The assay in Figure 3.8c was done in order to assess the topological state of the proteins upon purification. Indeed, one important aspect of HORMA domain proteins is that they have a preferred topology that is regulated by the energy barrier. If one of the two topologies presents a lower energetic state, that one would be preferred and over time, that topology would be in

majority. In eukaryotic cells, MAD2 is mostly held in the O conformation (Luo *et al.*, 2004; DeAntoni *et al.*, 2005; de Antoni *et al.*, 2005; Mapelli *et al.*, 2006, 2007), but can spontaneously convert to the C state *in vitro*. Samples of $MAD2^{WT}$ expressed and purified in *E. coli* are a mixture of both conformations in the absence of MAD1 or CDC20, because these two components favorite the C-MAD2 topology. This is partially a problem because we can't control the state of the conformer at the start of the experiments. Mutants have been developed to trap MAD2 in one of the two conformations at the expression level or to reduce movements of flexible regions for structural determination. $MAD2^{\Delta C}$ is in the open conformation like $MAD2^{WT}$ (Mapelli *et al.*, 2006). Musacchio's lab also designed an elegant 'loopless' (LL) mutant that traps MAD2 in a fixed O state (Mapelli *et al.*, 2007). Other 'open' mutants, like ΔC, are more flexible in the seatbelt region, and thus are not suited for crystallography (Mapelli *et al.*, 2007). The ΔN mutant presents a C conformation upon purification that was assessed by AE (Mapelli *et al.*, 2007). This ΔN, however, was not a locked C-MAD2, because it could convert to O in presence of a CDC20-bound C-MAD2 (DeAntoni *et al.*, 2005; Mapelli *et al.*, 2006). They concluded that $MAD2^{\Delta N}$ favors the C conformation while still competent in converting gradually into O. The $ATG13^{\Delta seatbelt}$ appeared to convert in a similar manner to what was observed in $MAD2^{\Delta N}$. One hypothesis is that in cells, $ATG13^{\Delta seatbelt}$ was in a different topological state (probably higher in energy). Therefore, we can suppose that in cells. $ATG13^{\Delta seatbelt}$ assumes the same topology as ATG101 because they can't interact. This data shows that ATG13 can temporarily assume a different conformation in cells, that slowly changes *in vitro*. This data also supports the idea that the dimerization of ATG13-ATG101 is conformational-dependent. This also suggests that the seatbelt of ATG13, even if it is not involved in directly interacting with ATG9, it has a role in defining the conformation of ATG13 without being the rate-limiting factor of the conversion.

We also performed the same experiment shown in figure 3.8c, with different mutants of ATG101. In this case, the seatbelt deletion did not seem to induce any consequence to the conformational state of ATG101, supporting the idea that the seatbelt in ATG101 does not control the conformational state of ATG101.

Figure 3.8 $ATG13^{\Delta seatbelt}$ mutant can form a dimer with ATG101 after conversion

(a) Summary of the mutants and frequent conformers of MAD2; ATG101-ATG13 conformers summary (Lou *et al.*, 2000; DeAntoni *et al.*, 2005; Mapelli *et al.*, 2006; Simonetta *et al.*, 2009; Qi *et al.*, 2015) **(b)** Schematic representation of the dimerization of known MAD2 conformers **(c)** *In vitro* affinity PD assay performed with ^{GST}ATG101 and the different mutants of ATG13: $^{6XHis\text{-}MBP}$-$ATG13^{\Delta seatbelt}$, $ATG13^{\Delta N}$ or $ATG13^{LL}$. ^{GST}-ATG101 was preincubated with GST beads. ATG13

mutants were incubated with beads for 1h on ice. The results were analyzed by SDS-PAGE; **(d)** quantification of (c); **(e)** *In vitro* PD kinetics assay performed with $^{6XHis\text{-}MBP\text{-}}ATG13^{WT}$ or $^{6XHis\text{-}MBP\text{-}}ATG13^{\Delta seatbelt}$ incubated with $^{GST\text{-}}ATG101^{WT}$. ATG13-ATG101 were incubated for the time indicated at 20ºC, then incubated on GST beads. The results were analyzed by SDS-PAGE; **(f)** quantification of (e), error bars depict only max error, but indicate both max and min error; **(g)** *In vitro* affinity PD assay performed with $^{GST}ATG13$ and different mutants of ATG101: $^{6XHis\text{-}MBP\text{-}}ATG101^{\Delta seatbelt}$, $ATG101^{\Delta N}$ or $ATG101^{LL}$. $^{GST\text{-}}ATG13$ was preincubated with GST beads. ATG101 mutants were incubated with beads for 1h on ice. The results were analyzed by SDS-PAGE; **(d)** quantification of (c);

Figure 3.8

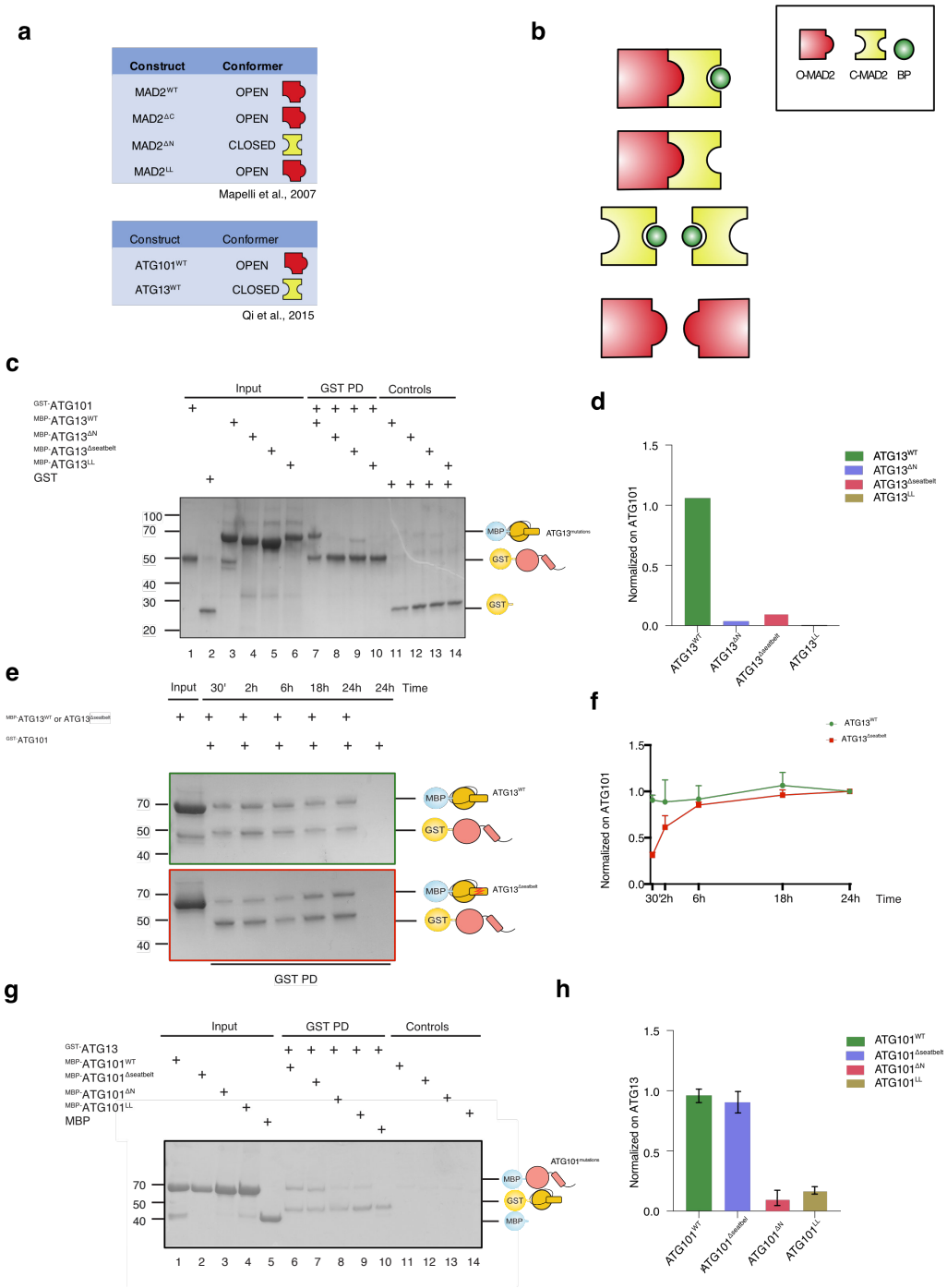

3.9 The interaction at the N-terminus of ATG9 is ATG13 conformer-dependent

In section 3.6 we showed that the binding of ATG13-101 interaction with to ATG9^{N} is much slower than to ATG9^{WT} or ATG9^{core+C}. The most conserved area within ATG9^{N} is directly adjacent to the core, centered around the conserve W37 (Figure 3.9a). The interaction motif of

ATG13 and ATG101 is currently not known and consensus motifs between other HORMA domains are not directly obvious (Sironi *et al.*, 2002b; Luo *et al.*, 2002; Hanafusa *et al.*, 2010). Often, they do include proline and there are indeed two prolines inside the $ATG9^{N}$ and one of them appears to be conserved in all the organisms where ATG101 is also present. We tried to perform a Phage Display assay to identify a consensus motif, however without success. The Phage display experiment shows a very high frequency of alignment to the KSPW region of $ATG9^{N}$ and also some to the two PP but, other than that, we could not extrapolate any definitive consensus. It is also clear from the data that the way in which ATG13-ATG101 interacts with ATG9 does not involve the canonical seatbelt interaction that C-REV7 and MAD2 form with their own specific binding partner.

We confirm a direct interaction between co-expressed ATG13 and $ATG9^{N}$ complex using SEC. The proteins coeluted in SEC with a 1:1 stoichiometry in the typical early elution of ATG13 (Figure 3.9b). To explain the co-expression requirement, we presume that the interaction between $ATG9^{N}$ and ATG13 involves a large activation barrier likely induced by the presence of a region within ATG13 that requires an incredible amount of energy to happen, which is not the C-terminus (Figure 3.7a). Therefore, we investigated whether a change of conformation was necessary for ATG13 to bind $ATG9^{N}$. We performed two pulldowns where we compared the ability of $ATG13^{WT}$, $ATG13^{\Delta C}$, or $ATG13^{\Delta seatbelt}$ to bind either ATG101 or $ATG9^{N}$, at two different times points: with protein fresh from the -80°C and proteins incubated overnight at 20°C. We preincubated the GST beads with either ^{GST}ATG101 or $^{GST}ATG9^{N}$ before adding the mutants. It is important to add that for both experiments, both ^{GST}ATG101 and $^{GST}ATG9^{N}$ are always used fresh. In the first panel (Figure3.9c), we can observe how fresh $ATG13^{WT}$ can interact immediately with ATG101 (first panel, lane 5), but not with $ATG9^{N}$ (first panel, lane 1). In contrast, fresh $ATG13^{\Delta C}$ and $ATG13^{\Delta seatbelt}$ prefer to bind to $ATG9^{N}$ over ATG101 (first panel, lanes 2 and 3 compared to 6 and 7). MBP was used as a negative control since all ATG13 mutants are tagged with MBP (both panels, lanes 4 and 8). After incubating the ATG13 mutants overnight at 20°C, $ATG13^{WT}$ still prefers to bind to ATG101 over $ATG9^{N}$ (second panel, lanes 1 and 5), confirming Figure 3.8c. Strikingly $ATG13^{\Delta C}$ and $ATG13^{\Delta seatbelt}$ switched preferences and favored to interact with ATG101 rather than $ATG9^{N}$ (second panel, lanes 2 and 3 compared to 6 and 7). The quantification of Figure 2.9c is shown in panel d.

Therefore, this experiment verifies the finding that ATG13 requires conversion to interact with $ATG9^{N}$. This also confirms that ATG13 dimerization is conformational dependent as observed previously with MAD2 (Figure 3.8e and f). ATG101 can convert topology, but probably only in presence of ATG9, marking a clear difference between the two HORMAs.

Structural analysis will be needed to fully understand the complex and unusual assembly mechanism of the ATG9-13-101 complex. Until then we decided to use AlphaFold Multimer to elucidate the interaction details between ATG13 and $ATG9^{N}$. AlphaFold Multimer is trained for multimeric protein complexes with known stoichiometry. As a specialized version of AlphaFold, AlphaFold Multimer predicts multimeric interfaces with more accuracy while preserving intra-chain precision (Evans *et al.*, 2021). The $ATG13^{HORMA}$-$ATG9^{N}$ interaction was detected with very high accuracy (over 90 of confidence level) with ATG101, $ATG13^{HORMA}$, and $ATG9^{N}$ as input (Figure 3.9e). pLDDT indicates the per-residue confidence score. Regions with pLDDT > 90 are likely to be accurately predicted. This is important for determining the reliability of the prediction. ATG13 folds as C also in the AlphaFold Multimer prediction. A superimposition of the predicted structure and the structure of Qi *et al.* doesn't show any significant difference: the seatbelt doesn't interact directly with the $ATG9^{N}$ (with the only exception of a salt bridge) and it is still docked on the β5. Most of the interactions between ATG9 and ATG13 happen between the ATG13 core. In particular, β6 and β4 appear particularly involved with hydrophobic residues that interact with both backbone and side-chains of $ATG9^{N}$. The highest confidence is observed at the $ATG9^{N\_W37}$, one of the most conserved residues we identified in the alignments (Figure 3.9a). This particular tryptophan is surrounded by charged and hydrophobic residues. In addition, the αC' has a charged $ATG13^{E64}$ that interacts with $ATG9^{N\_H39}$.

As a comparison, we also tested the $ATG13^{\Delta seatbelt}$-$ATG9^{N}$ complex, which yielded high confidence over a larger region around W37 (Figure 3.9f, second panel). We could not any variation in the conformation of ATG13 also in this case. These predictions will be validated with experiments using point mutants in these predicting interfaces both using purified proteins as well as cell-based assays to evaluate the phenotype of the mutants in cells.

Figure 3.9

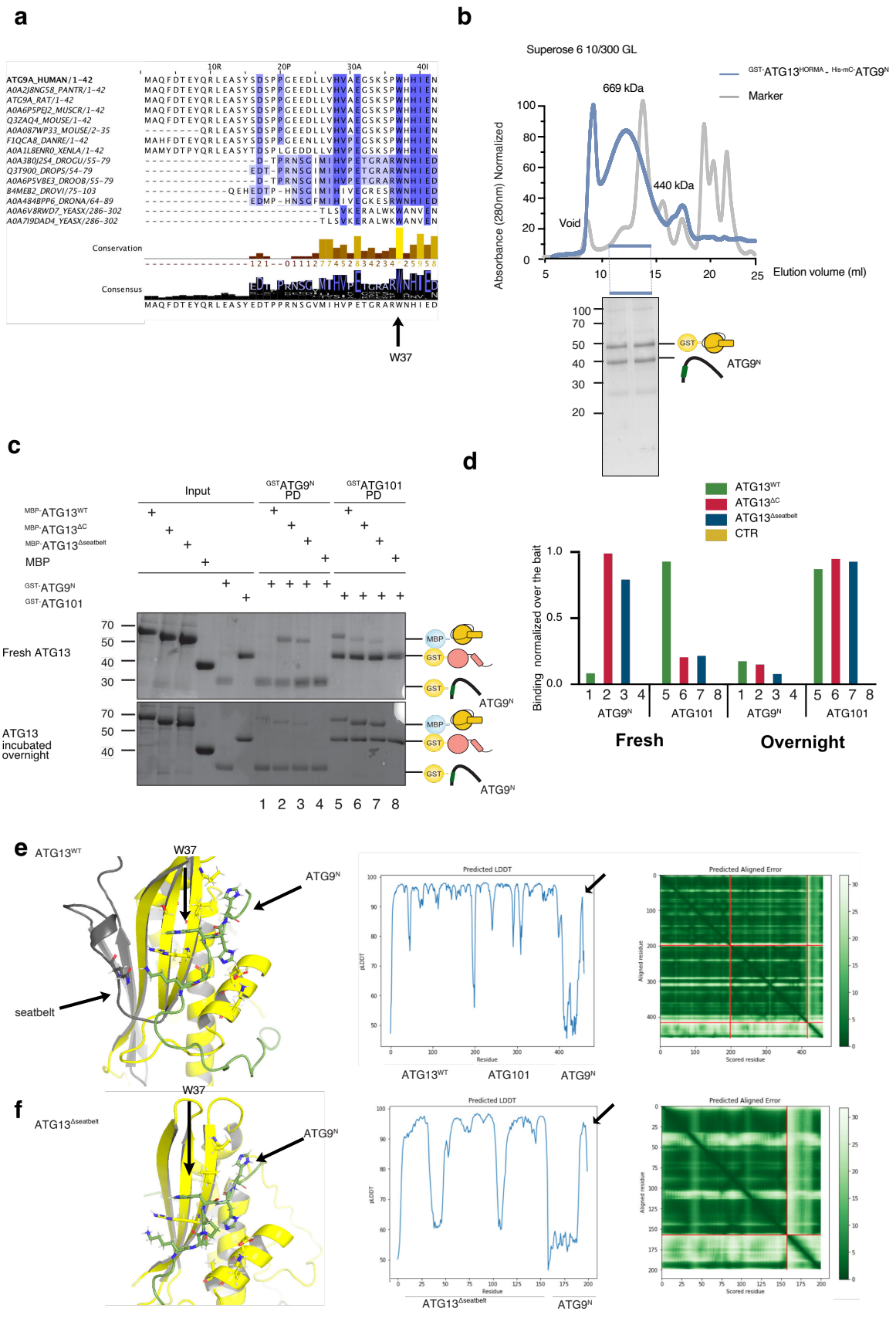

Figure 3.9 ATG13 conformational-dependent binding at the N-terminus of ATG9

(a) sequence alignment of $ATG9^{N}$ of different organisms; W37 is underlined by the arrow; **(b)** SEC of co-expressed $^{GST-}ATG13^{HORMA\_His-mC-}ATG9^{N}$ complex on S6 10/300 GL column. The elution profile of molecular weight standards is shown as a gray line with the native molecular mass of the standard indicated. Coomassie blue-stained SDS-PAGE of fractions indicated is shown in the bottom panel; **(c)** *In vitro* affinity PD assay performed with GST beads preincubated with $^{GST}ATG9^{N}$ and $^{GST}ATG101$. The two proteins were tested for interaction with $^{6XHis-MBP-}ATG13^{WT}$, $ATG13^{\Delta C}$, $ATG13^{\Delta seatbelt}$, or 6XHis-MBP -tag. $^{GST}ATG9^{N}$ and $^{GST}ATG101$ were freshly taken from -80, while ATG13 mutants were either used fresh (first panel), or left overnight at room temperature (second panel). ATG13 mutants were incubated for 5 minutes at on ice, then incubated with beads with pre-bound $^{GST}ATG9^{N}$ or $^{GST}ATG101$. The results were analyzed by SDS-PAGE; **(d)** quantification of (c); **(e)** AlphaFold Multimer prediction for the interaction between $ATG13^{HORMA}$ and $ATG9^{N}$ (ATG101 was included in the prediction); LDDT plot and predicted alignment error matrix shown on the side **(f)** AlphaFold Multimer prediction for the interaction between $ATG13^{\Delta seatbelt}$ and $ATG9^{N}$ (ATG101 was included in the prediction); LDDT plot and predicted alignment error matrix shown on the side

Overall, the data confirm that ATG13 and ATG101 can convert topology and bind directly to ATG9. At least for ATG13, conversion seems not to be energetically controlled and the conversion is necessary for ATG13 to interact with $ATG9^{N}$. ATG101 has a role in facilitating this conversion while also directly interacting with ATG9. The ATG13-ATG101 complex can bind two regions within ATG9, but the interaction at the N-terminus might represent the rate-limiting step for the formation of the accelerating unit composed by ATG9-ATG13-ATG101 involved in accelerating the lipid transfer activity of ATG2 and subsequent membrane expansion at the ER contact sites. We also propose that ATG13-ATG101 might create a hub for the initiation complexes by bridging the ATG14-BECN1-containing PI3KC1 and the membrane expansion active unit of ATG9-ATG2-WIPI4.

Model and supplementary figures are described in the discussion section.

4 Discussion

4.1 The use of the reconstitution method to explore autophagy initiation

ATG101 and ATG13 are the least explored out of all the HORMA domain proteins in mammals. This thesis provides insights into how two HORMA domain proteins, ATG13 and ATG101, interact with key components of the Autophagy initiation and regulate the complex formation. We determined, by characterizing the interaction kinetics of ATG13-ATG101-ATG9 complex formation, that ATG13 and ATG101 binding to ATG9 is slow and might represent the rate-limiting step for the autophagosome formation and expansion. We also determined that the ATG13 presents a metamorphic behavior that regulates the ATG13 propensity to form different interactions under different states. To prove this, we created a set of mutants similar to the ones previously described for other components of the HORMA domain family (Mapelli *et al.*, 2006, 2007; Simonetta *et al.*, 2009). We defined that ATG13 diverges from the canonical HORMA domain protein family component MAD2 in that it interacts with a binding partner without the typical seatbelt being actively participating in the direct interaction.

We also participated in a large-scale reconstitution effort together with Anh Nguyen in order to recapitulate the autophagy initiation at the ER contact sites and gain mechanistic insights into how autophagy machinery is recruited and formed under the guidance of these unique and uncharacterized HORMAs. To comprehend the intricacies and spatiotemporal regulation of autophagy, we focused our work on the use of *in vitro* techniques with purified and isolated components, while maintaining regulated conditions. This work was pursued in order to determine the minimal elements necessary to regulate the elegant but complicated biological activity that is the autophagosome nucleation and expansion at the ER contact sites (Moparthi and Wollert, 2019).

4.2 The impact of ATG13-ATG101 dimerization in Autophagy

In vitro systems have the great advantage to create biochemically-defined settings by limiting the number of variables that have to be considered when working with complex systems like cells (Laohakunakorn *et al.*, 2020). The biophysical properties of *in vitro* isolated components frequently do not always directly relate to their activities *in vivo* (Moparthi and Wollert, 2019). Combining *in vitro* and *in vivo* assays has proven to be a feasible way for circumventing this limitation. As a result, it has been critical for us to open communication with the Stork's Lab in Dusseldorf to find support for our findings.

In its previous work, Stork noted how mutating the interaction interface between ATG13-ATG101 impairs both ULK1 complex formation and autophagic flux (Wallot-Hieke *et al.,* 2018). However, they could not pinpoint whether the inhibitory effect on the autophagic flux was the secondary consequence of the missed ULK1 complex formation (Wallot-Hieke *et al.,* 2018) or the effect of the different roles that ATG13 and ATG101 might exert during autophagy progression that are ULK1-independent (H. Suzuki *et al.*, 2015b; Alers *et al.*, 2011; Hieke *et al.*, 2015; Kannangara *et al.*, 2021). Indeed, most ATG13-ATG101 are free circulating in the cells, and do not take part in the ULK1 kinase complex (Hosokawa *et al.*, 2009; H. Suzuki *et al.*, 2015c; Wallot-Hieke *et al.* 2018). Recently, a BioID screen identified ATG13-ATG101 as a potential interactor of ATG9 (Kannangara *et al.*, 2021). A BioID is a screen that searches for protein interactions within cells. A biotin ligase (Bir A) is employed by fusion to a protein of interest and expressed in cells. The ligase biotinylates proximal endogenous proteins based on their proximity. Streptavidin beads are used to bind biotin-labeled lysine residues from trypsin-digested proteins. The enriched peptides are then detected and identified by MS. They noticed how ATG13 was necessary for the interaction of ATG9-ATG101, while ATG101 was required for the interaction of ATG9A-ATG13 (Kannangara *et al.*, 2021). They propose that, during basal autophagy, the ATG13-ATG101 complex interacts with ATG9A to drive p62/SQSTM1 autophagic turnover and the binding between ATG13 and ATG101 seems to be essential for supporting this activity (Kannangara *et al.*, 2021). All this data correlate with the findings that ATG13-ATG101 dimerization is essential for accelerating ATG13 and ATG101 binding to ATG9 (Figure 3.5).

4.3 The impact of ATG13-ATG101 dimerization in starvation-induced Autophagy

We still missing the crucial information that ATG13-ATG101 dimerization is required for interaction with ATG9 in ULK1-dependent autophagy and that the ATG13-ATG101-FIP200-ULK1 complex directly interacts with ATG9 and forms a stable complex.

It is very likely that this HORMA-mediated regulation is not limited to the ULK1-independent pathway (Kannangara *et al.*, 2021), but is also essential for the starvation-induced autophagy pathway (Wallot-Hieke *et al.,* 2018). Wallot-Hieke's fractionation experiment (Wallot-Hieke *et al.,* 2018, Figure 5B) showing that the ULK1 complex does not form upon mutation of the ATG13-ATG101 interface, might also be explained by the fact that ULK1 and FIP200 are part of a major complex where also ATG9 is present together with ATG13-ATG101. Indeed, there is no other information that the HORMA domain of ATG13 and ATG101 is structurally essential for the ULK1 complex formation. One important experiment that could be done to address this point is performing the same fractionation experiment but selecting other components of the

autophagy initiation (ATG9, but also WIPI4, ATG2, and ATG14/BECN1, etc.) and comparing the fractions shifts of said proteins in cells lines with mutated ATG13 or ATG101 ($ATG13^{\Delta seatbelt}$, $ATG13^{\Delta N}$, $ATG101^{\Delta seatbelt}$, $ATG101^{\Delta N}$) and $ATG9^{N}$ (W37, e.g.).

In support of the fact that ULK1 might also take part inside this complex, at least under starvation-induced autophagy, are the work of Suzuki *et al.*, showing that Atg13-Atg9 interaction in yeast is enhanced upon starvation-mediated autophagy induction (S. W. Suzuki *et al.*, 2015b), and the fact that ULK1 also phosphorylates ATG9 to regulate its trafficking from the TGN in response to starvation (Young *et al.*, 2006; Egan *et al.*, 2015; Zhuo *et al.*, 2017).

4.4 Can also FIP200 be part of the ATG9-ATG13-ATG101 complex?

FIP200 is also regarded, in the canonical hierarchy of autophagy proteins (Suzuki *et al.*, 2007), to be the first protein to localize at ER-localized phagophores (Itakura and Mizushima, 2010; Orsi *et al.*, 2012). In the context of an ULK1-independent pathway, ATG13-FIP200 activity is inter-dependent (Alers *et al.*, 2011; Turco *et al.*, 2019; Shi *et al.*, 2020). It is not surprising that the phenotype of *ATG13*-/- MEF is not distinguishable from *FIP200* -/- MEF (Hara *et al.*, 2008). It appears that FIP200 scaffolding activity might be dependent on ATG13. Indeed, the FIP200 N-terminal domain is flexible but assumes a C-shaped structure when ATG13 is present (Shi *et al.*, 2020) which might be an important aspect of the scaffolding role FIP200 exerts in autophagy. Unfortunately, the lack of full-length ATG13 and FIP200 availability has impaired the biophysical characterization of this complex.

Atg17 (homolog of FIP200), together with Atg13-Atg1-Atg31-Atg29 (Atg1 complex, homolog of ULK1 complex) tethers Atg9 vesicles *in vitro*. Therefore, Atg17 has been proposed to directly bind to Atg9 (Rao *et al.*, 2016a). The fact that FIP200 binds p62/SQSTM1 and forms a scaffold around the condensates, supports the idea that also FIP200 might also take part in the ATG13-ATG101-ATG9 complex, at least in the context of ULK1-independent autophagy (Turco *et al.*, 2019). In this context, the recruitment of the ATG13 and the PI3KC1 to the condensates does not need FIP200, which is instead essential to appropriately anchor ATG13 and ATG9A vesicles by forming cup-shaped structures around p62 condensates (Turco *et al.*, 2019). Turco also noted how FIP200 is required for PIP3 production and the recruitment of WIPI2 (Turco *et al.*, 2019). From our findings and the collaboration with Anh Nguyen, we discovered that ATG13-ATG101-ATG9-ATG2-WIPI4 form a stable complex (Figure 3.3a, Figure 3.2), as well as ATG13-ATG101-ATG9-ATG14/BECN1 (Figure 3.4). Preliminary data from Anh Nguyen coupled with XL-MS also indicate that all these proteins form a single complex. FIP200 might take part in this complex for its scaffolding function. We can speculate that FIP200 influences ATG13-ATG101-

ATG9 localization and only indirectly, the PI3KC1 (Matsunaga *et al.*, 2010; Obara and Ohsumi, 2011; Jao *et al.*, 2013b, 2013c; Park *et al.*, 2016). On the other side, ATG2 is recruited by WIPIs at the PI3P-enriched membranes only in presence of the PI3KC1 (Obara, Sekito and Ohsumi, 2006; Obara, Sekito, *et al.*, 2008; Obara and Ohsumi, 2011; Chowdhury *et al.*, 2018; Otomo, Chowdhury, and Lander, 2018). This data supports the idea that ATG13-ATG101 are at the functional apex of autophagy in both ULK1-dependent and independent pathways.

4.5 How constitutive is the ATG13-ATG101 dimer?

Different publications propose that, in cells, ATG101 role is to protect ATG13 from proteasomal degradation, and expressing ATG13 in isolation from ATG101 is not possible (Mercer, Kaliappan and Dennis, 2009; H. Suzuki *et al.*, 2015b; Qi *et al.*, 2015). Therefore, the ATG13-ATG101 dimerization is not considered a particularly dynamic interaction. However, our collaborator observed a significant drop in fluorescence signal in HTRF assay when an untagged ATG101 was added to a preformed labeled-ATG13-ATG101 complex (Annabelle Friederich, Stork Group, Dusseldorf). Homogeneous time-resolved fluorescence (HTRF) assay uses the FRET principle where there is a transfer of energy between a donor and an acceptor molecule when they are in close proximity. Specifically, in HTRF, there is an introduction of a short time delay, in the μ-second range, between excitation and measurement of emission, in order to eliminate disturbing short-lived background fluorescence. In their experiment, the donor is coupled to an anti-GST antibody and the acceptor coupled to an anti-His antibody, which binds to $^{GST\text{-}}$ATG13 and $^{His\text{-}}$ATG101, respectively. When the two proteins are bound or, rather, are in close proximity the energy of the donor is not completely dissipated and it can be received by the acceptor, which then, consequently, can emit a fluorescence signal measurable at 665 nm. With the addition of untagged ATG101, the fluorescent signal dropped in significantly, indicating that the dimerization between ATG13 and ATG101 might be more dynamic than we thought.

In vitro, ATG101 and ATG13 do not need to form a stable dimer to interact with ATG9 (Figure 3.5c). However, dimerization is important for forming the ATG13-ATG101-ATG9 complex faster (Figure 3.5a). One question that is important to address in the future is how dynamic is the complex ATG13-ATG101 in the context of ATG9 interaction. It is still not clear from our experiments, for example, if ATG13 and ATG101 lose the dimerization after the interaction with ATG9 (Figure 3.2a) (see following sections for more information). The stoichiometry data (Figure 3.2f) support the hypothesis that at least one ATG101 might leave or never be recruited stably at the active subunit.

Different fractionation experiments show that while ATG13 always elutes in combination with ATG101, ATG101 is also found in a separate peak from ATG13 (Hosokawa *et al.*, 2009; H. Suzuki *et al.*, 2015c; Wallot-Hieke *et al.* 2018). One possible explanation is that ATG101 is in excess so that ATG13 is always maintained in a determinate conformational state to allow a time-efficient response upon autophagy complex assembly. If ATG13 is a target of proteasomal degradation in absence of ATG101 (Mercer, Kaliappan and Dennis, 2009), ATG101 might exert a role in balancing the levels of 'active' ATG13. ATG101 expression also depends on ATG13 presence: in MEF *ATG13* -/- ATG101 is not detected in the crude lysate (Wallot-Hieke *et al.*, 2018). The fact that ATG101 is also interacting with ATG9 is part of the mechanism for the stimulus of ATG13 conversion (Summary and model, panel d; Figure 3.9c) (this point is a later topic in the discussion).

According to the MAD2 model, the dimerization between two HORMAs is conformationally sensitive (DeAntoni *et al.*, 2005; Mapelli *et al.*, 2006). This means that two topologies can only dimerize when are opposite. There are exceptions to this: $p31^{comet}$ is closed upon itself, but the N-terminus is docked like in the open state (Figure 1.4d) and the two REV7 in the Shieldin complex (see following sections of the discussion). ATG13 and ATG101 seem to follow the MAD2 model. We could see that the $ATG13^{\Delta seatbelt}$ sample was purified with a mixture of O and C conformations (Figure 3.8c). Only over 6h, the $ATG13^{\Delta seatbelt}$ assumes a conformation favorable to interact with ATG101 (Figure 3.8e, f). Taken all together, this data proves that the dimerization of ATG13-ATG101 is a dynamic interaction, and is regulated by the conformational state of the HORMA domain.

4.6 How much do ATG13 and ATG101 differ from MAD2?

Most of the research about HORMAs focused on MAD2 conversion and binding to CDC20 (Lou *et al.*, 2000; Luo *et al.*, 2002; Sironi *et al.*, 2002a; DeAntoni *et al.*, 2005; Mapelli *et al.*, 2006, 2007; Simonetta *et al.*, 2009; Mariani *et al.*, 2012; Hara *et al.*, 2015). Evolutionarily, ATG13 and ATG101 are the most distant from MAD2, among the other HORMA domain proteins in human (Almutairi, 2018; Yajie Gu *et al.*, 2022) regarding their sequence, to the extent that there weren't identified by the original sequence alignment of Aravind and Koonin (Aravind and Koonin, 1998). The HORMA folds confer peculiar structural/functional features, one of them being the change of topology that creates an energetical barrier. Other than the characteristic core, HORMAs have flexible regions at the N-terminus and the C-terminus. This last contains an area termed 'safety belt' or 'seatbelt' that can pack against the HORMA domain core in two distinct ways, resulting in open (O) or closed (C) states. When the N-terminus is displaced from the core, the C-terminus is free to take its place and create an enclave for a binding partner to be embraced by the 'seatbelt'.

The O to C conversion and the asymmetric dimerization are at the base of the regulatory role of the HORMA protein (Lou *et al.*, 2000; Luo *et al.*, 2002; Sironi *et al.*, 2002a; DeAntoni *et al.*, 2005; Mapelli *et al.*, 2006, 2007; Simonetta *et al.*, 2009; Mariani *et al.*, 2012; Hara *et al.*, 2015). We were able to determine that ATG13 and ATG101 bind ATG9 with an incredibly slow reaction (24h at 20ºC) that could be accelerated by preforming the ATG13-ATG101 complex (1h on ice) (Figure 3.5c). In the context of HORMAs, the fact that ATG13 and ATG101 interact with ATG9 at an incredibly slow speed is a strong indication that both proteins undergo a conformational change before/during the interaction with ATG9. Furthermore, similarly to MAD2, the conversion is accelerated upon dimerization (Figure 3.5a).

In MAD2, the seatbelt is necessary for interacting with CDC20, while we discovered that, in the case of ATG13 and ATG101, the seatbelt is not involved in the direct binding with ATG9 (Figure 3.7a). Therefore, ATG101 and ATG13 might interact with ATG9 in a unique way. We also still detected a very slow interaction (Figure 3.7a), indicating that the seatbelt is not the key component that regulates the conformational change and creates the energy barrier, similarly to MAD2. In MAD2, the energetic barrier is created by the necessity to displace the N-terminus from β5 so that the C-terminus, localized near β6, can move around the protein and dock β5. While this happens, the N-terminus also tread through a loop located between αC and β5 (Figure 1.5a) (Lou *et al.*, 2000; Luo *et al.*, 2002; Sironi *et al.*, 2002a; Mapelli *et al.*, 2006, 2007; Simonetta *et al.*, 2009; Mariani *et al.*, 2012; Hara *et al.*, 2015).

The N-terminus of ATG13 is not reported in the structure of Qi *et al.* since it was removed for crystallization purposes (Qi *et al.*, 2015). In the AlphaFold2 prediction (Figure 3.8e and f) the N-terminus of ATG13 is mostly composed by the αA but also shows a short flexible unstructured region. In MAD2, the N-terminus creates a small αhelix separated αA and also comprises of a segment of the αA. Probably, the $ATG13^{N}$, given the more extensive involvement in the αA, simply requires more energy than MAD2 to pass through the loop. Thus, the N-terminus is most likely the energetic barrier that is keeping ATG13 in a not-ATG9-binding-prone state.

Qi *et al.* state that the seatbelt in ATG13, in particular, is likely too short to engage in any interaction with a binding partner (Qi *et al.*, 2015). This seems to agree with our findings. They also concluded that the ATG13 seatbelt is blocked to the core ('pinned') and unable to be part of any topological change. However, the fact that a HORMA does not use the seatbelt for interacting with the binding partner, does not imply the fact that it can't change conformation and have more than one state. Simply, the seatbelt is not involved in the interaction with the binding partner, but it might still dislocate with enough energy. The fact that all the ATG13 Δseatbelt mutant can still interact with ATG9 without a seatbelt, in a slow reaction and in a conformational state that is not

able to contemporarily interact with ATG101 (Figure 3.7a; Figure 3.9c) is a strong indication that the ATG13 seatbelt is used for maintaining ATG13 is a specific conformation rather than engaging in the binding partner interaction. To support the importance of the ATG13 seatbelt one of our collaborators, Björn Stork group, created an $ATG13^{\Delta seatbelt}$ KO cell line in MEF cell and observed a strong inhibitory effect on autophagic flux (data not shown). However, will be incredibly central to determine what is the upstream consequences of these defects, because it is safe to assume that this mutation is not affecting directly the interaction to ATG9 but rather the ATG13-ATG101 interaction given the effect observed in Figure 3.8.

Our data show that also ATG101 needs to undergo a topology change before interacting with ATG9 (Figure 3.5c). It is speculated that ATG101 is the only HORMA to be in an unchanged open conformation given the length of the N-terminus docked at the core that would cause the requirement of an extensive amount of energy to make space for the C-terminus to dock (Michel *et al.*, 2015; Qi *et al.*, 2015). NMR spectra of proteins incubated at 30ºC do not show any variation (Michel *et al.*, 2015) and support this theory. We also performed an Anion Exchange (AE) Chromatography that has been used before to isolate and identify the two conformers of MAD2 (Mapelli *et al.*, 2007). ResQ columns discriminate proteins in virtue of their surface charge. ATG101 incubated at 4 ºC or at 20ºC overnight eluted in only one peak in AE. There are two ways to explain these negative results. It might happen that the topological change does not significantly alter the total charge of the protein and the ResQ column would not detect any variation, therefore it is critical to combine this approach with other assays. Another option would be that the conformational change can indeed happen in ATG101, but only in the presence of the binding partner (in our case ATG9) and might be facilitated maybe by weak interactions happening between the two proteins. This weak interaction probably cannot be appreciated in pull-down experiments due to the extensive washing that the proteins undergo. In support of the possibility that $ATG101^{N}$ might undergo a topological change is a wide space formed by the loop between αC and β5 that is formed with the help of a more extensive αC than in MAD2. This wide space would allow for the treading of the long $ATG101^{N}$. Regarding the C-terminus of ATG101, few authors show different structures of ATG101 full-length (Mercer, Kaliappan and Dennis, 2009; Kim *et al.*, 2018) and, in these structures, the C-terminus tail of ATG101 is either free and flexible or is docked on one side of the core (β6). We removed the C-terminus and could not appreciate any variation in the conformational state of ATG101 (Figure 3.8g). However, removing the N-terminus it might have altered the conformational state of ATG101 since we could not appreciate any direct interaction between $ATG13^{WT}$ and $ATG101^{\Delta N}$ (Figure 3.8g). Some preliminary data indicate that

this might be the case since ATG101$^{\Delta N}$ would have the β5 free for the C-terminus to dock and close.

4.7 How much ATG13 and ATG101 differ from REV7

REV7 HORMA is a scaffolding protein that is involved in two critical DNA damage repair processes (Boersma *et al.*, 2015; Xu *et al.*, 2015; Gubta *et al.*, 2018; Noordermeer *et al.*, 2018; Setiaputra and Durocher, 2019). In particular, REV7 was discovered to influence DNA DSB (double-strand brakes) repair pathway choice. REV7 induces the formation of the Shieldin complex which is recruited to DSB sites by 53BP1–RIF1 complex and inhibits resection of damaged DNA ends, reducing HR (homologous recombination) repair and enhancing NHEJ (nonhomologous end-joining). SHLD3 (which facilitates binding to 53BP1–RIF1), and SHLD2, (which presents a DNA–binding activity) are brought together by REV7 (Gubta *et al.*, 2018; Noordermeer *et al.*, 2018; Setiaputra and Durocher, 2019). The REV7–SHLD3–SHDL2 complex was recently crystallized (Liang *et al.*, 2020). Liang *et al.*, show that REV7 dimerizes like MAD2, with one REV7 adopting the canonical seatbelt closure conformation (C-REV7- SHLD3^{RBM2}), while SHLD3^{RBM1}-SHLD2-'C/O'-REV7 is not canonical. This second REV7 shows a closure conformation, but the seatbelt does not seem to be involved in interacting with either of the SHLD proteins (therefore the authors termed it open, despite the conformation) (Figure 1.5c and d; Supplementary 2.c). Similarly, ATG13 doesn't use the seatbelt to directly interact with ATG9^{N} (Figure 3.7a; Figure 3.9c, e, f). Therefore, we propose that ATG13 might engage with ATG9 in a similar fashion. Indeed, in both cases, most of the residues involved in the interaction, on the HORMA side, are localized in β6, but in REV7 there is less involvement of β4 compared to the prediction we obtained of ATG13. The difference is that in REV7, SHLD2 is also forming a β-sandwich with SHLD3 (Figure 1.5c and d; Supplementary 2.c). One similarity between REV-SHLD2 and ATG13-ATG9^{N} is that in both cases, the region of the binding partner engaging with the HORMA β6 maintains its unstructured folding and does not augment the β-sheet after pairing with the β6 like in MAD2 (Mapelli *et al.*, 2007). SHLD2 and the ATG9^{N} engaging with REV7 and ATG13, respectively, have also another similarity: SHLD2 interacts with REV7 in a not-canonical manner through a consensus motif (FXPWFP) containing a key tryptophan (W11) (Liang *et al.*, 2020b). In our predicted structure, also a tryptophan (W37) on ATG9^{N} is central and is conserved among different organisms (Figure 3.9a). The SHLD2^{W11} is facing SHLD3 rather than the REV7, while in our structure, ATG9$^{N–W37}$ is buried within ATG13 β6 (Supplementary Figure 2c). This could support the hypothesis that ATG13 doesn't need to create any β-sandwich.

Our results do not completely appear discordant from REV7 not-canonical state. Indeed, both HORMA might create a tryptophan-centered rather than seatbelt-mediated interaction with a binding partner.

4.8 TRIP13-like mechanism in Autophagy

TRIP13 and p31^{comet} are important for the disassembly of HORMAs (Sarangi *et al.*, 2020; Ye *et al.*, 2017; Ma and Poon, 2018). PCH2/TRIP13 is part of the remodeler family AAA+ ATPase. The substrates (the N-terminus of MAD2 or REV7, for example) are pushed in the central pore to unfold, as ATP hydrolysis causes coordinated conformational changes in the ring-shaped homo-hexameric complex (Wang *et al.*, 2014; Ye *et al.*, 2015; Clairmont *et al.*, 2020). p31^{comet} binds PCH2/TRIP13 (Tipton *et al.*, 2012) and dimerizes with C-MAD2 (Yang *et al.*, 2007) for mediating the disassembly. Structurally p31comet is a unique HORMA because its structure resembles a C-MAD2, however, it appears self-closed. There is no indication in the literature that might undergo opening (Yang *et al.*, 2007). In the latest model of the MAD2 disassembly, the p31^{comet}-C-MAD2-CDC20 complex docks PCH2/TRIP13 on a helix of TRIP13. PCH2/TRIP13 pore interacts with the N-terminus of MAD2. MAD2 N-terminus is dragged inside the pore as a result of ATP hydrolysis, causing the MAD2 seatbelt to unfold locally. This disrupts the p31^{comet}-MAD2 interaction and releases CDC20. Through, this mechanism PCH2/TRIP13 accelerates the conversion of C-MAD2 to O-MAD2, so that MAD2 can start a new cycle.

Even though we discovered that also ATG13$^{\Delta seatbelt}$ could interact with ATG9, we evaluated the option that TRIP13 could also be involved in autophagy given that TRIP13 and p31^{comet} are also localized in the cytosol (Wang *et al.*, 2014) and the ATG13 HORMA domain is localized at the N-terminus of ATG13^{FL} and it would have a flexible easy-to-grab N-terminus. We also tested for direct binding between PCH2/TRIP13 and p31^{comet} and our complexes ATG13-ATG101 and ATG13-ATG101-ATG9. No direct interaction has been observed. We can entertain two hypotheses. For example, we can suppose that a TRIP13-MAD2 mechanism-like is not needed in autophagy, given the fact that the seatbelt of ATG13 doesn't have the same involvement as in MAD2. However, if the interaction between ATG13-ATG9 is strong, as in MAD2, an energy-mediated mechanism of disassembly might be required to accelerate the spontaneous disassembly reaction. If this is true, in our assay we might have missed some components or modifications necessary for the disassembly or used the wrong AAA+ ATPase. Our collaborators from Dusseldorf University Medicine, Céline, and Annabelle (Stork group) tested *TRIP13* KO cells for autophagy defects. However, no effect was detected on autophagic flux. AAA+ ATPase (like VCP/p97) is an interesting candidate. VCP/p97 binds BECN1 (Hill *et al.*, 2021) and enhances the

Ataxin-mediated stabilization of BECN1, and promotes assembly and activity of the PI3KC1. In this case, however, the ATPase would not promote the disassembly rather the assembly of the autophagy machinery. TRIP13 works in a similar manner in HORMADs (Herruzo *et al.*, 2021), where the 'inactive' form of HORMAD is converted to an 'active' HORMAD by the TRIP13, allowing for easier HORMAD recruitment at the chromosome axis. TRIP13 or a similar AAA+ ATPase might be always in action to maintain a pool or 'ready' HORMAs in autophagy: autophagy, differently from mitosis, meiosis, or DNA damage, is overall always an active pathway (Musiwaro *et al.*, 2012) and is upregulated under stress signals. Therefore, the mechanism for the inactivation might be different in autophagy compared to other quality control mechanisms where HORMA domain proteins are involved.

4.9 Why there are two binding sites on ATG9 for ATG13 and ATG101?

In our study, we established that both $ATG9^{N+core}$ and $ATG9^{core+C}$ were specifically able to bind directly to the ATG13-ATG101 complex. While the 'core' ($ATG9^{core}$) composed of all the transmembrane domains was not (Figure 3.6b). A recent paper set up a BioID screen and identified ATG13-ATG101 interacting with $ATG9^{C}$ (Kannangara *et al.*, 2021), in support of our unpublished findings. They choose ATG9 since is anchored on the membrane and therefore it would diminish the chance of promiscuous interactions. They proposed that the $ATG9^{C}$ is a hub for proteins recruitment. However, ATG9 shuttles among several compartments and choosing this protein might have lowered the confidence for autophagy-related components that are not involved in ATG9 trafficking. Indeed, they could not identify ATG2 and WIPIs. Probably ATG13 or ATG101 might have been a better target. In our XL-MS we did not find any cross-link between the $ATG9^{N}$ and ATG13-ATG101. Since ATG^{N} is only 43 residues long, it could be that the 1 lysine in the $ATG9^{N}$ was not accessible to the cross-linker when bound to complex ATG13-ATG101. In our AlphaFolds prediction, we could see that K34 is forming a salt bridge with the seatbelt of ATG13 (is the only interaction between the seatbelt and $ATG9^{N}$) (Figure 3.9e).

We speculate that the two sites of ATG9 might exert different roles in the establishment of the active unit of the ATG13-ATG101-ATG9 complex. Since ATG101-ATG13 interacts with the two regions with different kinetics (Figure 3.5c), probably each HORMA has specificity for one of the two. We already know that ATG13 binds the N-terminus (Figure 3.9b and c) and probably requires an extensive amount of energy to do so (See result section of Figure 3.9). One hypothesis is that ATG101 is specific for the C-terminus while ATG13 is specifically targeting the N-terminus. Therefore, the two regions will just be occupied by the two different proteins with their own interaction kinetics. Our hypothesis is that the ATG101-ATG13 complex interacts first with the C-terminus of ATG9 through ATG101, which consequently would accelerate the

interaction of ATG13 to the N-terminus ('template model', see Summary and model). We can prove with a simple experiment where we form the interaction between $ATG13^{WT}$ and $ATG9^{N}$ in presence of the $ATG9^{core+C}$ and with or without ATG101. It's interesting that in most yeast, Atg101 is not present, and Atg13 interacts with the N-terminus only (Suzuki *et al.*, 2009b). This might be a suggestion that ATG101 is a specialized HORMA that evolved to ensure that ATG13 is loaded on $ATG9^{N}$ at an appropriate speed.

4.10 How do ATG2-WIPI4 and ATG14-BECN1 fit in the picture?

ATG9 and ATG13-ATG101 localize at the ERES (Karanasios *et al.*, 2016), where ATG2 can also be found (Mari *et al.*, 2010; Obara and Ohsumi, 2011; S. W. Suzuki *et al.*, 2015a; Yamamoto *et al.*, 2016; Chowdhury *et al.*, 2018; Noda, 2021a). ATG2 is a ~20 nm long rod-like protein with an internal tubular channel that is assumed to transport lipids from the ER to the growing IM (Chowdhury *et al.*, 2018). Indeed, ATG2 is classified as a lipid transferase (Valverde *et al.*, 2019) known to bind WIPI3/4 (Chowdhury *et al.*, 2018). Atg18 (the yeast homolog of WIPIs) interacts with Atg2 (yeast ATG2 homolog) and PI3P simultaneously utilizing different binding sites (Obara *et al.*, 2008). Also, based on molecular dynamics simulations, ATG9A concentrates on highly curved membranes (Maeda *et al.*, 202) and ATG2 localizes at the expanding tip of the omegasome (Otomo and Maeda, 2019).

Since ATG9 interaction to ATG2 and WIPI4 was already established in the lab, we wanted to determine how ATG13 and ATG101 would fit in the picture of the phagophore expansion machinery. We could prove that ATG13-ATG101 could bind to ATG2-WIPI4 only in presence of ATG9 (Figure 3.3 a, b). Anh Nguyen pushed our knowledge even further proving that ATG2 is able to transfer lipid with the help of WIPI4. ATG9 binding to ATG2 induces an additional acceleration by, probably, scramblase the lipids from the outer to the inner leaflet of the omegasome and that, ATG13-ATG101, as a complex, can accelerate the activity of ATG9 over ATG2-WIPI4 up to 6 times (Supplementary Figure 1). To prove this, Anh combined a lipid transfer assay with a scramblase activity assay.

Since WIPI4 is a PI3P sensor and the conversion of PI to PI3P is mediated by the ATG14-containing PIKC1, it would be important to test if the presence and the continuous deposit of PI3P by the full PI3KC1 can accelerate even more the lipid transfer rate of ATG2 mediated by the presence of WIPI4, ATG9, and ATG13-ATG101. Suzuki and colleagues have shown that the Atg2-Atg18 complex in yeast could not be recruited to the PAS upon deletion of Atg14, indicating a hierarchy of recruitment between these two initiation subcomplexes (Suzuki *et al.*, 2007). ATG14

proposed role is to stabilize and shuttle the PI3KC1 to the omegasome and it contains BAR domain sensitive towards PI3P-containing high-curved membranes where also ATG2 and ATG9 localize.

4.10 Summary and model

The findings in this work are summarized in Figure 3.10:

1) ATG13-ATG101 can also bind ATG14-BECN1 and form a single complex with ATG9-ATG2-WIPI4 **(a)**
2) ATG13 and ATG101 can bind ATG9 in isolation, but their dimerization accelerates the reaction **(b)**
3) ATG13 can convert spontaneously over time **(c)**
4) ATG101-ATG13 dimer is conformational dependent **(c)**
5) The binding of ATG13 at the N-terminus of ATG9 is also conformation-dependent **(d)** and the dimerization might accelerate the reaction
6) The seatbelt of ATG13 is not involved in direct interaction with ATG9 **(e)**
7) ATG13-ATG101 bind $ATG9^{N}$ and $ATG9^{C}$ with slow and fast kinetics, respectively **(e)**

Combining the overall evidence presented in this thesis with literature and unpublished data from collaborators and colleagues, an updated model of autophagy initiation is presented in Figure 3.10.

We propose that ATG13 and ATG101 represent an autophagy module necessary for regulating in space and time the assembly of the most apical components of autophagosome nucleation and expansion (ATG14, BECN1, ATG9, ATG2, and WIPI4) by bridging through direct interaction the ATG14-containing PI3KC1 for PI3P production and the membrane elongation complex ATG9-ATG2-WIPI4. The binding of $ATG13^{HORMA}$ and ATG101 to ATG9 is incredibly slow, but it is accelerated by ATG13-ATG101 dimerization, which reduces the energetic barrier for the re-arrangement of ATG13 and its interaction to $ATG9^{N}$. First, the ATG13-ATG101 complex gets recruited at the C-terminus of ATG9 probably by ATG101. This interaction causes a rearrangement of ATG13, which is then handled to the N-terminus while losing its interaction to ATG101. This is then free to recruit new ATG13. We termed this model the 'handover model'. The slow interaction between the HORMA domain proteins to their respective binding region likely creates a kinetic bottleneck for the activation of the effector machinery at the autophagy initiation and might dictate the speed of the pathway itself.

Summary and Model

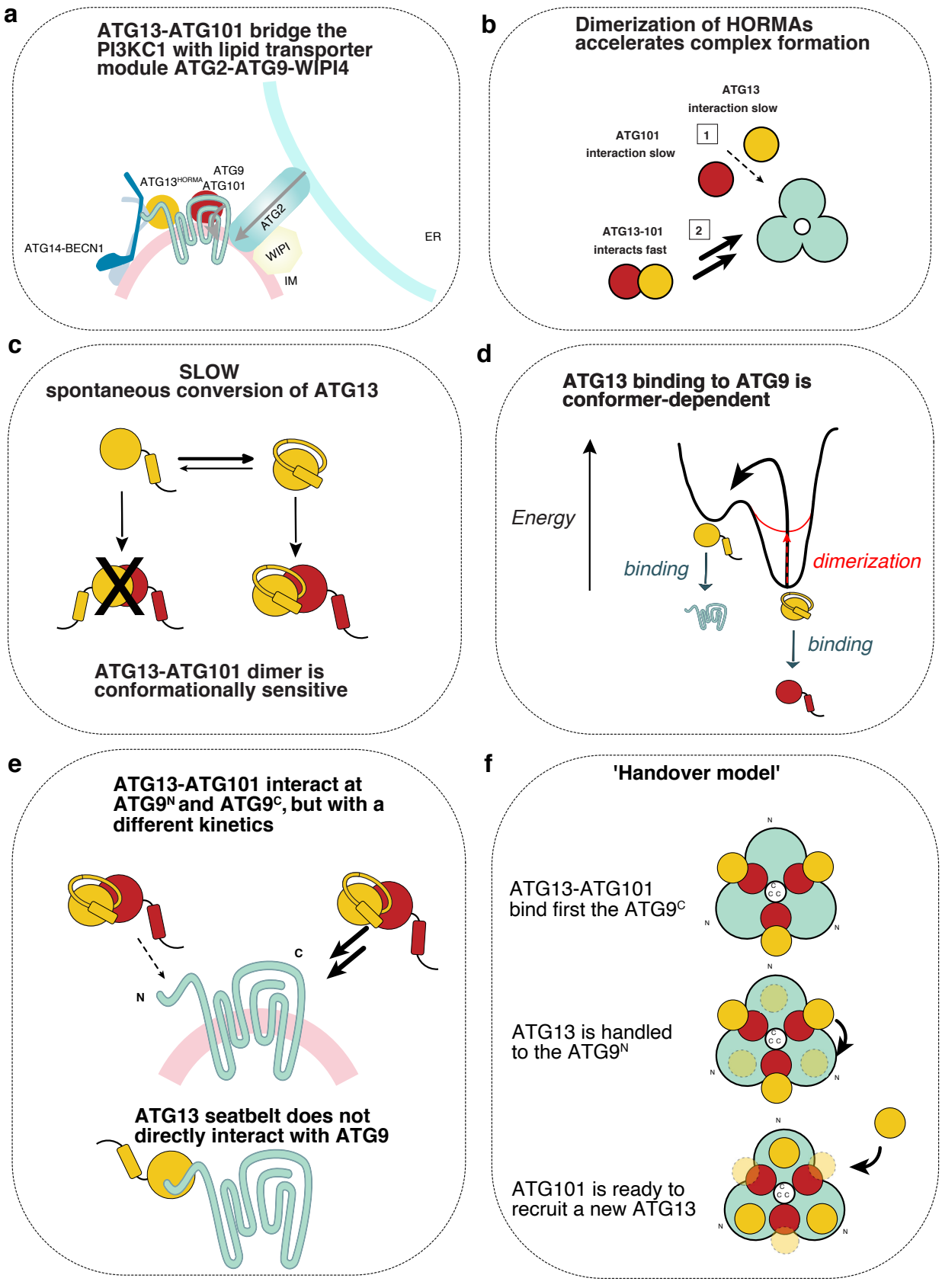

Figure 3.10 Summary and Model

(a) ATG13 and ATG101 form a hub for the autophagy initiation subcomplexes interacting directly with ATG9 and ATG14/BECN1. They also might favor ATG9 lipid scramblase while enhancing ATG2 lipid transfer activity; **(b)** ATG13 and ATG101 interaction to ATG9 is a rate-limiting step of the process and the dimerization of ATG13-ATG101 accelerate the complex formation; **(c)** ATG13 conversion of topology in a spontaneous and the dimerization of ATG13-ATG101 is controlled in a conformationally-sensitive fashion; **(d)** the seatbelt of ATG13 controls the conformational state while maintaining ATG13 in an ATG101-binding prone state. ATG13 binding to $ATG9^{N}$ is also conformational dependent; **(e)** there are two binding sites for ATG13-ATG101 on ATG9 and the interaction is characterized by different kinetics; ATG13 seatbelt doesn't interact with ATG9 directly; **(f)** The 'handover model' might describe how the binding of ATG101 the C-terminus of ATG9 might accelerate the conversion of ATG13, favoring the conformational change of ATG13 while accelerating its interaction at $ATG9^{N}$.

4.11 Short-term future prospective

Many questions have been raised as a result of these discoveries, which will need to be addressed in the near future.

The first question we can address is to determine if ATG101 is the first one to get recruited at the C-terminus. Determining the site where ATG101 is interacting on ATG9 is of key importance and it might help us to determine how ATG101 is able to mediate the acceleration for the interaction of ATG13 to $ATG9^{N}$. We clearly have to quantify all the interactions shown until now with more robust techniques to validate the kinetics trends observed in this work and to determine the interaction strengths between complexes to discriminate potential cooperative interaction between autophagy initiation subcomplexes to compare it with the overall autophagy initiation machinery stability. One far-fetched possibility is that the two regions of ATG9 might work independently rather than combine their effort to load ATG13 at the N-terminus. In this situation, an additional component might be involved. A good candidate might be ATG14-BECN1 since its interaction with ATG101 might accelerate the conversion of ATG13 in a similar manner to what has been described in the handover model with the interaction to $ATG9^{C}$. To address this point similar experiments shown in this work might help in determining the kinetics of ATG13-ATG101-ATG14-BECN1 complex formation also in the presence or absence of ATG9. It will also be useful to determine how ATG13-ATG101 can contemporarily interact with both complexes and confirm the regions of ATG101-ATG13 proposed to interact with ATG14 (Park

et al., 2016; *Kim et al.,* 2018). On top of this, it would be interesting to characterize the role of the phosphorylation deposited by ULK1, if they are able to modulate the conversion of ATG13 and accelerate the complex assembly. It is still unclear how ATG13-ATG101-ATG9 can accelerate ATG2 lipid transferase activity. Do they favor the two states of ATG9 described by Maeda and colleagues? Of key importance to address most of these questions it would also be useful to finally structurally characterize fully or partially the autophagy 7-components complex by CyoEM or crystallography.

4.12 Future prospective

Richard Feynman, the theoretical physicist who won the Nobel Prize in 1965, once said that we can't build what we can't comprehend. The phrase can be read in a variety of ways, however, the most basic is that an idea or proof should be easy to develop or comprehend from the bottom up using just fundamental principles.

The ultimate objective of reconstitution is to form an autophagosome just by using purified components. This is an incredible effort and might take years to see the end. Our work is a step forward towards that goal. We have established that two semi-globular proteins have distinctive conformers which are able to engage in different interactions but only one is the more likely trigger for the autophagy components to form a single super-machinery that, alone, is capable of transferring lipids between a source and a seeding membrane (this work and Anh's work). These findings are a significant step towards the effort to completely comprehend the molecular principles behind autophagy and autophagosome formation.

We can also speculate that the dimerization interface, as well as the binding region between ATG13 and ATG9, are a good target for the creation of drugs that precisely control autophagy, which could have significant therapeutic implications for the treatment of a variety of critical diseases.

Supplementary 1

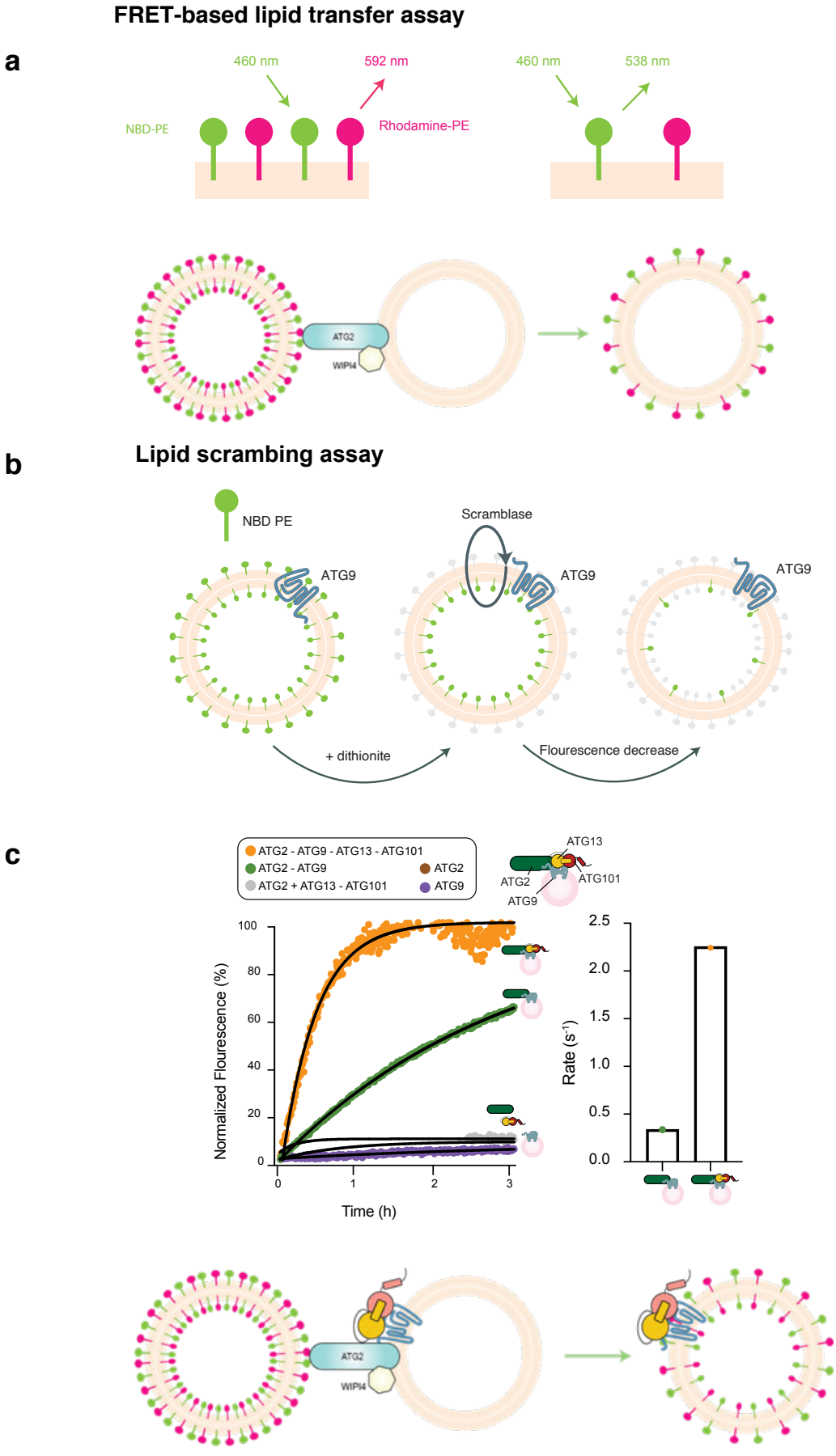

Figure 3.11 Supplementary 1 ATG13-ATG101 accelerate lipid transfer of ATG2 (data from Anh Nguyen)

(a) Schematic representation of FRET assay for ATG2 lipid transfer activity detection. The donor liposome contains NBD- and Rhodamine-labelled lipids, while the acceptor is free of labeling. The fluorescence resonance energy transfer (FRET) is measured. FRET between NBD and Rhodamine maintains NBD's fluorescence intensity (FI) low in donor liposomes. However, when these fluorescently tagged lipids are diluted by transport to acceptor liposomes mediated by ATG2, the FRET efficiency drops, increasing NBD FI inversely; **(b)** Schematic representation of the lipid scrambling activity assay for ATG9. The transport of fluorescently tagged lipids from the inner to the outer liposome leaflet can be studied using dithionite. Dithionite quenches fluorophores on the outer leaflet, lowering the fluorescent signal by 50%. If ATG9 flips lipids, after dithionite addition, the fluorescent signal will be reduced to the minimum (Matoba *et al.*, 2020); **(c)** Anh Nguyen experiment combining lipid transfer assay for ATG2 with ATG9 lipid scramble activity in the presence and the absence of ATG13-ATG101. The lipid transfer activity was normalized over the activity of ATG2.

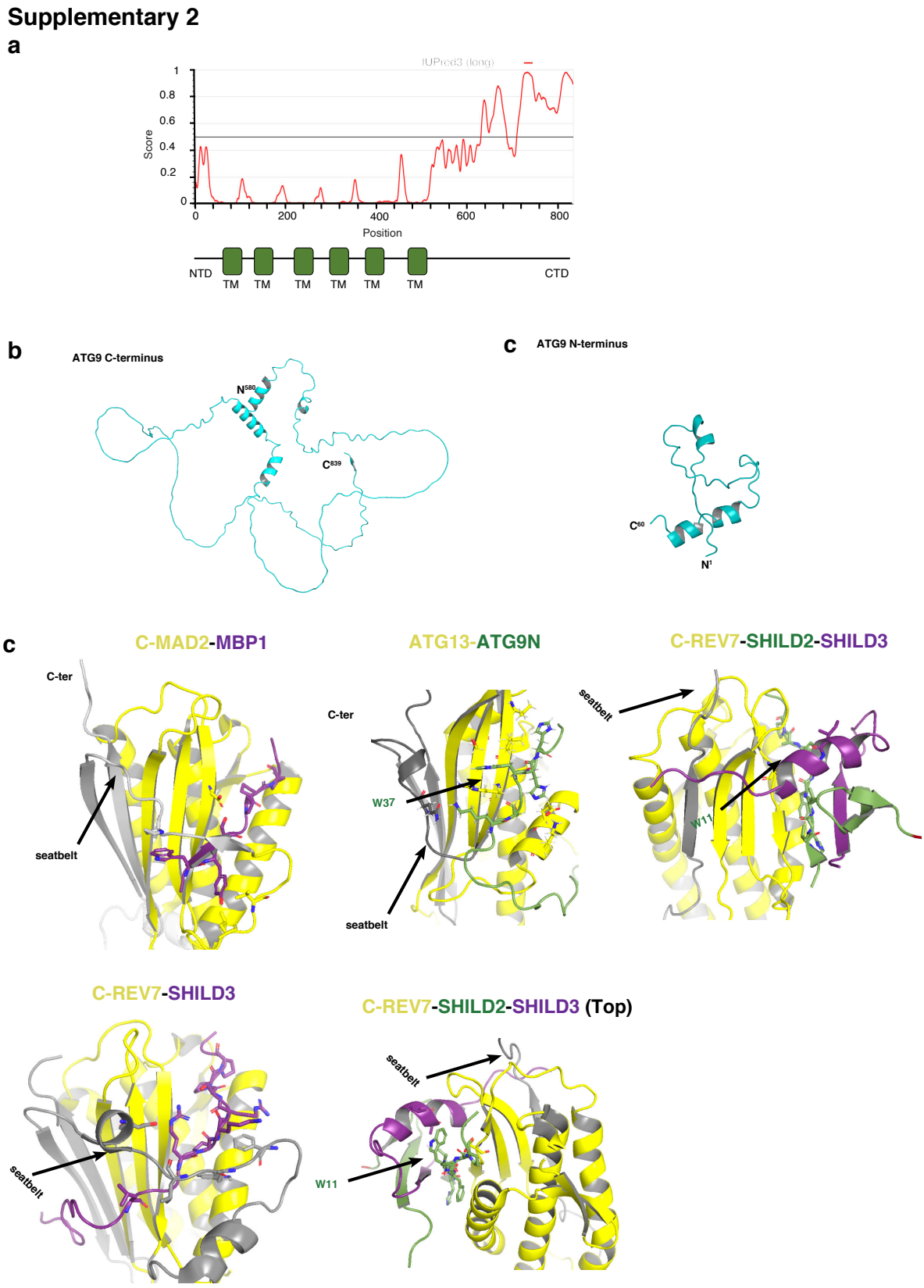

Figure 3.12 Supplementary 2 ATG9 binding regions and ATG13-ATG9^{N} structure prediction compared to other HORMA domain proteins

(a) IUPred prediction of IDR in ATG9; **(b)** AlphaFold prediction of ATG9 C-terminus (580-839); **(c)** AlphaFold prediction of ATG9 N-terminus (1); **(d)** Comparison of C-MAD2-MBP1 structure from Luo et al, 2002, structure prediction of AlphaFold Multimer of $ATG13^{HORMA}$-$ATG9^{N}$ and C-REV7-C-REV7-SHLD2-SHLD3 structure from Liang *et al.*, 2020 (two viewpoints).

5 Bibliography

Abdulrahman, W. *et al.* (2015) "The production of multiprotein complexes in insect cells using the baculovirus expression system," *Methods in Molecular Biology* [Preprint]. doi:10.1007/978-1-4939-2230-7_5.

Al-Bari, M.A.A. and Xu, P. (2020) "Molecular regulation of autophagy machinery by mTOR-dependent and -independent pathways," *Annals of the New York Academy of Sciences*. doi:10.1111/nyas.14305.

Alers, S. *et al.* (2011) "Atg13 and FIP200 act independently of Ulk1 and Ulk2 in autophagy induction," *Autophagy*, 7(12). doi:10.4161/auto.7.12.18027.

Alers, S., Wesselborg, S. and Stork, B. (2014) "ATG13: Just a companion, or an executor of the autophagic program?" *Autophagy*. doi:10.4161/auto.28987.

Alfieri, C., Chang, L. and Barford, D. (2018) "Mechanism for remodeling of the cell cycle checkpoint protein MAD2 by the ATPase TRIP13," *Nature*, 559(7713). doi:10.1038/s41586-018-0281-1.

Almutairi, Z.M. (2018) "Comparative genomics of HORMA domain-containing proteins in prokaryotes and eukaryotes," *Cell Cycle*. doi:10.1080/15384101.2018.1553402.

Anfinsen, C.B. (1973) "Principles that govern the folding of protein chains," *Science*. doi:10.1126/science.181.4096.223.

de Antoni, A. *et al.* (2005) "The Mad1/Mad2 complex as a template for Mad2 activation in the spindle assembly checkpoint," *Current Biology*, 15(3). doi:10.1016/j.cub.2005.01.038.

Aravind, L., and E.V. Koonin. 1998. The HORMA domain: A common structural denominator in mitotic checkpoints, chromosome synapsis and DNA repair. Trends Biochem. Sci. 23:284–286. https://doi.org/10.1016/S0968-0004(98)01257-2

Axe, E.L. *et al.* (2008) "Autophagosome formation from membrane compartments enriched in phosphatidylinositol 3-phosphate and dynamically connected to the endoplasmic reticulum," *Journal of Cell Biology*, 182(4). doi:10.1083/jcb.200803137.

Baba, M. *et al.* (1994) "Ultrastructural analysis of the autophagic process in yeast: Detection of autophagosomes and their characterization," *Journal of Cell Biology*, 124(6). doi:10.1083/jcb.124.6.903.

Bach, M. *et al.* (2011) "The serine/threonine kinase ULK1 is a target of multiple phosphorylation events," *Biochemical Journal*, 440(2). doi:10.1042/BJ20101894.

Bakula, D. *et al.* (2017) "WIPI3 and WIPI4 β-propellers are scaffolds for LKB1-AMPK-TSC signalling circuits in the control of autophagy," *Nature Communications*, 8. doi:10.1038/ncomms15637.

Balboni, M. *et al.* (2020) "COMET Functions as a PCH2 Cofactor in Regulating the HORMA Domain Protein ASY1," *Current Biology*, 30(21). doi:10.1016/j.cub.2020.07.089.

Berger, I., Fitzgerald, D.J. and Richmond, T.J. (2004) "Baculovirus expression system for heterologous multiprotein complexes," *Nature Biotechnology* [Preprint]. doi:10.1038/nbt1036.

Boersma, V. *et al.* (2015) "MAD2L2 controls DNA repair at telomeres and DNA breaks by inhibiting 5' end resection," *Nature*, 521(7553). doi:10.1038/nature14216.

Bordi, M. *et al.* (2021) "A gene toolbox for monitoring autophagy transcription," *Cell Death and Disease*, 12(11). doi:10.1038/s41419-021-04121-9.

Bowie, J.U. (2001) "Stabilizing membrane proteins," *Current Opinion in Structural Biology*. doi:10.1016/S0959-440X(00)00223-2.

Brulotte, M.L. *et al.* (2017) "Mechanistic insight into TRIP13-catalyzed Mad2 structural transition and spindle checkpoint silencing," *Nature Communications*, 8(1). doi:10.1038/s41467-017-02012-2.

Brunner, J.D., Schenck, S. and Dutzler, R. (2016) "Structural basis for phospholipid scrambling in the TMEM16 family," *Current Opinion in Structural Biology*. doi:10.1016/j.sbi.2016.05.020.

Bryan, P.N. and Orban, J. (2010) "Proteins that switch folds," *Current Opinion in Structural Biology*. doi:10.1016/j.sbi.2010.06.002.

Bueno-Arribas, M. *et al.* (2021) "A conserved ATG2 binding site in WIPI4 and yeast Hsv2 is disrupted by mutations causing β-propeller protein-associated neurodegeneration," *Human molecular genetics*, 31(1). doi:10.1093/hmg/ddab225.

Burroughs, A.M. *et al.* (2015) "Comparative genomic analyses reveal a vast, novel network of nucleotide-centric systems in biological conflicts, immunity and signaling," *Nucleic Acids Research*, 43(22). doi:10.1093/nar/gkv1267.

Busse, R.A. *et al.* (2015) "Characterization of PROPPIN-phosphoinositide binding and role of loop 6CD in PROPPIN-membrane binding," *Biophysical Journal*, 108(9). doi:10.1016/j.bpj.2015.03.045.
Cappadocia, L. and Lima, C.D. (2018) "Ubiquitin-like Protein Conjugation: Structures, Chemistry, and Mechanism," *Chemical Reviews*. doi:10.1021/acs.chemrev.6b00737.

Caryl, A.P. *et al.* (2000) "A homologue of the yeast HOP1 gene is inactivated in the Arabidopsis meiotic mutant asy1," *Chromosoma*, 109(1–2). doi:10.1007/s004120050413.

Chan, E.Y. and Tooze, S.A. (2009) "Evolution of Atg1 function and regulation," *Autophagy*. doi:10.4161/auto.8709.

Chan, E.Y.W. *et al.* (2009) "Kinase-Inactivated ULK Proteins Inhibit Autophagy via Their Conserved C-Terminal Domains Using an Atg13-Independent Mechanism," *Molecular and Cellular Biology*, 29(1). doi:10.1128/mcb.01082-08.

Chen, J. and Fang, G. (2001) "MAD2B is an inhibitor of the anaphase-promoting complex," *Genes and Development*, 15(14). doi:10.1101/gad.898701.

Chen, S. *et al.* (2016) "Distinct roles of autophagy-dependent and -independent functions of FIP200 revealed by generation and analysis of a mutant knock-in mouse model," *Genes and Development*, 30(7). doi:10.1101/gad.276428.115.

Choi, S., Houdek, X. and Anderson, R.A. (2018) "Phosphoinositide 3-kinase pathways and autophagy require phosphatidylinositol phosphate kinases," *Advances in Biological Regulation*, 68. doi:10.1016/j.jbior.2018.02.003.

Chowdhury, S. *et al.* (2017) "Structural analyses reveal that the ATG2A-WIPI4 complex functions as a membrane tether for autophagosome biogenesis," *bioRxiv* [Preprint].

Chowdhury, S. *et al.* (2018) "Insights into autophagosome biogenesis from structural and biochemical analyses of the ATG2A-WIPI4 complex," *Proceedings of the National Academy of Sciences of the United States of America*, 115(42). doi:10.1073/pnas.1811874115.

Clairmont, C.S. *et al.* (2020) "TRIP13 regulates DNA repair pathway choice through REV7 conformational change," *Nature Cell Biology*, 22(1). doi:10.1038/s41556-019-0442-y.

Dai, Y. *et al.* (2020) "Structural basis for shieldin complex subunit 3-mediated recruitment of the checkpoint protein REV7 during DNA double-strand break repair," *Journal of Biological Chemistry*, 295(1). doi:10.1074/jbc.RA119.011464.

DeAntoni, A. *et al.* (2005) "Explaining the oligomerization properties of the spindle assembly checkpoint protein Mad2," in *Philosophical Transactions of the Royal Society B: Biological Sciences*. doi:10.1098/rstb.2004.1618.

Demeter, A. *et al.* (2020) "ULK1 and ULK2 are less redundant than previously thought: computational analysis uncovers distinct regulation and functions of these autophagy induction proteins," *Scientific Reports*, 10(1). doi:10.1038/s41598-020-67780-2.

Denton, D. and Kumar, S. (2019) "Autophagy-dependent cell death," *Cell Death and Differentiation*. doi:10.1038/s41418-018-0252-y.

Egan, D.F. *et al.* (2015) "Small Molecule Inhibition of the Autophagy Kinase ULK1 and Identification of ULK1 Substrates," *Molecular Cell*, 59(2). doi:10.1016/j.molcel.2015.05.031.

Erdos, G., Pajkos, M. and Dosztányi, Z. (2021) "IUPred3: Prediction of protein disorder enhanced with unambiguous experimental annotation and visualization of evolutionary conservation," *Nucleic Acids Research*, 49(W1). doi:10.1093/nar/gkab408.

Evans, R. *et al.* (2021) "Protein complex prediction with AlphaFold-Multimer," *bioRxiv* [Preprint].

Faesen, A.C. *et al.* (2017) "Basis of catalytic assembly of the mitotic checkpoint complex," *Nature*, 542(7642). doi:10.1038/nature21384.

Feng, Y. *et al.* (2014) "The machinery of macroautophagy," *Cell Research*. doi:10.1038/cr.2013.168.

Fujiwara, Y. *et al.* (2020) "Meiotic cohesins mediate initial loading of HORMAD1 to the chromosomes and coordinate SC formation during meiotic prophase," *PLoS Genetics*, 16(9). doi:10.1371/journal.pgen.1009048.

Gan, B. *et al.* (2006) "Role of FIP200 in cardiac and liver development and its regulation of TNFα and TSC-mTOR signaling pathways," *Journal of Cell Biology*, 175(1). doi:10.1083/jcb.200604129.

Ganley, I.G. *et al.* (2009) "ULK1·ATG13·FIP200 complex mediates mTOR signaling and is essential for autophagy," *Journal of Biological Chemistry*, 284(18). doi:10.1074/jbc.M900573200.

Garcia, Y.A. *et al.* (2021) "Mapping Proximity Associations of Core Spindle Assembly Checkpoint Proteins," *Journal of Proteome Research*, 20(7). doi:10.1021/acs.jproteome.0c00941.

Gecchele, E. *et al.* (2015) "A comparative analysis of recombinant protein expression in different biofactories: Bacteria, insect cells and plant systems," *Journal of Visualized Experiments* [Preprint]. doi:10.3791/52459.

Geng, J. *et al.* (2008) "Quantitative analysis of autophagy-related protein stoichiometry by fluorescence microscopy," *Journal of Cell Biology*, 182(1). doi:10.1083/jcb.200711112.

Ghezraoui, H. *et al.* (2018) "53BP1 cooperation with the REV7–shieldin complex underpins DNA structure-specific NHEJ," *Nature*, 560(7716). doi:10.1038/s41586-018-0362-1.

Glick, D., Barth, S. and Macleod, K.F. (2010) "Autophagy: Cellular and molecular mechanisms," *Journal of Pathology*. doi:10.1002/path.2697.

Gómez-Sánchez, R. *et al.* (2018a) "Atg9 establishes Atg2-dependent contact sites between the endoplasmic reticulum and phagophores," *Journal of Cell Biology*, 217(8). doi:10.1083/jcb.201710116.

Gómez-Sánchez, R. *et al.* (2018b) "Atg9 establishes Atg2-dependent contact sites between the endoplasmic reticulum and phagophores," *Journal of Cell Biology*, 217(8), pp. 2743–2763. doi:10.1083/jcb.201710116.

Gradia, S.D. *et al.* (2017) "MacroBac: New Technologies for Robust and Efficient Large-Scale Production of Recombinant Multiprotein Complexes," in *Methods in Enzymology*. doi:10.1016/bs.mie.2017.03.008.

Graef, M. *et al.* (2013) "ER exit sites are physical and functional core autophagosome biogenesis components," *Molecular Biology of the Cell*, 24(18). doi:10.1091/mbc.E13-07-0381.

Grasso, D., Renna, F.J. and Vaccaro, M.I. (2018) "Initial steps in Mammalian autophagosome biogenesis," *Frontiers in Cell and Developmental Biology*. doi:10.3389/fcell.2018.00146.

Guardia, C.M., Tan, X.-F., *et al.* (no date) "Structure of Human ATG9A, the Only Transmembrane Protein of the Core Autophagy Machinery," *Cell Reports* [Preprint]. doi:10.1016/j.celrep.2020.107837.

Guardia, C.M., Christenson, E.T., *et al.* (no date) "The structure of human ATG9A and its interplay with the lipid bilayer," *Autophagy* [Preprint]. doi:10.1080/15548627.2020.1830522.

Gupta, R. *et al.* (2018) "DNA Repair Network Analysis Reveals Shieldin as a Key Regulator of NHEJ and PARP Inhibitor Sensitivity," *Cell*, 173(4). doi:10.1016/j.cell.2018.03.050.

Hanada, T. *et al.* (2007) "The Atg12-Atg5 conjugate has a novel E3-like activity for protein lipidation in autophagy," *Journal of Biological Chemistry*, 282(52). doi:10.1074/jbc.C700195200.

Hanafusa, T. *et al.* (2010) "Overlapping in short motif sequences for binding to human REV7 and MAD2 proteins," *Genes to Cells*, 15(3). doi:10.1111/j.1365-2443.2009.01380.x.

Hara, K. *et al.* (2009) "Purification, crystallization and initial X-ray diffraction study of human REV7 in complex with a REV3 fragment," *Acta Crystallographica Section F: Structural Biology and Crystallization Communications*, 65(12). doi:10.1107/S1744309109046181.

Hara, M. *et al.* (2015) "Structure of an intermediate conformer of the spindle checkpoint protein Mad2," *Proceedings of the National Academy of Sciences of the United States of America*, 112(36), pp. 11252–11257. doi:10.1073/pnas.1512197112.

Hara, T. *et al.* (2008) "FIP200, a ULK-interacting protein, is required for autophagosome formation in mammalian cells," *Journal of Cell Biology*, 181(3). doi:10.1083/jcb.200712064.

Hara , T and Mizushima N. 2009. Role of ULK-FIP200 complex in mammalian autophagy: FIP200, a counterpart of yeast Atg17? *Autophagy* 5: 85–87.

Harding, T.M. *et al.* (1995) "Isolation and characterization of yeast mutants in the cytoplasm to vacuole protein targeting pathway," *Journal of Cell Biology*, 131(3). doi:10.1083/jcb.131.3.591.

Harnett, M.M. *et al.* (2017) "From Christian de Duve to Yoshinori Ohsumi: More to autophagy than just dining at home," *Biomedical Journal*. doi:10.1016/j.bj.2016.12.004.

Hayashi-Nishino, M. *et al.* (2009) "A subdomain of the endoplasmic reticulum forms a cradle for autophagosome formation," *Nature Cell Biology*, 11(12). doi:10.1038/ncb1991.

Hegedus, K. *et al.* (2014) "The putative HORMA domain protein Atg101 dimerizes and is required for starvation-induced and selective autophagy in drosophila," *BioMed Research International*, 2014. doi:10.1155/2014/470482.

Herruzo, E. *et al.* (2021) "Pch2 orchestrates the meiotic recombination checkpoint from the cytoplasm," *PLoS Genetics*, 17(7). doi:10.1371/journal.pgen.1009560.

Hieke, N. *et al.* (2015) "Expression of a ULK1/2 binding-deficient ATG13 variant can partially restore autophagic activity in ATG13-deficient cells," *Autophagy*, 11(9). doi:10.1080/15548627.2015.1068488.

Hill, S.M. *et al.* (2021) "VCP/p97 regulates Beclin-1-dependent autophagy initiation," *Nature Chemical Biology*, 17(4). doi:10.1038/s41589-020-00726-x.

Hollenstein, D.M. and Kraft, C. (2020) "Autophagosomes are formed at a distinct cellular structure," *Current Opinion in Cell Biology*, 65, pp. 50–57. doi:10.1016/j.ceb.2020.02.012.

Hollingsworth, N.M., Goetsch, L. and Byers, B. (1990) "The HOP1 gene encodes a meiosis-specific component of yeast chromosomes," *Cell*, 61(1). doi:10.1016/0092-8674(90)90216-2.

"Homeostatic Control of Meiotic Prophase Checkpoint Function by Pch2 and Hop1" (no date) *Current Biology* [Preprint]. doi:10.1016/j.cub.2020.08.064.

Hosokawa, N., Sasaki, T., *et al.* (2009) "Atg101, a novel mammalian autophagy protein interacting with Atg13," *Autophagy*, 5(7). doi:10.4161/auto.5.7.9296.

Hosokawa, N., Hara, T., *et al.* (2009) "Nutrient-dependent mTORCl association with the ULK1-Atg13-FIP200 complex required for autophagy," *Molecular Biology of the Cell*, 20(7). doi:10.1091/mbc.E08-12-1248.

Huang, W.P. and Klionsky, D.J. (2002) "Autophagy in yeast: A review of the molecular machinery," *Cell Structure and Function*. doi:10.1247/csf.27.409.

Hurley, J.H. and Young, L.N. (2017) "Mechanisms of autophagy initiation," *Annual Review of Biochemistry*, 86. doi:10.1146/annurev-biochem-061516-044820.

Ichimiya, T. *et al.* (2020) "Autophagy and autophagy-related diseases: A review," *International Journal of Molecular Sciences*. doi:10.3390/ijms21238974.

Ichimura, Y. *et al.* (2000) "A ubiquitin-like system mediates protein lipidation," *Nature*, 408(6811). doi:10.1038/35044114.

Jao, C.C. *et al.* (2013a) "A HORMA domain in Atg13 mediates PI 3-kinase recruitment in autophagy," *Proceedings of the National Academy of Sciences of the United States of America* [Preprint]. doi:10.1073/pnas.1220306110.

Jao, C.C. *et al.* (2013b) "A HORMA domain in Atg13 mediates PI 3-kinase recruitment in autophagy," *Proceedings of the National Academy of Sciences of the United States of America*, 110(14), pp. 5486–5491. doi:10.1073/pnas.1220306110.

Jao, C.C. *et al.* (2013c) "What the N-terminal domain of Atg13 looks like and what it does: A HORMA fold required for PtdIns 3-kinase recruitment," *Autophagy*, 9(7), pp. 1112–1114. doi:10.4161/auto.24896.

Jung, C.H. *et al.* (2009) "ULK-Atg13-FIP200 complexes mediate mTOR signaling to the autophagy machinery," *Molecular Biology of the Cell*, 20(7). doi:10.1091/mbc.E08-12-1249.

Kabeya, Y. *et al.* (2000) "LC3, a mammalian homologue of yeast Apg8p, is localized in autophagosome membranes after processing," *EMBO Journal*, 19(21). doi:10.1093/emboj/19.21.5720.

Kabeya, Y. *et al.* (2005) "Atg17 functions in cooperation with Atg1 and Atg13 in yeast autophagy," *Molecular Biology of the Cell*, 16(5). doi:10.1091/mbc.E04-08-0669.

Kaizuka, T. and Mizushima, N. (2016) "Atg13 Is Essential for Autophagy and Cardiac Development in Mice," *Molecular and Cellular Biology*, 36(4), pp. 585–595. doi:10.1128/mcb.01005-15.

Kakuta, S. *et al.* (2012) "Atg9 vesicles recruit vesicle-tethering proteins Trs85 and Ypt1 to the autophagosome formation site," *Journal of Biological Chemistry*, 287(53). doi:10.1074/jbc.M112.411454.

Kamada, Y. *et al.* (2000) "Tor-mediated induction of autophagy via an Apg1 protein kinase complex," *Journal of Cell Biology*, 150(6). doi:10.1083/jcb.150.6.1507.

Kamada, Y. *et al.* (2010) "Tor Directly Controls the Atg1 Kinase Complex To Regulate Autophagy," *Molecular and Cellular Biology*, 30(4). doi:10.1128/mcb.01344-09.

Kannangara, A.R. *et al.* (2021) "BioID reveals an ATG9A interaction with ATG13-ATG101 in the degradation of p62/SQSTM1-ubiquitin clusters," *EMBO reports*, 22(10). doi:10.15252/embr.202051136.

Karanasios, E. *et al.* (2013) "Dynamic association of the ULK1 complex with omegasomes during autophagy induction," *Journal of Cell Science*, 126(22). doi:10.1242/jcs.132415.

Karanasios, E. *et al.* (2016) "Autophagy initiation by ULK complex assembly on ER tubulovesicular regions marked by ATG9 vesicles," *Nature Communications*, 7. doi:10.1038/ncomms12420.

Kawamata, T. *et al.* (2008) "Organization of the pre-autophagosomal structure responsible for autophagosome formation," *Molecular Biology of the Cell*, 19(5). doi:10.1091/mbc.E07-10-1048.

Kim, A.K. and Porter, L.L. (2021) "Functional and Regulatory Roles of Fold-Switching Proteins," *Structure*. doi:10.1016/j.str.2020.10.006.

Kim, B.W. *et al.* (2018) "The C-terminal region of ATG101 bridges ULK1 and PtdIns3K complex in autophagy initiation," *Autophagy*, 14(12), pp. 2104–2116. doi:10.1080/15548627.2018.1504716.

Kim, Y. *et al.* (2014) "The chromosome axis controls meiotic events through a hierarchical assembly of HORMA domain proteins," *Developmental Cell*, 31(4). doi:10.1016/j.devcel.2014.09.013.

Kirisako, T. *et al.* (2000) "The reversible modification regulates the membrane-binding state of Apg8/Aut7 essential for autophagy and the cytoplasm to vacuole targeting pathway," *Journal of Cell Biology*, 151(2). doi:10.1083/jcb.151.2.263.

Kraft, C. *et al.* (2012) "Binding of the Atg1/ULK1 kinase to the ubiquitin-like protein Atg8 regulates autophagy," *EMBO Journal*, 31(18). doi:10.1038/emboj.2012.225.

Krick, R. *et al.* (2012) "Structural and functional characterization of the two phosphoinositide binding sites of PROPPINs, a β-propeller protein family," *Proceedings of the National Academy of Sciences of the United States of America*, 109(30). doi:10.1073/pnas.1205128109.

de Krijger, I. *et al.* (2021) "MAD2L2 dimerization and TRIP13 control shieldin activity in DNA repair," *Nature Communications*, 12(1). doi:10.1038/s41467-021-25724-y.

de Krijger, I., Boersma, V. and Jacobs, J.J.L. (2021) "REV7: Jack of many trades," *Trends in Cell Biology*. doi:10.1016/j.tcb.2021.04.002.

Ktistakis, N.T. (2020) "ER platforms mediating autophagosome generation," *Biochimica et Biophysica Acta - Molecular and Cell Biology of Lipids*. doi:10.1016/j.bbalip.2019.03.005.

Kuma, A. *et al.* (2002) "Formation of the ~350-kDa Apg12-Apg5·Apg16 multimeric complex, mediated by Apg16 oligomerization, is essential for autophagy in yeast," *Journal of Biological Chemistry*, 277(21). doi:10.1074/jbc.M111889200.

Kumar, S. *et al.* (2021) "Mammalian hybrid pre-autophagosomal structure HyPAS generates autophagosomes," *Cell*, 184(24). doi:10.1016/j.cell.2021.10.017.

Kundu, M. *et al.* (2008) "Ulk1 plays a critical role in the autophagic clearance of mitochondria and ribosomes during reticulocyte maturation," *Blood*, 112(4). doi:10.1182/blood-2008-02-137398.

Lai, L.T.F. *et al.* (2020) "Subnanometer resolution cryo-EM structure of Arabidopsis thaliana ATG9," *Autophagy*, 16(3). doi:10.1080/15548627.2019.1639300.

Lang, T. *et al.* (2000) "Autophagy and the cvt pathway both depend on AUT9," *Journal of Bacteriology*, 182(8), pp. 2125–2133. doi:10.1128/JB.182.8.2125-2133.2000.

Laohakunakorn, N. *et al.* (2020) "Bottom-Up Construction of Complex Biomolecular Systems With Cell-Free Synthetic Biology," *Frontiers in Bioengineering and Biotechnology*. doi:10.3389/fbioe.2020.00213.

Lara-Gonzalez, P. *et al.* (2021) "A tripartite mechanism catalyzes Mad2-Cdc20 assembly at unattached kinetochores," *Science*, 371(6524). doi:10.1126/science.abc1424.

Lawrence, C.W. (2002) "Cellular roles of DNA polymerase ζ and Rev1 protein," *DNA Repair*. doi:10.1016/S1568-7864(02)00038-1.

Lawrence, C.W., Das, G. and Christensen, R.B. (1985) "REV7, a new gene concerned with UV mutagenesis in yeast," *MGG Molecular & General Genetics*, 200(1). doi:10.1007/BF00383316.

Lee, E. *et al.* (2014) "Autophagy is essential for cardiac morphogenesis during vertebrate development," *Autophagy*, 10(4). doi:10.4161/auto.27649.

Lee, E.J. and Tournier, C. (2011) "The requirement of uncoordinated 51-like kinase 1 (ULK1) and ULK2 in the regulation of autophagy," *Autophagy*, 7(7). doi:10.4161/auto.7.7.15450.

Lemontt, J.F. (1971) "Mutants Of Yeast Defective In Mutation Induced By Ultraviolet Light," *Genetics*, 68(1). doi:10.1093/genetics/68.1.21.

Levine, B. and Klionsky, D.J. (2004) "Development by self-digestion: Molecular mechanisms and biological functions of autophagy," *Developmental Cell*. doi:10.1016/S1534-5807(04)00099-1.

Levine, B. and Kroemer, G. (2008) "Autophagy in the Pathogenesis of Disease," *Cell*. doi:10.1016/j.cell.2007.12.018.

Li, X., He, S. and Ma, B. (2020) "Autophagy and autophagy-related proteins in cancer," *Molecular Cancer*. doi:10.1186/s12943-020-1138-4.

Li, X. and Schimenti, J.C. (2007) "Mouse pachytene checkpoint 2 (Trip13) is required for completing meiotic recombination but not synapsis," *PLoS Genetics*, 3(8). doi:10.1371/journal.pgen.0030130.

Liang, L. *et al.* (2020a) "Molecular basis for assembly of the shieldin complex and its implications for NHEJ," *Nature Communications*, 11(1). doi:10.1038/s41467-020-15879-5.

Liang, R. *et al.* (2019) "Structural Conservation of the Two Phosphoinositide-Binding Sites in WIPI Proteins," *Journal of Molecular Biology*, 431(7). doi:10.1016/j.jmb.2019.02.019.

Lin, F.C., Shi, H. bin and Liu, X.H. (2021) "Similarities and Differences of Autophagy in Mammals, Plants, and Microbes," in *Advances in Experimental Medicine and Biology*. doi:10.1007/978-981-16-2830-6_7.

Liu, C.C. *et al.* (2016) "Cul3-KLHL20 Ubiquitin Ligase Governs the Turnover of ULK1 and VPS34 Complexes to Control Autophagy Termination," *Molecular Cell*, 61(1). doi:10.1016/j.molcel.2015.11.001.

Liu, Y. and Levine, B. (2015) "Autosis and autophagic cell death: The dark side of autophagy," *Cell Death and Differentiation*. doi:10.1038/cdd.2014.143.

Lorenz, A. *et al.* (2004) "S. pombe meiotic linear elements contain proteins related to synaptonemal complex components," *Journal of Cell Science*, 117(15). doi:10.1242/jcs.01203.

Lou, X. *et al.* (2000) "Structure of the Mad2 spindle assembly checkpoint protein and its interaction with Cdc20," *Nature Structural Biology*, 7(3), pp. 224–229. doi:10.1038/73338.

Luckow, V.A. *et al.* (1993) "Efficient generation of infectious recombinant baculoviruses by site-specific transposon-mediated insertion of foreign genes into a baculovirus genome propagated in Escherichia coli," *Journal of Virology* [Preprint]. doi:10.1128/jvi.67.8.4566-4579.1993.

Luo, X. *et al.* (2002) "The Mad2 spindle checkpoint protein undergoes similar major conformational changes upon binding to either Mad1 or Cdc20," *Molecular Cell*, 9(1). doi:10.1016/S1097-2765(01)00435-X.

Luo, X. *et al.* (2004) "The Mad2 spindle checkpoint protein has two distinct natively folded states," *Nature Structural and Molecular Biology*, 11(4). doi:10.1038/nsmb748.

Luo, X. and Yu, H. (2008) "Protein Metamorphosis: The Two-State Behavior of Mad2," *Structure*. doi:10.1016/j.str.2008.10.002.

Lynch-Day, M.A. and Klionsky, D.J. (2010) "The Cvt pathway as a model for selective autophagy," *FEBS Letters*, 584(7), pp. 1359–1366. doi:10.1016/j.febslet.2010.02.013.

Maeda, S. *et al.* (no date) "Structure, lipid scrambling activity and role in autophagosome formation of ATG9A," *Nature Structural and Molecular Biology* [Preprint]. doi:10.1038/s41594-020-00520-2.

Maeda, S., Otomo, C. and Otomo, T. (2019) "The autophagic membrane tether ATG2A transfers lipids between membranes," *eLife*, 8. doi:10.7554/eLife.45777.

Maiato, H. *et al.* (2004) "The dynamic kinetochore-microtubule interface," *Journal of Cell Science*. doi:10.1242/jcs.01536.

Mapelli, M. *et al.* (2006) "Determinants of conformational dimerization of Mad2 and its inhibition by p31comet," *EMBO Journal*, 25(6). doi:10.1038/sj.emboj.7601033.

Mapelli, M. *et al.* (2007) "The Mad2 Conformational Dimer: Structure and Implications for the Spindle Assembly Checkpoint," *Cell*, 131(4). doi:10.1016/j.cell.2007.08.049.

Mari, M. *et al.* (2010) "An Atg9-containing compartment that functions in the early steps of autophagosome biogenesis," *Journal of Cell Biology*, 190(6). doi:10.1083/jcb.200912089.

Mari, M., Tooze, S.A. and Reggiori, F. (2011) "The puzzling origin of the autophagosomal membrane," *F1000 Biology Reports*. doi:10.3410/B3-25.

Mariani, L. *et al.* (2012) "Role of the Mad2 dimerization interface in the spindle assembly checkpoint independent of kinetochores," *Current Biology*, 22(20), pp. 1900–1908. doi:10.1016/j.cub.2012.08.028.

Martinez-Perez, E. and Villeneuve, A.M. (2005) "HTP-1-dependent constraints coordinate homolog pairing and synapsis and promote chiasma formation during C. elegans meiosis," *Genes and Development*, 19(22). doi:10.1101/gad.1338505.

Matoba, K. *et al.* (2020) "Atg9 is a lipid scramblase that mediates autophagosomal membrane expansion," *Nature Structural & Molecular Biology* [Preprint]. doi:10.1038/s41594-020-00518-w.

Matsunaga, K. *et al.* (2009) "Two Beclin 1-binding proteins, Atg14L and Rubicon, reciprocally regulate autophagy at different stages," *Nature Cell Biology*, 11(4). doi:10.1038/ncb1846.

Matsunaga, K. *et al.* (2010) "Autophagy requires endoplasmic reticulum targeting of the PI3-kinase complex via Atg14L," *Journal of Cell Biology*, 190(4). doi:10.1083/jcb.200911141.

Mercer, C.A., Kaliappan, A. and Dennis, P.B. (2009) "A novel, human Atg13 binding protein, Atg101, interacts with ULK1 and is essential for macroautophagy," *Autophagy*, 5(5). doi:10.4161/auto.5.5.8249.

Michel, M. *et al.* (2015) "The mammalian autophagy initiator complex contains 2 HORMA domain proteins," *Autophagy*, 11(12), pp. 2300–2308. doi:10.1080/15548627.2015.1076605.

Miller, J.H. (1992) *A short course in bacterial genetics*, *Cold Spring Harbor Laboratory Press, Cold Spring Harbor*.

Miniowitz-Shemtov, S. *et al.* (2015) "Mode of interaction of TRIP13 AAA-ATPase with the Mad2-binding protein p31comet and with mitotic checkpoint complexes," *Proceedings of the National Academy of Sciences of the United States of America*, 112(37). doi:10.1073/pnas.1515358112.

Mizushima, N. *et al.* (1998) "A protein conjugation system essential for autophagy," *Nature*, 395(6700). doi:10.1038/26506.

Mizushima, N. (2018) "A brief history of autophagy from cell biology to physiology and disease," *Nature Cell Biology*. doi:10.1038/s41556-018-0092-5.

Mizushima, N., Noda, T. and Ohsumi, Y. (1999) "Apg16p is required for the function of the Apg12p-Apg5p conjugate in the yeast autophagy pathway," *EMBO Journal*, 18(14). doi:10.1093/emboj/18.14.3888.

Moparthi, S.B. and Wollert, T. (2019) "Reconstruction of destruction – In vitro reconstitution methods in autophagy research," *Journal of Cell Science*. Company of Biologists Ltd. doi:10.1242/jcs.223792.

Moreau, K. and Rubinsztein, D.C. (2012) "The plasma membrane as a control center for autophagy," *Autophagy*. doi:10.4161/auto.20060.

Morishita, H. *et al.* (2020) "Autophagy Is Required for Maturation of Surfactant-Containing Lamellar Bodies in the Lung and Swim Bladder," *Cell Reports*, 33(10). doi:10.1016/j.celrep.2020.108477.

Murakumo, Y. *et al.* (2000) "A human REV7 homolog that interacts with the polymerase ζ catalytic subunit hREV3 and the spindle assembly checkpoint protein hMAD2," *Journal of Biological Chemistry*, 275(6). doi:10.1074/jbc.275.6.4391.

Murzin, A.G. (2008) "Biochemistry: Metamorphic proteins," *Science*. doi:10.1126/science.1158868.

Musacchio, A. and Salmon, E.D. (2007) "The spindle-assembly checkpoint in space and time," *Nature Reviews Molecular Cell Biology*. doi:10.1038/nrm2163.

Nagata, S., Sakuragi, T. and Segawa, K. (2020) "Flippase and scramblase for phosphatidylserine exposure," *Current Opinion in Immunology*. doi:10.1016/j.coi.2019.11.009.

Nakatogawa, H., Ichimura, Y. and Ohsumi, Y. (2007) "Atg8, a Ubiquitin-like Protein Required for Autophagosome Formation, Mediates Membrane Tethering and Hemifusion," *Cell*, 130(1). doi:10.1016/j.cell.2007.05.021.

Nao Hosokawa, † *et al.* (2009) "Nutrient-dependent mTORC1 Association with the ULK1–Atg13–FIP200 Complex Required for Autophagy," *Molecular biology of the cell*, 20(m).

Noda, N.N. (2021a) "Atg2 and Atg9: Intermembrane and interleaflet lipid transporters driving autophagy," *Biochimica et Biophysica Acta - Molecular and Cell Biology of Lipids*. doi:10.1016/j.bbalip.2021.158956.

Noda, N.N. (2021b) "Atg2 and Atg9: Intermembrane and interleaflet lipid transporters driving autophagy," *Biochimica et Biophysica Acta - Molecular and Cell Biology of Lipids*. Elsevier B.V. doi:10.1016/j.bbalip.2021.158956.

Noda, N.N. and Mizushima, N. (2016) "Atg101: Not just an accessory subunit in the autophagy-initiation complex," *Cell Structure and Function*. doi:10.1247/csf.15013.

Noda, T. *et al.* (2000) "Apg9p/Cvt7p is an integral membrane protein required for transport vesicle formation in the Cvt and autophagy pathways," *Journal of Cell Biology*, 148(3). doi:10.1083/jcb.148.3.465.

Noda, T. (2017) "Autophagy in the context of the cellular membrane-trafficking system: The enigma of Atg9 vesicles," *Biochemical Society Transactions*. Portland Press Ltd, pp. 1323–1331. doi:10.1042/BST20170128.

Noda, T. and Ohsumi, Y. (1998) "Tor, a phosphatidylinositol kinase homologue, controls autophagy in yeast," *Journal of Biological Chemistry*, 273(7). doi:10.1074/jbc.273.7.3963.

Noda, T., Suzuki, K. and Ohsumi, Y. (2002) "Yeast autophagosomes: De novo formation of a membrane structure," *Trends in Cell Biology*. doi:10.1016/S0962-8924(02)02278-X.

Noordermeer, S.M. *et al.* (2018) "The shieldin complex mediates 53BP1-dependent DNA repair," *Nature*, 560(7716). doi:10.1038/s41586-018-0340-7.

Obara, K., Sekito, T., *et al.* (2008) "The Atg18-Atg2 complex is recruited to autophagic membranes via phosphatidylinositol 3-phosphate and exerts an essential function," *Journal of Biological Chemistry*, 283(35). doi:10.1074/jbc.M803180200.

Obara, K., Noda, T., *et al.* (2008) "Transport of phosphatidylinositol 3-phosphate into the vacuole via autophagic membranes in Saccharomyces cerevisiae," *Genes to Cells*, 13(6). doi:10.1111/j.1365-2443.2008.01188.x.

Obara, K. and Ohsumi, Y. (2011) "Atg14: A key player in orchestrating autophagy," *International Journal of Cell Biology* [Preprint]. doi:10.1155/2011/713435.

Obara, K., Sekito, T. and Ohsumi, Y. (2006) "Assortment of phosphatidylinositol 3-kinase complexes-Atg14p directs association of complex I to the pre-autophagosomal structure in Saccharomyces cerevisiae," *Molecular Biology of the Cell*, 17(4). doi:10.1091/mbc.E05-09-0841.

Ohsumi, Y. (1999) "Molecular mechanism of autophagy in yeast, Saccharomyces cerevisiae," *Philosophical Transactions of the Royal Society B: Biological Sciences*, 354(1389). doi:10.1098/rstb.1999.0501.

Oliver, R.C. *et al.* (2013) "Dependence of Micelle Size and Shape on Detergent Alkyl Chain Length and Head Group," *PLoS ONE*, 8(5). doi:10.1371/journal.pone.0062488.

Orii, M. *et al.* (2020) "Transmembrane phospholipid translocation mediated by Atg9 is involved in autophagosome formation," *Journal of Cell Biology*, 220(3). doi:10.1083/JCB.202009194.

Orsi, A. *et al.* (2012) "Dynamic and transient interactions of Atg9 with autophagosomes, but not membrane integration, are required for autophagy," *Molecular Biology of the Cell*, 23(10). doi:10.1091/mbc.E11-09-0746.

Orth, M. *et al.* (2011) "Shugoshin is a Mad1/Cdc20-like interactor of Mad2," *EMBO Journal*, 30(14). doi:10.1038/emboj.2011.187.

Osawa, T. *et al.* (2019) "Atg2 mediates direct lipid transfer between membranes for autophagosome formation," *Nature Structural and Molecular Biology*, 26(4). doi:10.1038/s41594-019-0203-4.

Osawa, T., Ishii, Y. and Noda, N.N. (2020) "Human ATG2B possesses a lipid transfer activity which is accelerated by negatively charged lipids and WIPI4," *Genes to Cells*, 25(1). doi:10.1111/gtc.12733.

Osawa, T. and Noda, N.N. (2019) "Atg2: A novel phospholipid transfer protein that mediates de novo autophagosome biogenesis," *Protein Science*. doi:10.1002/pro.3623.

Otomo, T., Chowdhury, S. and Lander, G.C. (2018) "The Rod-Shaped ATG2A-WIPI4 Complex Tethers Membranes In Vitro," *Contact*, 1. doi:10.1177/2515256418819936.

Otomo, T. and Maeda, S. (2019) "ATG2A transfers lipids between membranes in vitro," *Autophagy*. doi:10.1080/15548627.2019.1659622.

Papa, A. and Pandolfi, P.P. (2019) "The pten–pi3k axis in cancer," *Biomolecules*. doi:10.3390/biom9040153.

Papinski, D. *et al.* (2014) "Early Steps in Autophagy Depend on Direct Phosphorylation of Atg9 by the Atg1 Kinase," *Molecular Cell*, 53(3). doi:10.1016/j.molcel.2013.12.011.

Papinski, D. and Kraft, C. (2016) "Regulation of Autophagy by Signaling Through the Atg1/ULK1 Complex," *Journal of Molecular Biology*. doi:10.1016/j.jmb.2016.03.030.

Park, J. *et al.* (2019) "Quaternary structures of Vac8 differentially regulate the Cvt and PMN pathways," *Autophagy*, 00(00), pp. 1–16. doi:10.1080/15548627.2019.1659615.

Park, J.M. *et al.* (2016) "The ULK1 complex mediates MTORC1 signaling to the autophagy initiation machinery via binding and phosphorylating ATG14," *Autophagy*, 12(3). doi:10.1080/15548627.2016.1140293.

Pfleger, C.M. *et al.* (2001) "Inhibition of Cdh1-APC by the MAD2-related protein MAD2L2: A novel mechanism for regulating Cdh1," *Genes and Development*, 15(14). doi:10.1101/gad.897901.

Piano, V. *et al.* (2021) "CDC20 assists its catalytic incorporation in the mitotic checkpoint complex," *Science*, 371(6524), pp. 67–71. doi:10.1126/science.abc1152.

Polson, H.E.J. *et al.* (2010) "Mammalian Atg18 (WIPI2) localizes to omegasome-anchored phagophores and positively regulates LC3 lipidation," *Autophagy*, 6(4). doi:10.4161/auto.6.4.11863.

Proikas-Cezanne, T. *et al.* (2004) "WIPI-1α (WIPI49), a member of the novel 7-bladed WIPI protein family, is aberrantly expressed in human cancer and is linked to starvation-induced autophagy," *Oncogene*, 23(58). doi:10.1038/sj.onc.1208331.

Qi, S. *et al.* (2015) "Structure of the human Atg13-Atg101 HORMA heterodimer: An interaction hub within the ULK1 complex," *Structure*, 23(10). doi:10.1016/j.str.2015.07.011.

Ragusa, M.J., Stanley, R.E. and Hurley, J.H. (2012) "Architecture of the atg17 complex as a scaffold for autophagosome biogenesis," *Cell*, 151(7). doi:10.1016/j.cell.2012.11.028.

Rao, Y. *et al.* (2016a) "The Atg1-kinase complex tethers Atg9-vesicles to initiate autophagy," *Nature Communications*, 7. doi:10.1038/ncomms10338.

Rao, Y. *et al.* (2016b) "The Atg1-kinase complex tethers Atg9-vesicles to initiate autophagy," *Nature Communications*, 7. doi:10.1038/ncomms10338.

Reggiori, F. *et al.* (2004) "The Atg1-Atg13 complex regulates Atg9 and Atg23 retrieval transport from the pre-autophagosomal structure," *Developmental Cell*, 6(1), pp. 79–90. doi:10.1016/S1534-5807(03)00402-7.

Rizzo, A.A. *et al.* (2018) "Rev7 dimerization is important for assembly and function of the Rev1/Polζ translesion synthesis complex," *Proceedings of the National Academy of Sciences of the United States of America*, 115(35). doi:10.1073/pnas.1801149115.

Rosenberg SC Corbett KD (2015) The multifaceted roles of the HORMA domain in cellular signaling The Journal of Cell Biology 211:745–755.

Sarangi, P. *et al.* (no date) "p31comet promotes homologous recombination by inactivating REV7 through the TRIP13 ATPase," *Proceedings of the National Academy of Sciences of the United States of America* [Preprint]. doi:10.1073/pnas.2008830117.

Sarangi, P., Clairmont, C.S. and D'Andrea, A.D. (2020) "Disassembly of the Shieldin Complex by TRIP13," *Cell Cycle*. doi:10.1080/15384101.2020.1758435.

Sauer, R.T. and Baker, T.A. (2011) "AAA+ Proteases: ATP-fueled machines of protein destruction," *Annual Review of Biochemistry*, 80. doi:10.1146/annurev-biochem-060408-172623.

Sawa-Makarska, J. *et al.* (2020) "Reconstitution of autophagosome nucleation defines Atg9 vesicles as seeds for membrane formation.," *Science (New York, N.Y.)*, 369(6508). doi:10.1126/science.aaz7714.

"Secret of Atg9: lipid scramblase activity drives de novo autophagosome biogenesis" (no date) *Cell Death and Differentiation* [Preprint]. doi:10.1038/s41418-020-00663-1.

Setiaputra, D. and Durocher, D. (2019) " Shieldin – the protector of DNA ends ," *EMBO reports*, 20(5). doi:10.15252/embr.201847560.

Shi, X. *et al.* (2020) "ULK complex organization in autophagy by a C-shaped FIP200 N-terminal domain dimer," *Journal of Cell Biology*, 219(7). doi:10.1083/JCB.201911047.

Shima, T., Kirisako, H. and Nakatogawa, H. (2019) "COPII vesicles contribute to autophagosomal membranes," *Journal of Cell Biology*, 218(5). doi:10.1083/jcb.201809032.

Shintani, T. *et al.* (1999) "Apg10p, a novel protein-conjugating enzyme essential for autophagy in yeast," *EMBO Journal*, 18(19). doi:10.1093/emboj/18.19.5234.

Simonetta, M. *et al.* (2009) "The influence of catalysis on Mad2 activation dynamics," *PLoS Biology*, 7(1). doi:10.1371/journal.pbio.1000010.

Simunovic, M. *et al.* (2019) "Curving cells inside and out: Roles of BAR domain proteins in membrane shaping and its cellular implications," *Annual Review of Cell and Developmental Biology*. doi:10.1146/annurev-cellbio-100617-060558.

Sironi, L. *et al.* (2002a) "Crystal structure of the tetrameric Mad1-Mad2 core complex: Implications of a 'safety belt' binding mechanism for the spindle checkpoint," *EMBO Journal*, 21(10). doi:10.1093/emboj/21.10.2496.

Sironi, L. *et al.* (2002b) "Crystal structure of the tetrameric Mad1-Mad2 core complex: Implications of a 'safety belt' binding mechanism for the spindle checkpoint," *EMBO Journal*, 21(10), pp. 2496–2506. doi:10.1093/emboj/21.10.2496.

Stjepanovic, G. *et al.* (2014) "Assembly and dynamics of the autophagy-initiating Atg1 complex," *Proceedings of the National Academy of Sciences of the United States of America*, 111(35), pp. 12793–12798. doi:10.1073/pnas.1407214111.

Suzuki, H. *et al.* (2015a) "Open and closed HORMAs regulate autophagy initiation," *Autophagy*, 11(11), pp. 2123–2124. doi:10.1080/15548627.2015.1091144.

Suzuki, H. *et al.* (2015b) "Structure of the Atg101-Atg13 complex reveals essential roles of Atg101 in autophagy initiation," *Nature Structural and Molecular Biology*, 22(7), pp. 572–580. doi:10.1038/nsmb.3036.

Suzuki, H. *et al.* (2015c) "Structure of the Atg101-Atg13 complex reveals essential roles of Atg101 in autophagy initiation," *Nature Structural and Molecular Biology*, 22(7). doi:10.1038/nsmb.3036.

Suzuki, H. *et al.* (2017) "Structural biology of the core autophagy machinery," *Current Opinion in Structural Biology*. doi:10.1016/j.sbi.2016.09.010.

Suzuki, K. *et al.* (2001) "The pre-autophagosomal structure organized by concerted functions of APG genes is essential for autophagosome formation," *EMBO Journal*, 20(21). doi:10.1093/emboj/20.21.5971.

Suzuki, K. *et al.* (2013) "Fine mapping of autophagy-related proteins during autophagosome formation in Saccharomyces cerevisiae," *Journal of Cell Science*, 126(11). doi:10.1242/jcs.122960.

Suzuki, K. and Ohsumi, Y. (2010) "Current knowledge of the pre-autophagosomal structure (PAS)," *FEBS Letters*. doi:10.1016/j.febslet.2010.02.001.

Suzuki, S.W. *et al.* (2015a) "Atg13 HORMA domain recruits Atg9 vesicles during autophagosome formation," *Proceedings of the National Academy of Sciences of the United States of America*, 112(11), pp. 3350–3355. doi:10.1073/pnas.1421092112.

Suzuki, S.W. *et al.* (2015b) "Atg13 HORMA domain recruits Atg9 vesicles during autophagosome formation," *Proceedings of the National Academy of Sciences of the United States of America*, 112(11), pp. 3350–3355. doi:10.1073/pnas.1421092112.

Takeshige, K. *et al.* (1992) "Autophagy in yeast demonstrated with proteinase-deficient mutants and conditions for its induction," *Journal of Cell Biology*, 119(2). doi:10.1083/jcb.119.2.301.

Tanida, I. *et al.* (1999) "Apg7p/Cvt2p: A novel protein-activating enzyme essential for autophagy," *Molecular Biology of the Cell*, 10(5). doi:10.1091/mbc.10.5.1367.

Tanida, I. *et al.* (2005) "Lysosomal turnover, but not a cellular level, of endogenous LC3 is a marker for autophagy.," *Autophagy*, 1(2). doi:10.4161/auto.1.2.1697.

Teter, S.A. and Klionsky, D.J. (2000) "Transport of proteins to the yeast vacuole: Autophagy, cytoplasm-to-vacuole targeting, and role of the vacuole in degradation," *Seminars in Cell and Developmental Biology*, 11(3). doi:10.1006/scdb.2000.0163.

Thumm, M. *et al.* (1994) "Isolation of autophagocytosis mutants of Saccharomyces cerevisiae," *FEBS Letters*, 349(2). doi:10.1016/0014-5793(94)00672-5.

Tomida, J. *et al.* (2015) "REV7 is essential for DNA damage tolerance via two REV3L binding sites in mammalian DNA polymerase ζ," *Nucleic Acids Research*, 43(2). doi:10.1093/nar/gku1385.

Tooze, S.A. and Yoshimori, T. (2010) "The origin of the autophagosomal membrane," *Nature Cell Biology*. doi:10.1038/ncb0910-831.

Torpey, L.E. *et al.* (1994) "IX. Yeast sequencing reports. Cloning and sequence of REV7, a gene whose function is required for DNA damage-induced mutagenesis in Saccharomyces cerevisiae," *Yeast*, 10(11). doi:10.1002/yea.320101115.

Tromer, E.C. *et al.* (2019) "Mosaic origin of the eukaryotic kinetochore," *Proceedings of the National Academy of Sciences of the United States of America*, 116(26). doi:10.1073/pnas.1821945116.

Tsukada, M. and Ohsumi, Y. (1993) "Isolation and characterization of autophagy-defective mutants of Saccharomyces cerevisiae," *FEBS Letters*, 333(1–2). doi:10.1016/0014-5793(93)80398-E.

Turco, E. *et al.* (2019) "FIP200 Claw Domain Binding to p62 Promotes Autophagosome Formation at Ubiquitin Condensates," *Molecular Cell*, 74(2). doi:10.1016/j.molcel.2019.01.035.

Valverde, D.P. *et al.* (2019) "ATG2 transports lipids to promote autophagosome biogenesis," *Journal of Cell Biology*, 218(6). doi:10.1083/JCB.201811139.

Voges, D., Zwickl, P. and Baumeister, W. (1999) "The 26S proteasome: A molecular machine designed for controlled proteolysis," *Annual Review of Biochemistry*. doi:10.1146/annurev.biochem.68.1.1015.

Wallot-Hieke *et al.*, 2018 „Systematic analysis of ATG13 domain requirements for autophagy induction"Autophagy, 14 (2018), pp. 743-763, 10.1080/15548627.2017.1387342

Wang, C. *et al.* (2018) "Phosphorylation of ULK1 affects autophagosome fusion and links chaperone-mediated autophagy to macroautophagy," *Nature Communications*, 9(1). doi:10.1038/s41467-018-05449-1.

Wang, X. *et al.* (2019) "REV7 has a dynamic adaptor region to accommodate small GTPase RAN/Shigella IpaB ligands, and its activity is regulated by the RanGTP/GDP switch," *Journal of Biological Chemistry*, 294(43). doi:10.1074/jbc.RA119.010123.

Watanabe, Y., Taguchi, K. and Tanaka, M. (2020) "Ubiquitin, Autophagy and Neurodegenerative Diseases," *Cells*. doi:10.3390/cells9092022.

West, A.M.V., Komives, E.A. and Corbett, K.D. (2018) "Conformational dynamics of the Hop1 HORMA domain reveal a common mechanism with the spindle checkpoint protein Mad2," *Nucleic Acids Research*, 46(1). doi:10.1093/nar/gkx1196.

Westhorpe, F.G. *et al.* (2011) "p31 comet-mediated extraction of Mad2 from the MCC promotes efficient mitotic exit," *Journal of Cell Science*, 124(22). doi:10.1242/jcs.093286.

Wojtasz, L. *et al.* (2009) "Mouse HORMAD1 and HORMAD2, two conserved meiotic chromosomal proteins, are depleted from synapsed chromosome axes with the help of TRIP13 AAA-ATPase," *PLoS Genetics*, 5(10). doi:10.1371/journal.pgen.1000702.

Wong, A.S.L., Cheung, Z.H. and Ip, N.Y. (2011) "Molecular machinery of macroautophagy and its deregulation in diseases," *Biochimica et Biophysica Acta - Molecular Basis of Disease*. doi:10.1016/j.bbadis.2011.07.005.

Xie, W. *et al.* (2021) "Molecular mechanisms of assembly and TRIP13-mediated remodeling of the human Shieldin complex," *Proceedings of the National Academy of Sciences of the United States of America*, 118(8). doi:10.1073/pnas.2024512118.

Xu, G. *et al.* (2015) "REV7 counteracts DNA double-strand break resection and affects PARP inhibition," *Nature*, 521(7553). doi:10.1038/nature14328.

Yajie Gu *et al.*, 2022 Evolutionary Dynamics and Molecular Mechanisms of HORMA Domain Protein Signaling Yajie Gu, Arshad Desai, Kevin D. Corbett Annual Review of Biochemistry 2022 91:1

Yamamoto, H. *et al.* (2012) "Atg9 vesicles are an important membrane source during early steps of autophagosome formation," *Journal of Cell Biology*, 198(2). doi:10.1083/jcb.201202061.

Yamamoto, H. *et al.* (2016) "The Intrinsically Disordered Protein Atg13 Mediates Supramolecular Assembly of Autophagy Initiation Complexes," *Developmental Cell*, 38(1), pp. 86–99. doi:10.1016/j.devcel.2016.06.015.

Yang, M. *et al.* (2007) "p31comet Blocks Mad2 Activation through Structural Mimicry," *Cell*, 131(4). doi:10.1016/j.cell.2007.08.048.

Yang, M. *et al.* (2008) "Insights into Mad2 regulation in the spindle checkpoint revealed by the crystal structure of the symmetric Mad2 dimer," *PLoS Biology*, 6(3). doi:10.1371/journal.pbio.0060050.

Yang, Y. *et al.* (2021) "Autophagosomal Membrane Origin and Formation," in *Advances in Experimental Medicine and Biology*. doi:10.1007/978-981-16-2830-6_2.

Ye, Q. *et al.* (2015) "TRIP13 is a protein-remodeling AAA+ ATPase that catalyzes MAD2 conformation switching," *eLife*, 2015(4). doi:10.7554/eLife.07367.

Ye, Q. *et al.* (2020) "HORMA Domain Proteins and a Trip13-like ATPase Regulate Bacterial cGAS-like Enzymes to Mediate Bacteriophage Immunity," *Molecular Cell*, 77(4), pp. 709-722.e7. doi:10.1016/j.molcel.2019.12.009.

Young, A.R.J. *et al.* (2006) "Starvation and ULK1-dependent cycling of mammalian Atg9 between the TGN and endosomes," *Journal of Cell Science*, 119(18). doi:10.1242/jcs.03172.

Zhou, C. *et al.* (2017) "Regulation of mATG9 trafficking by Src- and ULK1-mediated phosphorylation in basal and starvation-induced autophagy," *Cell Research*, 27(2). doi:10.1038/cr.2016.146.

6 Acknowledgments

I've been working on this project in Faesen Lab at the Max Planck Institute for Biophysical Chemistry since the end of 2017. Out of all the things that might have happened during the most challenging time of my academic life, I would say, a pandemic wasn't in the frame of my thoughts. I consider myself extremely fortunate to have had the chance to survive a PhD and a pandemic, at the same time.

I was also very lucky to have shared my struggles and joyful academic moments with motivated, creative, and hardworking people like all the components of Faesen Lab. I will surely remember this journey all of you for years to come as a stressful, but incredible experience.

First of all, I had the opportunity to challenge myself professionally thanks to this amazing and stimulating project and, surely, Alex who guided me and supported me at any time, and was always there to listen to me whenever I had a doubt, I needed an opinion or wanted a confrontation. His ability to see things from a different perspective has always fascinated me and it has always been part of the reason why I have never been afraid to come in his office even with the most stupid theory or the most unexpected result. Without his extensive understanding of HORMAs, my thesis would not have been conceivable.

I would also like to thank Alex Stein who guided my colleagues and me through the fascinating realm of transmembrane proteins and detergents. I would also like to ancknowledge Prof. Thumm to have had the patience to accept to be part of my TAC during the last year. His impact on the Autophagy field is outstanding and I feel honored to have him in my committee. I want to thank Prof. Blanch Schwappach who was also part of my TAC at the beginning and I have tried to learn as much as I could from her opinions and ideas.

Additionally, I would like to thank all of my collaborators. Bjorn Stork, Annabelle and Céline. Our confrontational meetings have been incredibly expiring and our monthly exchange maintained me focused on the goal. I also would like to thank the full Urlaub lab and Iwan for their help.

I'd like to convey my heartfelt gratitude to the people of the lab who have also sustained me throughout the years and during the pandemic have been part of my support circle.

First of all, Vivek. He has been with me from the beginning to the end. Doing something alone is nice, doing it with a friend is better. Anh, I am grateful for the fact I met him more than ever, I don't know how to express how important he has been for me and this project. Anoshi, for her support at any time of these years. Her kindness is brighter than the light of the old gel lamp downstairs. Bastian, because I admire his ability to apply logic to anything. I have tried to learn

from him every day. Laura, for being caring and supporting to all of us with her dedication and energy. You are the strongest of all of us. Steffi and Gertrude, the pillars of the lab, I will never be able to share how much I am grateful they didn't give up on us. If the lab is not burned to the ground yet, is because of them. I also wish to thank Juliane, for her help and support with administrative issues and her amazing precision and kindness.

Lastly, I would like to thank my family and friends who taught me to approach everything with love, care, and commitment. I want to thank my parents and my sister, Chiara, the other amazing part of me; Zia Ale and Zio Carlo and Andrea for being on my side at any moment of my life; Simran and Dev, who are the most beautiful human beings on this earth; to Ahmad to be part of what I want to be; to Gabriela, Luca, and Antonio to be my supportive circle at any moment of my life; to Sham and Chiara, who were always ready to be a temporary family whenever I needed it.

I dedicate this work to you, even if I was my first motivation during this hell of a PhD.

(Infine, vorrei ringraziare la mia famiglia e i miei amici che mi hanno insegnato ad affrontare tutto con amore, cura e impegno. Voglio ringraziare i miei genitori e mia sorella, Chiara, l'altra parte meravigliosa di me; Zia Ale e Zio Carlo e Andrea per essere stati al mio fianco in ogni momento della mia vita; Simran e Dev, che sono gli esseri umani più belli su questa terra; ad Ahmad per essere parte di ciò che voglio essere; a Gabriela, Luca e Antonio per essere il mio circolo solidale in ogni momento della mia vita; a Sham e Chiara, che sono sempre state una famiglia temporanea ogni volta ne avessi bisogno.

Dedico a voi questo lavoro, anche se io sono stata la mia prima motivazione durante quest'inferno di PhD).

"**E quindi uscimmo a riveder le stelle"**

– Dante, Inferno, Canto XXXIV

("And thence we emerged to gaze upon the stars again")